Cortical Resting State Circuits:

Connectivity and Oscillations

Tristan T. Nakagawa

TESI DOCTORAL UPF / ANY 2014

DIRECTOR DE LA TESI

Dr. Gustavo Deco
Dr. Salvador Soto-Faraco
Departament Department of Information and
Communication Technologies - DTIC;
Center for Brain and Cognition CBC

Abstract

Ongoing spontaneous brain activity patterns raise ever-growing interest in the neuroscience community. Complex spatiotemporal patterns that emerge from a structural core and interactions of functional dynamics have been found to be far from arbitrary in empirical studies. They are thought to compose the network structure underlying human cognitive architecture. In this thesis, we use a biophysically realistic computer model to study key factors in producing complex spatiotemporal activation patterns. For the first time, we present a model of decreased physiological signal complexity in aging and demonstrate that delays shape functional connectivity in an oscillatory spiking-neuron network model for MEG resting-state data. Our results show that the inclusion of realistic delays maximizes model performance. Furthermore, we propose embracing a datadriven, comparative stance on decomposing the system into subnetworks.

Resumen

Últimamente, el interés de la comunidad científica sobre los patrones de la continua actividad espontanea del cerebro ha ido en aumento. Complejos patrones espacio-temporales emergen a partir de interacciones de un núcleo estructural con dinámicas funcionales. Se ha encontrado que estos patrones no son aleatorios y que componen la red estructural en la que la arquitectura cognitiva humana se basa. En esta tesis usamos un modelo computacional detallado para estudiar los factores clave en producir los patrones emergentes. Por primera vez, presentamos un modelo simplificado de la actividad cerebral en envejecimiento. También demostramos que la inclusión del desfase de transmisión en un modelo para grabaciones magnetoencefalográficas del estado en reposo maximiza el rendimiento del modelo. Para ello, aplicamos un modelo con una red de neuronas pulsantes ('spiking-neurons') y con dinámicas oscilatorias. Además, proponemos adoptar una posición comparativa basada en los datos para descomponer el sistema en subredes.

Preface

In this thesis, we lay out a perspective on the structure and dynamics of spontaneous brain activity as expression of a complex, metastable system of active and interacting, but distinguishable brain networks. In Chapter 1, we trace the development of the idea of the brain as a self-organizing, complex network at the large scale, and the development of a whole 'resting state' brain connectivity research field, and the contributions of methodological advances, such as advances in structural imaging and new data analysis and description methods, from graph theory and new connectivity measures to clustering and decomposition approaches.

In Chapter 2, we review how computational modeling can help us to bridge the gap between structure and function by exploring and proposing mechanisms of the brain's network dynamics. In Chapter 3, we give an example of a spiking-neuron network model approach that suggests that decreases in multiscale entropy in aging are an expression of displacement of the brain (as an attractor network) from an optimal dynamical working point due to structural connectivity decreases. We extend on the modeling work and the importance of specific model aspects in Chapter 4: we examine in a dynamic mean field model the importance of considering network propagation delays in the presence of alpha-band oscillations, which are typically found in resting state recordings of MEG alpha. We show how the model can intrinsically generate the typically observed resting-alpha rhythms by spike-frequency adaptation, and that the functional network organization is best (and most robustly) fitted in the presence of delays within physiologically ranges at propagation speeds of 5-10 m/s.

Finally, we turn towards analyzing the resting state networks both in time and space in Chapter 5. We utilize Parallel Factor Analysis (PARAFAC), a multiway factorization method related to higher-dimensional PCA/ICA, to identify distinct networks in MEG resting state recordings. We show

how this method sucessfully identifies several of the established RSNs and traces their time courses simultaneously. To conclude, in Chapter 6 we summarize and discuss our findings and their implications, how our work may contribute to understanding spontaneous human brain function as an expression of a multistable, self-organizing system, and give an outlook on future research and application possibilities.

For the digital version of this document, please note that the Table of Contents, chapter numbers, and other brown text elements are in-document links to text sections, figures, or the glossary [1] Citations (in blue) link to the bibliography, and `typeface` elements are links to webpages of cited papers or other web resources (functional at the time of writing this thesis).[2]

Chapters 2, 3 and 4 reproduce the below listed publications as indicated in the corresponding chapters:

Nakagawa, T. T., Jirsa, V. K., Spiegler, A., McIntosh, A. R., & Deco, G. (2013). Bottom up modeling of the connectome: Linking structure and function in the resting brain and their changes in aging. NeuroImage, 10.1016/j.neuroimage.2013.04.055. http://www.linkinghub.elsevier.com/retrieve/pii/S1053811913004023.
Nakagawa, T. T., et al. (2014). How delays matter in an oscillatory whole-brain spiking-neuron network model for MEG alpha-rhythms at rest. NeuroImage, 87, 383–394, 10.1016/j.neuroimage.2013.11.009. http://www.sciencedirect.com/science/article/pii/S1053811913011014.

[1] On various pdf readers, *Alt+left* or *Command+left* jumps back to the previous view
[2] The author is not affiliated with, nor responsible for any linked web content

Contents

1. Introduction

1.1. Idle minds - the brain at rest

When we say a person is at rest, we generally mean they are in a state of inactivity and motionless. While the description can be valid for a dead, a sleeping, or an awake person, the common point is the absence of activity, including concentration or effortful thought. However, while a person may be said to be thinking nothing in a colloquial way, the same is not true for a profounder conceptualization of cognition. Even without any external affordances, the brain is very much active and may come up with a wider variety of ideas and plans. That these are not limited to a productive or socially accepted framework is nicely illustrated by an old saying:

> "An idle brain is the devil's shop."[1]

That the brain is in fact also constantly active physiologically, producing a rich array of rhythms and patterns that change by its wakefulness state, became quickly clear from the first times electrical brain activity was recorded from 1875 onward by Caton, Berger, and others (Haas, 2003). From this, and the fact that brain metabolism is only minimally affected when comparing active concentration and rest (Sokoloff et al., 1955; Buckner & Vincent, 2007), we have known for a long time that the brain is never idle in the sense of 'inactive' or 'unused'. Nonetheless, it has only been increasingly appreciated over the last two decades how spontaneous brain activity is far from idle also in the senses of 'pur-

[1] (Bohn & Ray, 1855, p.106)

poseless', 'pointless' or 'vain', while many of its specific functions and mechanisms are just beginning to be understood.

Initial findings of spontaneous correlations of activity during wakeful rest (Biswal et al., 1995, 1997; Lowe et al., 1998; Xiong et al., 1999), and of a subset of brain regions consistently deactivated during tasks (Shulman et al., 1997), pioneered a shift in paradigm from studying the effect of external stimuli and affordances on brain activity to studying the internal dynamics themselves. The properties and interactions of these spontaneous ('intrinsic') activity patterns are being extensively studied today in a field somewhat unfortunately known as 'resting state research' (describing the state of the person, not the brain).

But where do these networks and their fluctuations and interactions in time originate, and what purpose do their spontaneous fluctuations serve? The current undertaking of large collaborative research efforts to map and model the brain at many scales, like the Human Connectome Project, the Human Brain Project and the BRAIN Initiative, express both the importance and complexity of the task at hand. They raise high hopes in deciphering the inner workings of our brain, and promise to provide us with a wealth of invaluable data and insights into brain network function. At the same time, care must be taken that we do not oversimplify and reduce ourselves to the structural connections in our brain, chanting: 'I am my connectome'.[2]

To understand the origin of resting state (RS) dynamics, one must combine the underlying structure, that is, the physical connection pathways between brain areas, with the dynamic activity patterns resulting from these mutual connections. As far as structure is concerned, advances in fiber-tracking, both by tract-tracing in animals (Stephan et al., 2001; Bakker et al., 2012; Bezgin et al., 2012), and by diffusion tensor/spectrum imaging (DTI/DSI) in humans (Wedeen et al., 2005; Sporns et al., 2005; Hagmann et al., 2010; Cammoun et al., 2012), have led to the identifica-

[2] http://www.ted.com/talks/sebastian_seung

tion of a structural core of human cortical connections (Hagmann et al., 2008), so that the connectome map is ever-increasing in detail (Cammoun et al., 2012; Daducci et al., 2012).

For investigating RS brain dynamics, functional connectivity and higher order statistics have been used. By its nature, spontaneous brain activity cannot be investigated by the classic subtraction paradigm of taking the mean difference of stimulus- or task-locked activation levels between two or more conditions. Therefore, connectivity measures such as correlations, phase synchronizations, mutual information, Granger causality and others that are independent of mean differences are commonly applied in RS research.

By now, we know that spontaneous brain activity is complex yet structured both in space and time, featuring slow fluctuations of correlated activity within groups of brain areas (so called resting state networks, RSNs). Slow (<.1 Hz) fluctuations were repeatedly found in resting state functional magnetic resonance imaging (rsfMRI) blood oxygenation level dependent (BOLD) signal (Biswal et al., 1995; Cordes et al., 2001; Fox & Raichle, 2007), and drive the large-scale connectivity patterns between different cortical areas. They have been linked both to alpha/beta power and gamma band activity (Becker et al., 2011; Scheeringa et al., 2012; Tagliazucchi et al., 2012b; Ritter et al., 2013; Neuner et al., 2014) in neurophysiological studies, and their detailed correspondence is a highly active field of investigation. Concerning the spatial structure of these fluctuations, several functional networks have been identified. Originally, a task-negative (or default mode network, DMN) and a task-positive network were found in fMRI BOLD and Positon Emission Tomography (PET) studies (Mazoyer et al., 2001; Raichle et al., 2001; Greicius et al., 2003; Fox et al., 2005). Subsequently, the existence of several functionally relevant RSNs has been corroborated by many studies both in fMRI (De Luca et al., 2006; Damoiseaux et al., 2006; Smith et al., 2009; van den Heuvel & Hulshoff Pol, 2010) and MEG/EEG (MEEG) (Laufs et al., 2003; Tagliazucchi et al., 2012b; Brookes et al., 2011c; Mantini

et al., 2007; de Pasquale et al., 2010). The variability in number (and exact composition) of components identified in different studies illustrate that they are somewhat variable in their compositions and not completely unconnected, so criteria to merge subnetworks may influence the results (Lee et al., 2012; Uddin et al., 2009; Buckner et al., 2008a). Even so, several core functional networks including the DMN, a dorsal attention network (DAN), a ventral attention network (VAN), a visual network (VN), a frontoparietal (FPN) and a somatosensory network (SMN) are robustly identified in most studies (even though there might be a methodological bias to extract certain *types* of networks, as discussed in Chapter 5).

A key question for investigating the internal dynamics of the brain and, ultimately, the way they shape our perceptions and cognition, is that of how the observed functional patterns originate from the underlying structural core of physical connections, and what mechanisms and network properties are important and characteristic for the human brain. To this end, it is convenient to view the brain as a complex network of connected units, which are subject of study of graph theory (which we will introduce in more detail in Section 1.3.2). As the brain is a complex system with many interacting brain areas, it is impractical to describe it in terms of all its objects and individual interactions. Instead, we want to describe the system in terms of its most important (statistical) properties, and identify the mechanisms and parameters shaping these properties. In this context, a network, or *graph*, comprises several objects, or *nodes* (here representing brain areas), connected by links, or *edges*. The brain has been shown to share similarities in key graph properties, such as being *small-world*,[3] with many other real world networks with complex structured patterns, such as neural networks, power grids, and social networks (Watts & Strogatz, 1998; Bullmore & Sporns, 2009; Van Steen, 2010; Stam & van Straaten, 2012). This may be partly due to spatial constraints of cortical wiring cost, but some graph properties, such as the high modularity

[3]Combining high modularity, i.e. more strongly intra- than interconnected groups of nodes, with short mean pathlength, meaning a low mean number of intermediate nodes that have to be passed to connect any two nodes of the network.

and strong s-core (Figure 1.1), suggest that the connectome layout follows specific functional aspects beyond metabolic considerations (Samu et al., 2014).

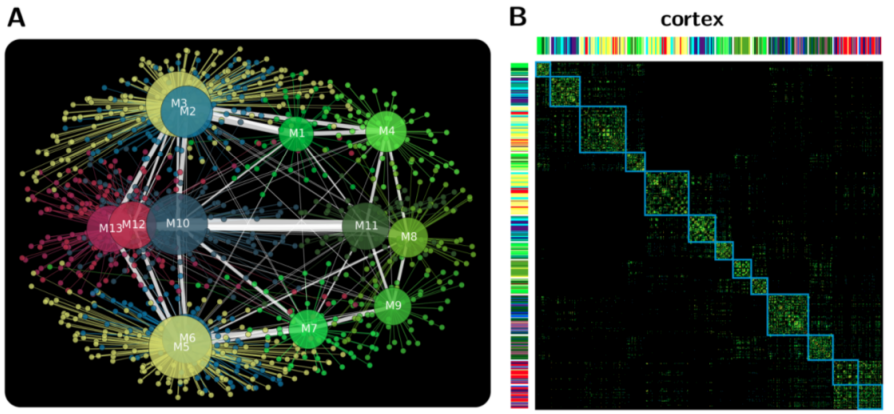

Figure 1.1: Graph representation of modules (large circles in A, blue squares in B) from high-resolution DSI imaging, which show high modularity and a stronger s-core when compared to surrogate graphs. Adapted from Samu et al. (2014), their Figure 5 A, B

1.2. From noise to networks - structure in spontaneous brain activity

1.2.1. A network of task-deactivating regions - a default brain mode?

In the tradition of behavioural experimentalists such as Galton, Donders, or Posner, controlled laboratory conditions and mean differences in response to experimental variations were the obvious tools of choice to

study brain function. For example, much of the two-streams hypothesis about functional specialization between action and perception in the visual stream (Goodale & Milner, 1992) was obtained by a subtraction paradigm based on differences in impairment for different tasks.

With the advent of fMRI in the 1990s, a safe, widely applicable way of measuring brain activation with high spatial resolution became available to scientists. Many important findings about the specific functions of brain areas were uncovered by comparing blockwise or event-related means between conditions, such as the existence of a brain area more responsive to faces than to other objects (Kanwisher et al., 1997). The subtraction paradigm states that brain areas involved in a task should be more active during that task than during a nonactive baseline or a control condition. To isolate functions, only the aspect of interest would be varied, so all changes in measured brain activity would either be connected to the variable of interest, or they would be noise and even out over many trials. However, Arieli et al. (1996) found that ongoing activity can predict single trial evoked responses in visual cat cortex. Shulman et al. (1997), looking at surprisingly reliable task-deactivations in a set of brain areas for a wide array of tasks, also rejected the idea that the baseline would be just noise. They suggested that increased activity found during passive conditions may reflect ongoing mental processes such as monitoring the environment, emotional states and spontaneous thoughts (conceptual processing, Binder et al., 1999). Others directly studied the baseline activity by itself, and found functional connectivity in brain areas such as the homologous motor cortices (Biswal et al., 1995, 1997; Lowe et al., 1998; Xiong et al., 1999). These studies, by embracing a new paradigm of studying functional connectivity in ongoing brain dynamics, triggered a wealth of studies and new perspectives on how to research the internal dynamics and networks of the brain.

The existence of a 'default mode network' (Greicius et al., 2003), a set of regions which deactivated during various tasks (Shulman et al., 1997), was quickly attested by different measures of brain activity: this network

had a higher-than-mean oxygen-extraction fraction during rest (Raichle et al., 2001), and showed correlated spontaneous BOLD activity (Greicius et al., 2003). Of the regions identified by Shulman et al. (1997) (see Table 1.1 and their Figure 1), Greicius et al. (2003) found all but two (right amygdala and left lateral inferior frontal cortex) to be correlated to PCC in their RS BOLD time series.

Table 1.1: *Task-deactivating regions found by Shulman (BA=Brodman Area)*

Region description	BA	Focus nr
posterior cingulate cortex / precuneus	31/7	1
inferior parietal cortex	40,39/19	2,3,4
left dorsolateral frontal cortex	8	5
left lateral inferior frontal cortex	10/47	11
left inferior temporal gyrus	20	13
medial frontal regions	8,9,10,32	6,7,8,9,10,12
right amygdala		14

In spite of slight differences in the involvement of some areas such as the amygdala or the hippocampus, they agree about the core regions of the default mode network: the posterior cingulate cortex (PCC), and medial prefrontal cortex (MPFC), with involvement also in medial and lateral (infero-) parietal cortex and ventral anterior cingulate cortex. Subsequent fMRI studies (Fox et al., 2005; Fransson, 2005) found the DMN to slowly (<.1 Hz) fluctuate in anticorrelation with another network of task-related/task-positive regions including intraparietal sulcus, dorsolateral PFC, (pre-)supplementary motor area, ventral anterior cingulate cortex (ACC), fusiform gyrus, and insula (see Figure 1.2).

Functionally, these later regions are known to be implicated in top-down

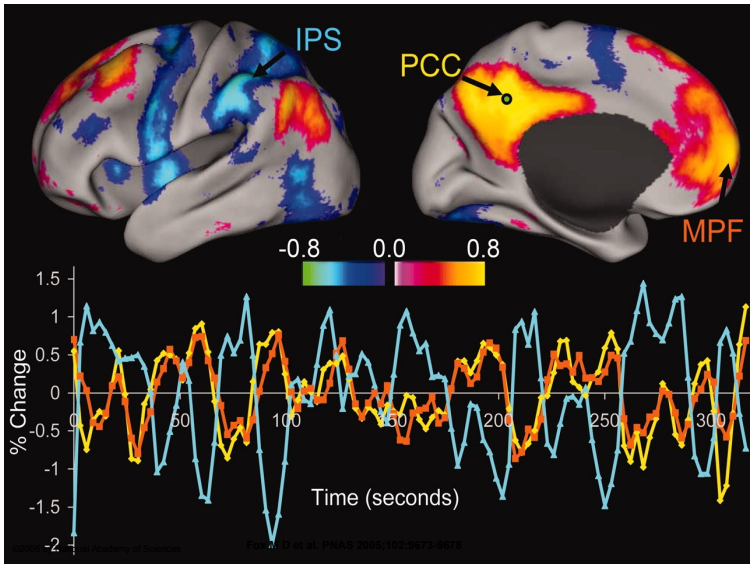

Figure 1.2: RS anticorrelations]*Slow, anticorrelated BOLD fluctuations between DMN regions (PCC, MPF) and IPS. Adapted from Fox et al. (2005), ©by PNAS*

attention (intraparietal sulcus, dorsolateral PFC: dorsal attention network, DAN) (Corbetta & Shulman, 2002), saliency and awareness (insula) (Craig, 2002, 2009), and a wide array of motor and cognitive tasks in general (Cabeza & Nyberg, 2000).

The DMN areas, on the other hand, are implicated in episodic memory (Desgranges et al., 1998; Cabeza et al., 2002), information retrieval (Desgranges et al., 1998; Cabeza et al., 2002; Maguire & Mummery, 1999), and conceptual processing. Binder et al. (1999); Greicius et al. (2003) also proposed integrative connections between these networks in IFC and MPFC, as they overlap in the region of interest (ROI) maps of both PCC (DMN) and ventral ACC (DAN).

Although physiological noise has been shown to importantly contribute to slow BOLD fluctuations (Wise et al., 2004; Birn et al., 2006; Birn,

2012), and the interpretability and the conceptual usefulness of a default mode has been disputed (Morcom & Fletcher, 2007), the slow functional connectivity patterns at rest remain after considering physiological noise (Birn, 2012; Damoiseaux et al., 2006). Another critique of the task-positive/task-negative dichotomy was based on the fact that the global signal regression used in previous studies (Greicius et al., 2003; Fox et al., 2005; Fransson, 2005) may introduce artifactual anticorrelations into the voxel time-series (Buckner et al., 2008a; Murphy et al., 2009). However, different analyses circumventing or correcting for global signal regression have confirmed a connectivity bipartition distinguishing the DMN and a task-positive network (Fransson, 2005; Golland et al., 2008; Fox et al., 2009).

Yet another approach to avoid the use of ROI analysis and global signal regression suggested that spontaneous brain activity is not separable in just two, but several different functional networks.

1.2.2. Resting State Networks

Damoiseaux et al. (2006) utilized a tensor probabilistic ICA (PICA) approach (Beckmann et al., 2005; Beckmann & Smith, 2005) to better quantify distinct RS patterns and to separate such effects from artifacts such as respiratory or cardiac cycles. Though not ultimately asserting a neural origin, they found nine consistent RS components in two datasets, describing similar activation maps as in earlier studies (De Luca et al., 2006; Fox et al., 2005), and known functional implications: an occipital lateral visual network (VN), the DMN, two lateralized parietofrontal 'memory' networks consistent with the Dorsal Attention Network (DAN), a medial VN, a somatosensory network centered around the central sulcus, a ventral stream network including superior temporal with some cingulate and frontal involvement, a network of mainly superior parietal areas, with some occipitotemporal and precentral involvement, an auditory network (AN) consistent of superior temporal, postcentral and insular cortex. An-

other component resembles part of the DMN in one, and a frontopolar network in the other dataset.

Several fMRI ICA studies have corroborated that several RSN (e.g. Beckmann et al., 2005; De Luca et al., 2006; Chen et al., 2008; Biswal et al., 2010) with similar functional interpretations can be distinguished. The difference in number of components is mainly due to the amount of components chosen for extraction, so lateral and medial visual areas may be included in one (De Luca et al., 2006) or in two separate (Damoiseaux et al., 2006) components. While this may seem somewhat arbitrary, one has to take into consideration that apart from data variability, preprocessing and parcellation effects as well as prewhitening and artifact component rejection, none of these networks are completely segregated. Therefore, there is no absolute ground truth in how many components the brain consists of, and our answer concerning how many components there are will depend on how we ask the question: different compositions may for example be incorporated and set in relation to each other, e.g. by hierarchical clustering (Doucet et al., 2011; Cordes et al., 2002; Zhou et al., 2006). Importantly, cumulative evidence from fMRI ROI and ICA as well as from electrophysiological studies (detailed below), indicates that RSNs are indeed reliable, robust, distinguishable entities. Across studies, these networks can be identified with qualitatively similar shapes and conceivable functional significance, and across modalities and analysis measures. Their most appropriate representation is a field of active research, and as new methods become available, the possible biases of decompositions such as the 'spatial independence' constraint typically used in RS ICA can be tackled (Smith et al., 2012). In Chapter 5, we will present a datadriven, maximally unbiased approach of how to decompose threedimensional brain data into components with minimal assumptions on data structure.

1.2.3. Electrophysiological evidence

While EEG has been used to study brain oscillations in wakeful rest long before the emergence of fMRI (Berger, 1929), today's large interest in the internal dynamics and functional networks of the brain were triggered by several fMRI studies (Shulman et al., 1997; Greicius et al., 2003; Fox et al., 2005; Damoiseaux et al., 2006). Due to its excellent spatial resolution, fMRI can be used to map slow activity changes, and in rsfMRI, functional connectivity between voxels and areas. These properties predisposed fMRI for the detection of functional connectivity in slow dynamics of RS brain signals. However, besides its limitation to capturing only slow processes (< ~1-2 Hz), rsfMRI suffers from the setback that it does not directly measure neural activity. Initially, it was unclear whether the RSNs found, while reliable, were actually of neural origin, and if so, how they related to neural dynamics. Since then, EEG studies, while by themselves suffering from low spatial resolution and source leakage, have confirmed the existence of several RSNs both by using spatial priors gained from fMRI research and from independently obtained decompositions. Within the last decade, electrophysiological studies have refined and extended the characterization of functionally significant RSNs. Studying important frequencies and oscillatory dynamics, these studies, whose main results we summarize here, importantly complement the understanding that we gained from fMRI about internal brain dynamics.

What causes the slow BOLD fMRI oscillations so robustly appearing in RS recordings? While the question of large-scale functional connectivity between delineated areas has not been a primary focus in EEG research, the existence and modulations of different brain oscillations during different consciousness states has always been of interest to researchers. The alpha rhythm has been linked to spontaneous brain activity since Berger (1929). While its origins, discussed in more detail in Chapter 4, are still not understood in detail, spike-frequency adaptation (SFA) and a feedback-loop between cortex and thalamus are considered the main generators. Accordingly, thalamus and alpha activity may be related pos-

itively (Gonçalves et al., 2006; Feige et al., 2005). Alpha power, along with beta (Tagliazucchi et al., 2012b), was later shown to relate to lower cortical BOLD activity (Robinson et al., 2001; Goldman et al., 2002; Gonçalves et al., 2006; Tagliazucchi et al., 2012b; Sato et al., 2010) and decreased connectivity, implying stronger inhibition (Scheeringa et al., 2012). Alpha suppression can hence be regarded as a landmark of cortical activation (Tagliazucchi et al., 2012b), and accordingly, alpha increases upon closing the eyes (Yang et al., 2010; Barry et al., 2007). Concerning lower consciousness states, sleep and unconsciousness, as well as meditation, have been associated with slower delta/theta rhythms and more local connectivity (Larson-Prior et al., 2011; Lehmann et al., 2012).

Accordingly, recent research using conjoint EEG/fMRI also (negatively) related ICA-derived RSN mainly to alpha and beta-band activity (Mantini et al., 2007; Jann et al., 2010), although a more complex picture emerges over studies: Jann et al. (2010) find fMRI related decreases in alpha and beta in sensory networks when compared to lower frequencies (limiting their study to <=30 Hz). Mantini et al. (2007) find VN and AN also in low frequencies, as well as a frontopolar, 'self-referential' network mainly in the gamma band. Within alpha and beta, the SMN has been associated more with beta and the VN more with alpha activity, but connectivity overlaps borders between frequency bands and does not allow for clean-cut, exclusive distinctions (Mantini et al., 2007). Newer studies complicate the picture even more, in that DMN BOLD activity may be related to alpha in eyes open, but not in eyes closed condition (Mo et al., 2013), and that different nodes of the DMN may relate to different frequency bands (PCC/precuneus - beta; parahippocampus - delta), highlighting different functional involvement (Neuner et al., 2014). These are only a few examples in an actively evolving field, illustrating that the decomposition and functional role of different areas and frequency bands together is an important current research question. In Chapter 5, we will present a datadriven time-space-frequency decomposition with minimal assumptions and discuss network decomposition methods in greater detail.

Similarly to EEG, RS networks have recently also been investigated with MEG technology. MEG is related to neural discharges as well as EEG, but differs due to the different properties of propagation of electric and magnetic fields. As MEG is only sensitive to tangential signal components, it mainly picks up signals from sulci, while at the same time signal loss due to distance from the skull is higher than for EEG. This results in a more limited, yet less distorted and better localizable signal for cortical sources at a high temporal resolution. In relation to the early work in EEG described above, Nikouline et al. (2001) found slow, correlating amplitude fluctuations (<.1 Hz) between the two hemispheres as well as near-zero lag phase synchronization for spontaneous beta-band oscillations. As the study was limited to interhemispheric comparison, the magnetic fields showed little overlap and source leakage is not a major concern (along with the somewhat continuous phase-lag pattern, showing significant phase locking also at nonzero phase lags). Liu et al. (2010) confirmed slow (<.1 Hz) interhemispheric power modulations after ICA-based artifact rejection in the beta band. While also found in alpha and gamma bands, the latter showed a sharp spatial decrease, suggesting slow oscillations to dominate slow global brain dynamics. de Pasquale et al. (2010) conducted a network study of the DMN and DAN, deriving seed-based internodal coherence maps from windows of maximal correlations in the data. They find expression of transient formation of these RSNs in the slow modulation of theta, alpha, and beta power, and stress the nonstationarity of the signal, as short periods of high correlations (tens of milliseconds) alternate with periods of low correlations (hundreds of milliseconds). Shortly after, Brookes et al. (2011a) demonstrated good agreement between rsfMRI and source-reconstructed MEG, and independently replicated eight RSN from bandpass filtered power envelopes in the alpha (DMN) and beta bands which closely resemble fMRI derived RSNs (Figure 1.3, Brookes et al., 2011c).

Even though the beamforming algorithm, which suppresses spatially separate but temporally correlated sources, minimizes crosstalk, some source-leakage could have affected the analysis due to correlated beam-

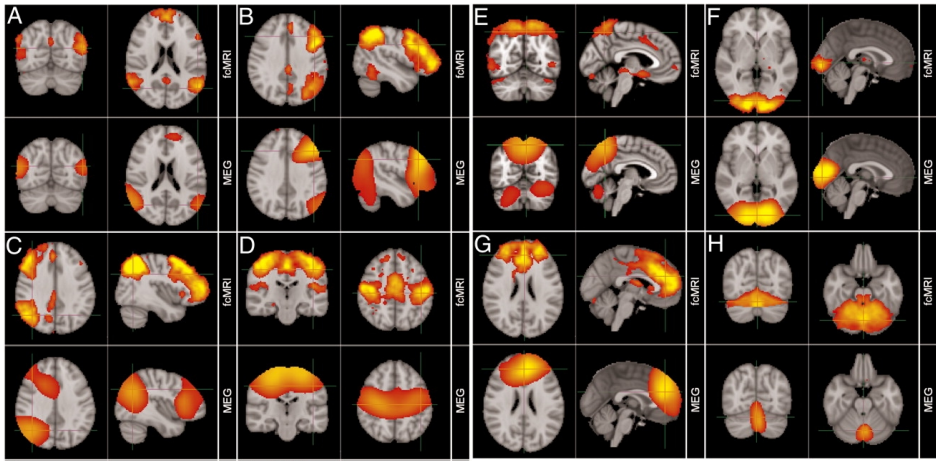

Figure 1.3: RSNs found by ICA](*spatial) fcMRI (first and third row) and corrseponding (temporal) MEG Independent Components (second and fourth row) of RSNs; DMN (A) in alpha, all others in beta band. Adapted from Brookes et al. (2011c), ©by PNAS

former weights (Brookes et al., 2012). Notwithstanding, the similarity to networks derived from functional connectivity MRI (fcMRI) demonstrates the robustness of RSNs, and localization in envelope carrier-frequency in the alpha and beta bands is in line with earlier findings on RS oscillations but with an additional topographic component. Using a source-leakage correction method by subtracting pairwise common linear signal components between reconstructed sources, Hipp et al. (2012) found functional connectivity in alpha and beta band power envelopes with a peak around 16 Hz and highest global connectivity at that frequency for the regions LPC, MPFC, DPFC and MT+ in parietal cortex, which formed an interconnected network combining DMN and a frontoparietal control network (FPN, Vincent et al., 2008). In contrast to fMRI, posterior midline areas were not identified either by Hipp et al. or Brookes et al. (2011c) as part of the network, which may be affected by the MEG signal drop with increasing distance from the cortical surface.

Using mutual information (MI) on bandlimited MEG signal between areas of distances > 40 mm to avoid source leakage, Jin et al. (2013) found network hubs in left superior frontal and middle temporal gyrus, as well as posterior cingulate cortices in frequency bands from theta to gamma, and medial cingulate cortex in gamma only. Other measures to improve signal detection (Hall et al., 2013) or to measure leakage-corrected (nonzero lag), phase-related functional connectiviy have since been proposed, such as a multivariate interaction measure (MIM) (Ewald et al., 2012) and the phase lag index PLI (Hillebrand et al., 2012). The latter found frequency-dependent phase connectivity patterns closely related to relative source power (except for gamma), with connectivity hubs in occipitoparietal and superior temporal areas for alpha, sensorimotor cortex for beta, and more widespread connectivity for gamma PLI across temporal, sensorimotor, inferior parietal and inferior cortices. Marzetti et al. (2013) found phase-shifted MIM interactions between homologous DAN areas in delta and alpha, and alpha and beta connectivity with DAN for visual and somatosensory regions, respectively. Due to the methodological difficulties and the lack of understanding of the mechanisms driving spontaneous brain dynamics, it is yet too early to draw final conclusions. However, the uncovering of phase relations is another essential piece of the puzzle, complementing the aspects already illuminated by other neuroimaging and neurophysiological techniques (Palva & Palva, 2012).

As we have seen, evidence from fMRI and neurophysiology alike point to the existence of slowly fluctuating, interacting but distinguishable functional networks that are related to bandlimited power and phase relationships mostly in the alpha and beta bands in quiet rest. The core connectivities remain identifiable, but connectivity is affected both by changes in states of consciousness (e.g. sleep, meditation) and neurological and psychiatric diseases. To quantify connectivities and changes, and bring together all the puzzle pieces from different studies, a framework of the brain as a complex graph, a network of networks, has emerged. Graph Theory, namely, the study of complex systems and their abstract representations as graphs composed of nodes (objects) linked by edges (connec-

tions), provides us the tools to quantify and systematically compare network statistics and properties. In the following section, we will embrace a network theory perspective, departing for now from brain dynamics in favor of a structural description and the structural layout of the brain's pathways. This perspective will be reintegrated with the so far presented findings in Section 2.3, where we introduce computational models of the resting state to model spontaneous brain activity as a result of local neuronal dynamics, driven by and driving their surrounding network.

1.3. Measuring brain connectivity

1.3.1. Fiber tracking: Diffusion imaging

Up until the 21st century, neural fiber tracts were mainly mapped invasively through staining techniques such as with horseradish peroxidase (van der Want et al., 1997). In a large effort, the collation of connectivity data on the macaque brain (*CoCoMac*) has been implemented to create a large-scale, comprehensive primate brain connectivity database (Stephan et al., 2001; Kötter, 2004), which is still in constant progress in a second edition (Bakker et al., 2012). The same approach has not been pursued in the human brain, but technological improvements in the tracing of water diffusion by diffusion tensor imaging DTI (Basser et al., 1994; Le Bihan et al., 1986; Le Bihan, 2014) and diffusion spectrum / diffusion weighted imaging DSI/DWI (Wedeen et al., 2005; Huisman, 2003). These techniques have made it possible to make neural fiber tracts traceable noninvasively by means of the inhomogeneities they cause in the diffusion tensors of water molecules in the brain. While still limited in accuracy, the development of DSI has made it possible to distinguish several crossing fibers within a single voxel of ~3mm size given sufficient directional difference between them. Over the last years, the increasingly anticipated 'human connectome' (Sporns et al., 2005), a global map of connections between

brain areas, has been mapped for the human brain, and is ever-increasing in detail thanks to advancing technology (Cammoun et al., 2012; Daducci et al., 2012). Figure 1.4 shows how parcellation at different spatial scales, combined with DSI tractography, leads to the construction of connectivity matrices of different sizes. As the brain is not completely segregated into structural modules, however, the choice of parcellation into brain areas is nontrivial, and affects the distribution and strength of connections. For a long time, the gold standard to describe brain areas were the cytoarchitectonic maps of Brodmann (Brodmann, 1909; Brodmann & Gary, 2006). However, functional and structural borders do not always coincide, and cytoarchitectonic borders may not readily be identifiable on imaging datasets. Other parcellations with varying numbers of nodes and delineation criteria (e.g. anatomical, cyto-, myeloarchitectonic) have been developed over the years, such as the 90 node automatic anatomical labeling atlas (AAL, Tzourio-Mazoyer et al., 2002) and the Talairach Atlas (Lancaster et al., 2000) (for a recent review, see Craddock et al., 2013).

Once having chosen a parcelleation, one can construct connectivity maps. These matrices typically result from summing all fibers between each pair of nodes and hold a connectivity strength in the sense of the cumulative thickness of fibers connecting two brain areas, but distance matrices considering the Euclidean distance or fiber length can also be constructed. Due to the inability of DSI to identify fiber directionality, connectivity matrices are symmetrical in their raw form, although they may lose symmetry due to normalization of connections by brain area size. This is an important point, as directed and undirected graphs may have different properties and information flow (Woodman & Jirsa, 2013), and further research is needed to determine in detail the extent of reciprocity of connections and the tightness of the link between fiber thickness and signaling strength. However, combined DSI and autoradiography found bidirectionality of all studied long association pathways in the monkey brain (Schmahmann et al., 2007), making a symmetric approximation appear reasonable. All in all, the developments over the last decade, that have

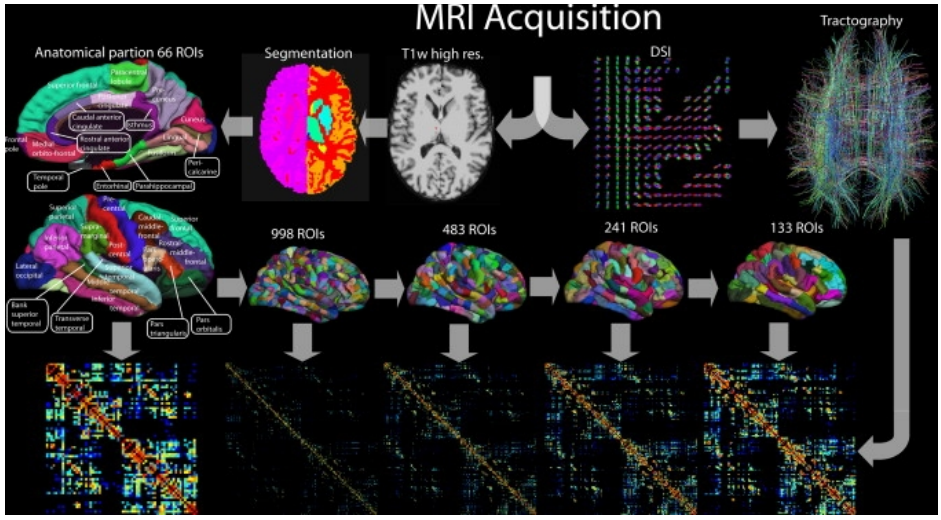

Figure 1.4: DTI

]*Construction of normalized connection matrices at different scales from structural MRI, brain parcellation, and DSI tractography. Adapted from Cammoun et al. (2012), ©Elsevier.*

been providing us with whole brain, high-resolution connectivity maps, are an invaluable asset for the study of cerebral networks and interactions, and crucial for developing models of internal brain dynamics.

1.3.2. Graph Theory - measuring graphs

One important question that arises with the ability to trace fiber connections in the brain globally is that of how to represent and analyze them. The study of networks of connected objects (nodes) is the subject of Graph Theory, which has been popular in social science for a long time and provides tools for describing, classifying and comparing different graphs and their properties. In a graph, nodes connected by links (edges) are said to be neighbors. The *path length L(p)* is the average of

the number of edges in the shortest path between to nodes. The *clustering coefficient C* is the average fraction of all possible connections between the neighbors of a node, for all nodes. Many different graph properties can be computed, both for the network as a whole, and for each node locally, such as *node degree* (the number of direct connections of a node) or its *centrality* (the fractions of all shortest paths in the network which include the node), as illustrated in Figure 1.5. Different elemental connectivity patterns between 3 or more nodes such as *triangles* are called *motifs* and their arrangements and combination into connected *modules* determine the larger graph's shape and properties. High centrality nodes are called *connector hubs* if they reside between, or *local hubs*, if they lie within a densely interconnected module of nodes. For a more in-depth review on graph theory measures and applications in neuroscience, see Rubinov & Sporns (2010).

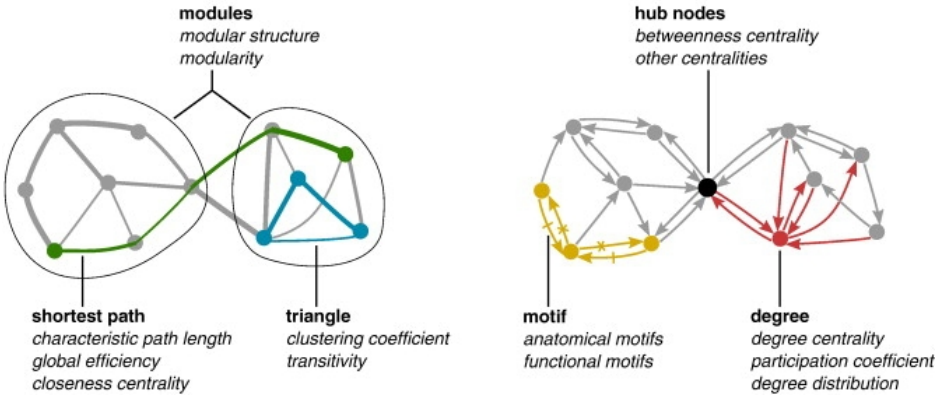

Figure 1.5: *Basic Network measures as explained in the text, adapted from Rubinov & Sporns (2010), ©Elsevier Publishing Group*

In a seminal paper, Watts & Strogatz (1998) demonstrated a basic model for networks that, while very different in size and nature, share an interesting property: The western U.S. power grid, a collaboration graph for movie actors, and the neural connectome of the worm *C. elegans* were all *small-world* (Milgram, 1967; Travers & Milgram, 1969) networks com-

bining short path lengths and high clustering coefficients. This means that, on average, all other nodes can be reached from a given node by far fewer steps than this would be the case on a regular graph or a random graph (see Figure 1.6).

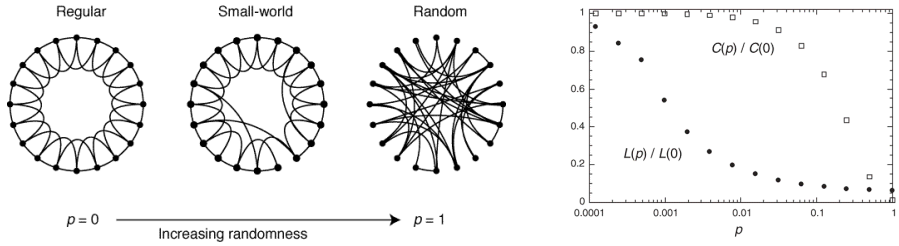

Figure 1.6: *Left: example for graphs with increasingly random connections through rewiring. Right: small-world networks combine short mean path lengths L with a high clustering coefficient C. Adapted from Figures 1 (left) and 2 (right) of Watts & Strogatz (1998), ©Nature Publishing Group.*

In studying simple model dynamics in different systems, Watts & Strogatz (1998) found that in small-world networks, coupled phase oscillators readily synchronize. Their speculation that this may be relevant to neural synchronization, and the brain may have a small-world architecture, foreboded both the now widely accepted small-world structure of brain connectivity and the usefulness of oscillator nodes to study its dynamics in computational large-scale models, which we will introduce in Section 2.3.

In 2007, Iturria-Medina et al. (2007) presented a DWI proof of concept and brain connectivity maps with respect to strength, density, and probability. Hagmann et al. (2007) used DSI to similarly construct a whole-brain connectivity graph, and confirmed the small-world structure of the brain, combining shorter path-lengths and higher clustering than surrogate graphs with the same degree-distribution as the DSI-derived network. With these techniques, the known structural connectivity of occipital areas was replicated, and a highly connected 'structural core' on the brain graph was identified (Hagmann et al., 2008), consisting mostly of high de-

gree, strength, efficiency, and centrality nodes in posterior medial cortex (precuneus, paracentral lobule, posterior cingulate, superior and inferior parietal cortex as well as cuneus, pericalcarine and superior temporal areas). Nijhuis et al. (2013) confirmed many of these areas to be connector hubs (combining high degree with betweenness centrality) and is in line with network analysis of macaque and cat cortices (Sporns et al., 2007). The important role of network hubs in human brain function and dysfunction has become a major focus of cognitive neuroscience, and while graph analyses have helped identify key structural and functional patterns of brain organization, the influences of data preprocessing, connectivity measure and model choices pose important new challenges for the use and interpretations of network approaches (Sporns, 2014; van den Heuvel & Sporns, 2013). For example, while DSI technology gives us a formerly unknown resolution of anatomical fiber tracts, one has to keep in mind that there is only information about fiber thickness and density, and not about directionality or synaptic efficacy. Also, due to the brain's inherent multiscale connectivity, resulting connection patterns will depend on the spatial scale and normalization (or lack thereof) of fiber strengths by brain area surface and parcellation size. This, and the fact that smaller fibers may either be missed or misspecified (giving rise to connectivity probability maps additionally to weight maps), are a few of the factors profoundly affecting graph properties. In spite of these limitations, advanced fiber imaging has provided a consistent map of a highly structured connectivity architecture of human cortex, with strongly connected hubs and functional modules, which are in line with many functional connectivity patterns and modules identified in functional or combined studies.

1.3.3. Functional Connectivity

But what is the precise relationship between large scale structural and functional connectivity in the human brain? This is much more difficult to answer, as functional connectivity is a multi-faceted ('elusive' - Horwitz, 2003) concept (Rogers et al., 2007), and may vary both with

connectivity measures (based on phases, bivariate or multivariate correlations, coherency or mutual information) and time scales (frequency bands, time windows) considered. This higher dimensionality of FC shows that there is no single correct answer on the relation between FC and SC, but may also slightly vary with scale and connectivity measure applied. Seed-based correlational MRI analysis first led to the discovery of spontaneous coactivations and the existence of distinguishable networks in the motor cortex (Biswal et al., 1995), and later in task-related (e.g. IPS) and task-negative (often PCC and MPFC) networks (Corbetta & Shulman, 2002; Greicius et al., 2003; Fransson, 2005; Fox et al., 2005). Due to its time resolution, capturing slow brain dynamics, correlations were successfully used to measure FC, in spite of methodological concerns.

One main point of controversy was whether routinely performed global signal regression (removal of BOLD fluctuations co-occurring in the whole brain) is a necessary preprocessing step or artifactual itself, introducing artificial anticorrelations (Fox et al., 2005; Buckner et al., 2008a; Honey et al., 2009; Murphy et al., 2009). By comparison between analysis methods, though, Fox et al. (2009) resumed that, while global signal regression does mathematically introduce anticorrelations and global signal distributions must especially be considered in group comparison studies, the global signal is not strongly localized to the task-positive or task-negative networks. Instead, this signal is indeed rather spatially global and linked to physiological artifacts, so that after regression, FC better matches SC, and thalamocortical activity is more consistent with previous findings. Also, anticorrealtions can be found even without global signal regression, so that the authors conclude that, while the influence of the procedure must be considered and studied carefully, global signal regression may improve FC estimation and is not primarily artifactual.

Extension of the seed-based analysis over all ROIs yields a symmetrical correlation matrix indexing correlations/coherence for all brain area pairs, which can be used to describe the system, build functional graphs, and compare FC and SC on a system level. Studies concerned with these

aspects have consistently shown the existence of RSNs, specifically the DMN (e.g by cluster analysis, van den Heuvel et al., 2008), as outlined in Section 1.2.1.

However, correlational analysis is limited in different ways: Correlations are by nature hypothesis driven, and when computed on pairs of voxels, many significance tests have to be performed to get statistically meaningful activation maps. Artifacts introducing global correlations have to be corrected beforehand, but spurious correlations often remain. ICA was soon proposed as an alternative to overcome these limitations (see Section 1.2.2), as it allows for simultaneous decomposition of the signal into maximally independent components, and artifact rejection and coactivation maps are computed in a single analysis step. After performing a PCA to reduce the data dimensionality to K (a process termed prewhitening), an eigenvalue-decomposition is performed on the data that extracts maximally independent components while maximizing the variance of the data explained by these components. As ICA needs manifold more datapoints than components, and fMRI typically delivers many spatial but few temporal datapoints, spatially independent components have been predominant (Kiviniemi et al., 2003; Beckmann & Smith, 2004; Damoiseaux et al., 2006; De Luca et al., 2006), while EEG/MEG studies typically extract temporally independent signal components (Brookes et al., 2011c; Mantini et al., 2007; Yuan et al., 2012). In both cases, the data is represented as a combination of K independent components (IC), and each original data channel $x_n(t) = 1, ..., N$ (voxels, sources or sensors) is assigned a coefficient c_k on each of the components, so that

$$x_n(t) = c_{n,1} * IC(t)_1 + ... + c_{n,K} * IC(t)_K. \tag{1.1}$$

Artifactual components are typically identified and rejected manually, and the number of extracted components is also chosen by hand, so that the technique is not completely datadriven and both ICA and correlational analyses should be regarded as complementary (De Luca et al., 2006). As treated in more detail in Chapter 5, another important question is whether

independence is an optimal constraint for data decomposition, and higher dimension generalizations of ICA and PCA are further discussed. So while the existence and identifiability of various RSNs with functional importance has been robust over data recording and analysis methodology, their detailed characterization and interactions in time are a matter of active research. Considering the correspondence of SC and FC, though, studies also highlight that connectivity patterns change with frequency (Salvador et al., 2005) and that the overall concordance of functional and structural links is only part of the picture (Skudlarski et al., 2008). Overall, structurally stronger connected nodes are also functionally strongly connected, while this relation decreases for weaker anatomical connections. In fact, functional connections are commonly observed in the absence of direct structural links (Honey et al., 2009), raising interest in the question of how the collective brain network gives rise to functional interactions more complex than what is explainable purely by direct physical links between nodes. Another question is how changes in anatomical connectivity, e.g. through learning, injury, aging, or disease, directly affect functional connectivity and how symptoms may give us insight into the structure-function relationship in the brain. On the other hand, new diagnostic and treatment opportunities are likely to arise if the key implicated network communications and pathways can be identified.

1.3.4. Connectivity alterations in diseases

Brain connectivity is implicated in a wide range of neuropsychological diseases, and in the last years a wealth of studies has been published on the subject. As each disease is its own field of study, a comprehensive overview is out of the scope of this thesis. We will give an overview and explore the effects of SC changes on brain dynamics and FC in Chapter 3 in the context of aging. To give an impression of the importance of connectivity changes in many conditions, we here recapture some key findings on altered SC and FC in mental illness, whereby SC alterations are so far better corroborated (see also review by Griffa et al., 2013). The

investigation of many conditions regarding their functional connectivity both in task and at rest is a highly active field of research.

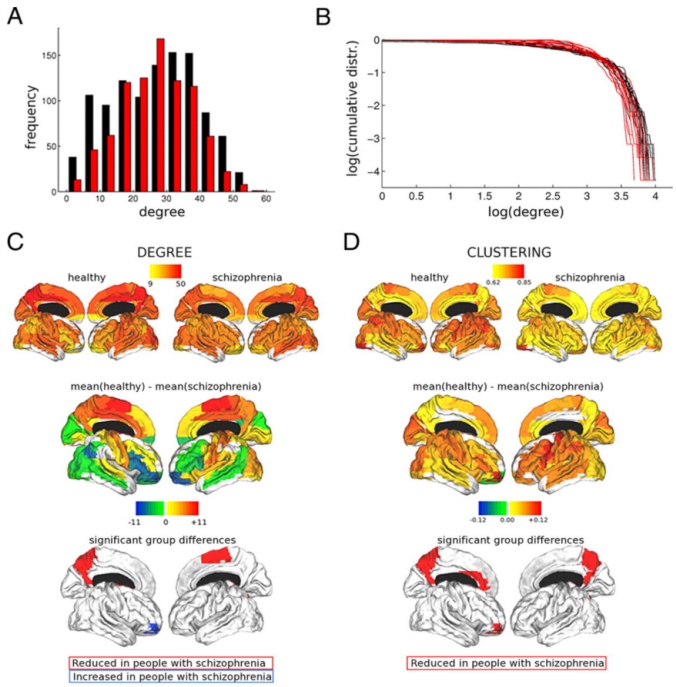

Figure 1.7: *Group differences in topological properties of brain functional networks: Lower probabilities for high-degree network hubs (A,B - red lines), and differences in clustering and degree distribution over the cortex (C,D) are apparent in schizophrenia patients when compared to healthy controls. Adapted from (Lynall et al., 2010, their Figure 4), ©Society for Neuroscience.*

Griffa et al. (2013) categorize three global dimensions of structural changes: changes in integration, segregation, and architecture. In a graph theoretical context, both segregation and integration capacity are related to small-worldness, which combines both so that information travels quickly due to short mean path lengths (high integration capacity), while local processing is supported by strong clustering and local efficiency (segregation). Although small-worldness, a robust macro-scale

property of the brain, is typically preserved, the integration/segregation ratio, clustering and degree-distribution (Figure 1.7) are often altered.

For Alzheimer's Disease patients, Griffa et al. (2013) report increased characteristic path length and clustering coefficients. The correlation with cognitive decline both in AD and normal aging (see also Section 3), supports the hypothesis that decreasing long range connectivity (especially interhemispheric) supports the symptoms. This is reflected in decreases in functional connectivity, which increasingly affect all systems with ongoing disease progression (Greicius et al., 2004; Zhou et al., 2010; Damoiseaux et al., 2012; Supekar et al., 2008).

Schizophrenia has long been viewed as a disconnection disorder (Friston, 1998), and though connection alterations are complex and widespread, a trend towards higher path lengths and clustering coefficients, together with decreased local efficiency of various brain regions, supports the disconnection hypothesis. However, symptoms and pathology lack homogeneity at the macro-level, and alterations may be specific to certain sub-systems, or rather subtle global configuration alterations difficult to pinpoint to specific areas (Liang et al., 2006; Liu et al., 2008; Lynall et al., 2010; Salomon et al., 2011). In MS, besides grey matter losses, widespread white matter losses affected both long-range and short-range efficiency in various functional subsystems including the cerebellum (Dogonowski et al., 2013), leading to decrease in network efficiency, (Bonavita et al., 2011; Lowe et al., 2008; Roosendaal et al., 2010). In temporal lobe epilepsy, cortical thickness correlation analysis (Bernhardt et al., 2011) showed symptom-progression related network disruptions in the form of increased path length, clustering coefficient, and a relative accentuation of paralimbic and temporal hubs when compared to healthy controls. Results vary for different types of epilepsy, and the amount of studies is rapidly increasing, although it is still difficult to ascertain general findings from the limited amount of data (see Griffa et al., 2013). Recent FC studies on Depression have also found hyperconnectivity in an introspective socioaffective network (ISA, Schilbach et al., 2014), along

with DMN and others (Zeng et al., 2012). While this is not an exhaustive list of examples for findings of altered connectivity in diseases, reliable data is still outstanding for confident clinical application. This is a highly active and promising field of potentially useful applications of RS and brain connectivity recordings (Fox & Greicius, 2010), and many advances can be expected in the understanding of how certain network alterations lead to specific symptoms of a disease and how they are connected. For some disorders, group-based distinctions are already possible (Burklund & Lieberman, 2012), and clinical applications are foreseeable in the future. Combined with tasks or stimulus presentation, otherwise badly distinguishable groups such as recovered Major Depression patients could be better identified with this method. Yet, to ultimately understand why certain connectivity alterations lead to specific symptoms, we also need to understand in more depth the basic principles of the healthy brain as a complex, dynamic, and plastic self-organizing system, and how its network structure and dynamics are connected to specific functions on the one hand, and interrelate on the other hand.

1.3.5. Conclusions - a complex network perspective

A complex-network view was already voiced twenty years ago (Tononi et al., 1994; Haken, 1996), and inspired by first connectivity datasets, a graph theoretical approach to studying the human brain took its course and is still growing (recounted by Sporns, 2012). The complex network perspective defines a new era after a large gap from blackbox and purely modular models of the brain, as well as following behavioralism and cognitivism, and has superseded pioneering but more unidirectional and mechanic functional processing models such as the two visual processing streams of Mishkin & Ungerleider (1982); Goodale & Milner (1992) by emphasizing dynamic and multidirectional self-organizing principles and emergent properties. These properties are being intensively studied in a quest to fundamentally understand how brain function, and with it cognition, emerges, develops, and adapts to external and internal stimuli and

contingencies without an external, teleological module. There is now accumulating evidence suggesting that the brain is small-world in structure and functional states, consisting of interacting, hierarchical (Stam & van Straaten, 2012) modules forming networks (Sporns, 2013), and that this network of networks shows critical or scale-free/fractal dynamics (Reijneveld et al., 2007; Bullmore et al., 2009). However, many of the details and extents of how these properties emerge from the architecture and physiological processes are still very blurry. Here, computational models have successfully been used to demonstrate the emergence of certain properties such as critical dynamics from certain structures such as simulated brain networks, and the changes and deterioration that can be induced by structural changes (Deco et al., 2013a).

Therefore, in the following, we will turn to the question of how complex RS patterns arise from the structural core and dynamics of the brain. We will explore computational models and their attempts at explaining and predicting many empirical findings by creating and manipulating complex, self-organizing networks as virtual brains, with different states and dynamics.

In the following Chapter, we briefly recapture the rationale behind computational modeling of large-scale resting state networks, and present then the fundamental paradigm of how SC and local dynamics are combined to create simulated brain dynamics with the example of a spiking-neuron network. We then exemplarily study changes in dynamics caused by structural changes in aging, before giving a comparative overview over computational models of different complexity and behaviors in Section 2.3.

2. From structure to function - large scale models of the resting state

In the last years, a wealth of network models has been developed by integrating computational models of neural population activity with structural empirical data on the brains' connectivity pathways. In the following chapter, we introduce the rationale and implementation of large-scale computational models for RS activity in the brain or cortex as a whole. The chapter reproduces part of a paper with the title "Bottom up modeling of the connectome: linking structure and function in the resting brain and their changes in aging". The work was published in NeuroImage (NeuroImage 87 (2013) 15 318-329, http://dx.doi.org/10.1016/j.neuroimage.2013.04.055) by Nakagawa T. T., Jirsa V. K., Spiegler A., McIntosh A. R., and Deco G. The text underwent minor formatting and structural (e.g. figure counts) changes to better integrate into the thesis format.

For comprehensiveness, a description of different dynamical models are included that, except for the spiking model description, do not form part of the published paper in Section 2.3. The application of such a model for aging, also included in the paper listed above, is given in Chapter 3.

The abstract of the paper reads:

> With the increasing availability of advanced imaging technologies, we are entering a new era of neuroscience. Detailed descriptions of the complex brain network enable us to map out a structural connectome, characterize it with graph the-

oretical methods, and compare it to the functional networks with increasing detail. To link these two aspects and understand how dynamics and structure interact to form functional brain networks in task and in the resting state, we use theoretical models. The advantage of using theoretical models is that by recreating functional connectivity and time series explicitly from structure and predefined dynamics, we can extract critical mechanisms by linking structure and function in ways not directly accessible in the real brain. Recently, resting state models with varying local dynamics have reproduced empirical functional connectivity patterns, and given support to the view that the brain works at a critical point at the edge of a bifurcation of the system. Here, we present an overview of a modeling approach of the resting brain network and give an application of a neural mass model in the study of complexity changes in aging.

2.1. Introduction

With the turn of the millennium, a paradigm shift slowly occurred in the field of brain science. In the 1990s, driven by the maturation of fMRI and its high spatial resolution, studies mainly focused on the precise localization of specific brain functions, leading to a new level of understanding of many perceptual processing streams, the mapping of two visual pathways in the brain, and localization of various specific functions. However, with time it also became clear that many neural responses depend strongly on context. Also, complex brain functions such as attention and consciousness interact widely throughout the brain, and there are also networks of brain areas actively structuring brain dynamics in the absence of any task. Especially the latter sparked interest in the dynamics of the fixation-only or eyes-closed awake 'resting state' condition as a potential baseline for various task conditions, and the investigation of intrinsic structure, self-

organizing principles and dynamics of the brain as a network of networks (Gusnard & Raichle, 2001).

With concurring advances in DTI/DSI and related technologies it has been possible to create a first generation of structural macro-connectomes (Hagmann et al., 2008, 2010; Sporns et al., 2005; Sporns, 2011) as well as large-scale functionally connected networks in fMRI-BOLD (Damoiseaux et al., 2006; Doucet et al., 2011; Fox & Raichle, 2007; Fox et al., 2005; Greicius et al., 2003), and, most recently, MEG and EEG recordings (Brookes et al., 2011a,c; Hipp et al., 2012; Mantini et al., 2007; Yuan et al., 2012). Furthermore, we are now in the process of obtaining detailed structural and physiological descriptions of the brain on multiple scales at once for large, physiologically detailed reconstructions of its networks (Van Essen & Ugurbil, 2012; Van Essen et al., 2012). However, a major challenge we will face in the coming years will not only be the pure recreation of realistic brain connectivity and dynamics. It will be the extraction of important features and mechanisms of these dynamics and of the network structure that are critical to brain function. This is critical to understand how this most complex network self-organizes into a very stable and consistent, yet flexible and adaptive system and its core components.

In the following, we will review and discuss how large-scale theoretical brain models are crucial to bridging the gap between purely anatomical brain networks and their cognitive architectures by identifying key network properties underlying the empirically observable network dynamics. We will outline how modeling evidence supports the idea that the brain works in a critical region close to a bifurcation, and that these dynamics are common to resting state models capturing the spatial patterns of spontaneous brain activity. Finally, we will apply this modeling approach to the study of Multiscale Entropy (MSE) in the aging brain, and give an outlook on how capturing spatiotemporal dynamics such as complexity and oscillatory dynamics presents the next big challenge for computational

models, to contribute further to understanding cognitive architecture of the brain and its relation to the underlying structural connectome.

In the following section, we will first describe how large scale computational models link the structural connectome to functional networks and dynamics. We then exemplarily review the underlying architecture of a biophysically sophisticated resting state model and its reduction to a neural mass model in Section 2.3. Finally, in Section 3, we give an application of the model for studying changes in cognitive architecture and complexity of spontaneous dynamics in aging.

2.2. Linking structure and dynamics: model approaches

An important question which remains to be answered in spite of the advances in structural mapping of the human connectome and intrinsic functional networks, is how they are related in detail. For large scale spontaneous fMRI dynamics, it has been shown that functional correlations of slow fluctuations are mainly determined by the underlying structural large-scale connectivity in the long run (Greicius et al., 2009; Hagmann et al., 2008; Honey et al., 2009; Skudlarski et al., 2008), and both functional and structural network characteristics can be described using graph theory (Bullmore & Bassett, 2011; Sporns, 2011). However, this structure-function mapping is imperfect, as functional connectivities are also influenced by indirect links and network dynamics, especially on shorter time intervals (Honey et al., 2009). In this sense, the structural connectome is like a road system, in which traffic volume (functional connections) and street size are closely connected in the long run, but depend much more on the dynamics of the population on shorter time scales. Even though this analogy does not extend to the specific dynamics of the systems, it nicely illustrates the enabling (and limiting) role of structure

for function. Analogously, our observations of functional relations and states may be strongly influenced by sampling window and frequency, as well as the aspects of the dynamics we focus on, such as mean activity, peak activity, or oscillatory phases.

As these dynamics enable the brain's rich repertoire of functional states, it is of fundamental theoretical interest to understand the critical features and mechanisms that link anatomical structure and recordings of brain dynamics. Theoretical models bridge this gap by constructing explicit network dynamics to capture the relations between structural connections and resulting resting state recordings (Deco & Jirsa, 2012; Cabral et al., 2011; Deco et al., 2009, 2013b; Honey et al., 2007, 2009; Knock et al., 2009).

These models are all implemented on graphs with nodes (brain areas), edges (connections), and local node dynamics, as illustrated in Figure 2.1. Spatial connectivity is determined by the parcellated structural connectome, derived from diffusion imaging (Hagmann et al., 2008) and tracing studies and databases (Gong et al., 2009; Kötter, 2004).

For modeling brain areas as nodes on the graph, raw diffusion data are parcelled, and areas and connectivities are down-sampled to the brain-area level and normalized. The resulting structural connectivity matrices are taken as fiber tracts between brain areas, and their functional transmission strength in the model is taken as the relative density of these tracts. The topological properties of the extracted brain network depend on, and are limited by the precision of several parameters such as fiber extraction algorithms (see e.g. Hagmann et al., 2008, methods section, for an exemplary analysis pipeline), extraction of connectivity direction, and cortex parcellation (Jbabdi et al., 2009; Wang et al., 2009; Zalesky et al., 2010). At least on low resolution parcellations, though, our earlier work shows model robustness over different parcellations for exploration of large-scale BOLD patterns of structural and functional networks (Cabral et al., 2012).

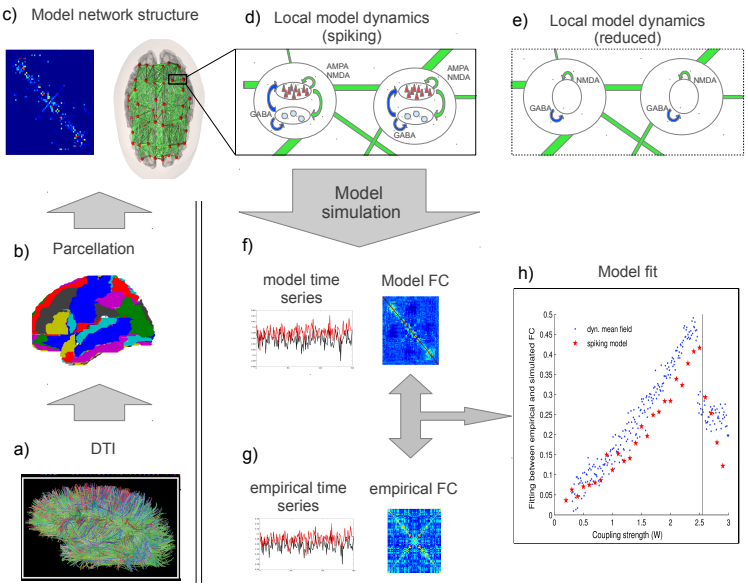

Figure 2.1: resting state networks

]*Modeling resting state networks. a) Fiber tract measurements (here depicting DTI, adopted and modified under a creative commons attribution license, from (Hagmann et al., 2007), b) parcellated from voxel space to brain areas, are used to build a brain graph (c, right), with nodes (red) representing brain areas and edges (green) represent links between nodes.The coupling matrix (c, left), determining the relative weights of connections between nodes, allows the network nodes to interact with each other, depending on their local dynamics. Local model dynamics are exemplarily sketched out for the full spiking model (d) and its dynamic mean field reduction (e) as described in section 2.3. Functional connectivity from simulations (f) and empirical resting state recordings (g) can then be compared to find the model's working point, as depicted in (f) for the described model (adapted with permission from the authors from Deco et al., 2013b). The vertical black line shows the location of the bifurcation at which the spontaneous stable state loses its stability.*

Delays, reflecting finite transmission velocities along axonal fiber tracts,

and which may reach up to 200 ms in the human brain (Nunez, 1995) further shape the full spatiotemporal structure, especially in the presence of oscillatory local dynamics (Campbell, 2007; Freyer et al., 2009; Jirsa & Ding, 2004). Intrinsic local dynamics have been captured in models by simple (Cabral et al., 2011; Deco et al., 2009; Ghosh et al., 2008a,b) and chaotic (Honey et al., 2007, 2009) oscillators as well as by detailed biophysically realistic descriptions of spiking neuron populations (Deco & Jirsa, 2012). Noise is added to keep the system active and in a dynamic regime in the absence of structured external input (Deco et al., 2009; Ghosh et al., 2008b).

The simulated time series for every node are then constructed as a forward model on the basis of local dynamics and input from other nodes arriving through the network structure. Functional connectivities are computed from the time series' raw, phase or power correlations and related functional connectivity measures. Generally, for low couplings, the system nodes are in a state dominated by low activity (Deco & Jirsa, 2012; Ghosh et al., 2008b; Honey et al., 2007) or intrinsic oscillations (Deco et al., 2009; Cabral et al., 2011). With increasing coupling, the system transitions to higher activity or synchronization states, which are spatially structured by the topography of the underlying anatomical connectome.

As the global strength level of the connections is not known *a priori*, the optimal model working point can be determined by comparing the model and the empirical functional connectivities for different coupling strengths. For the different resting state models, this has commonly been found to be at the critical point of a bifurcation at the edge of instability; i.e. at the border between a stable homogenous baseline state and emergent activation or synchronization patterns (see Figure 2.1 h). Critical dynamics of fluctuations between unstable functional brain states have been suggested to occur in neural networks (Beggs, 2008; Haken, 1996; Rabinovich et al., 2001, 2008), and there is ever increasing empirical and model evidence for criticality as an organizing principle in the brain as

a whole (Bassett et al., 2006; Kitzbichler et al., 2009; Poil et al., 2008, 2012; Tagliazucchi et al., 2012a).

For global resting state dynamics, the working location of the system at a critical point may maximize its flexibility and enable it to explore various functional states. Typical resting state dynamics with fluctuations between functional states occur as nodes transiently synchronize into sets of coactivated brain regions when being pushed beyond the bifurcation by noise. While the structure of the network depends on the underlying connectome, degree and variability of expression for specific networks are shaped by the proximity to the bifurcation and the noise of the dynamics. From this perspective, the emergence of Resting State Networks (RSN) reflects the dynamical capacity of the system to explore the brain's state space spontaneously while remaining able to efficiently respond to minimal external inputs. Recently, Deco & Jirsa (2012) have found such critical dynamics in a detailed and realistic spiking neuron attractor model, represented by populations of excitatory (AMPA and NMDA) and inhibitory (GABA-A receptor) integrate and fire neurons.

In the non-oscillatory, asynchronous state, as in the presented model, the key component to the model and its dynamics depend on the topography of its spatial connectivity structure and the location of its bifurcation, where the available states may change mainly with the graph properties of the network. In this case, the consistently reduced dynamic mean field model captures the resting state dynamics and bifurcation structure of the spiking model (Deco et al., 2013b). This is not necessarily true in the presence of oscillations, as the delay structure and fast dynamics become important and must be taken into account as additional factors and the network interactions become more complex.

In the following, we will illustrate the bifurcation from a trivial low activity state to multistable attractors with this model, and how its reduction to a neural mass model can help us appreciate its main mechanisms and necessary preconditions.

2.3. Biophysical model characterization of the resting state

In the previous sections, we presented the rationale and the fundamental working steps of the basic RS modeling paradigm, from brain parcellation, SC and FC connectivity measurements, to the simulation of RS activity in a model network, and extracting functional markers and graph measures of interest. As we saw, at each step of the processing pipeline, nontrivial decisions have to be made, which depend on the nature and quality of the data available, and influence the interpretability and possible conclusions we can draw from results.

In computational modeling, which strives to elucidate the probable links between structure and activation and uncover mechanisms and dynamics of brain function, a key question is that of how to implement neural dynamics into the model. All models simplify brain dynamics, but the extents and the levels of abstraction vary. Every model has different assumptions of the intrinsic behavior of local brain areas, and may help us understand brain behavior only if we keep in mind their nature and limitations when drawing conclusions. While a spiking neuron model may help us identify neurophysiological mechanisms or simulate drug-effects in more detail, a simple oscillator model can elucidate changes in synchronization over a wide set of parameters with much higher computational efficiency. In the following, we will present a nonexhaustive list of mesoscopic models that similarly used a large-scale connectome combined with different models of intrinsic local dynamics and discuss their assumptions, conclusions, similarities and differences. While the majority of models presented here consider slow, asynchronous BOLD fMRI signals, in Chapter 4, we will explore how different parameters influence model dynamics, considering the importance of delays in the presence of oscillatory dynamics in the case of MEG bandlimited power signals.

Mesoscopic models describe the activity of populations of neurons, as-

suming that their collective behavior is not strongly sensitive to the details of individual neuron activity (Breakspear & Jirsa, 2007). Mean field models represent lowdimensional representations of collective neuronal dynamics in one or more parameters and modes, the most important being firing rate or mean activity, but extendable to include variability parameters (Brunel & Wang, 2003). These models still connect to some biophysiological behaviors of individual neurons (Stefanescu & Jirsa, 2011; Jirsa & Stefanescu, 2011) while even simpler models inspired by physical systems such as the Kuramoto model or the Ising spin glass model fully abstract population behavior from underlying biomechanical processes of individual neurons. In Section 2.3.6, we also present a biophysically realistic global spiking attractor model with populations of integrate-and-fire neurons on the microscopic scale, along with its reduction to a mesoscopic dynamic mean field model.

2.3.1. Conductance-based biophysical models

The biophysical neural mass model of Breakspear et al. (2003) was the first one to be extended into a full cortical network model with nodes for brain areas and a datadriven long-range connectivity matrix as network links (Kötter, 2004) in a work by Honey et al. (2007). They implement the conductance-based local model for neural dynamics by Morris & Lecar (1981), which describes neuron behavior as a function of voltage- and ligand-gated membrane channels. Sigmoidally voltage-dependent sodium (Na) and calcium (Ca) channels, along with exponentially relaxing potassium (K) channels describe the local populations, which are interconnected by long-range excitatory to excitatory connections, implementing glutamate-induced synaptic currents.

In this model, the neural activity is captured by the mean membrane po-

tential of the excitatory pyramidal cells *V*, and governed by:

$$C\frac{dV}{dt} = -g_{Ca}m_{Ca}(V - V_{Ca}) - g_{Na}m_{Na}(V - V_{CNa}) \\ -g_K W(V - V_K) - g_L(V - V_L), \tag{2.1}$$

where g_{ion} is the maximum conductance of each ion species, and g_L is the passive conductivity of leaky ions. m_{ion} is the fraction of open channels and V_{ion} is the Nernst potential for that ion species. *W* is the average number of 'open' potassium channels. All related equations and parameters are nondimensional and normalized to neural capacitance $C = 1$. As each voltage-gated channel opens when the membrane potential crosses a given threshold T_{ion} from below, the relationship between membrane conductance and the single channel is governed by a step function. For the population average over such channels, assuming an ion-specific Gaussion distribution of T_{ion}, the sigmoid-shaped neural activation function for each ion is given by

$$m_{ion} = 0.5(1 + tanh(\frac{V - T_{ion}}{\delta_{ion}}), \tag{2.2}$$

where δ_{ion} is the variance of the distribution. For the fraction of open potassium channels (*W*), an exponential 'relaxation' is achieved by *W* being governed by

$$\frac{dW}{dt} = \frac{\phi(m_K - W)}{\tau}, \tag{2.3}$$

where ϕ is a temperature scaling factor and τ is the relaxation time constant. Synaptic interactions between neurons within the same local population, feedback terms subsequent to cell firing, representing neurotransmitter release, are introduced. At the soma, the membrane potential triggers and action potential if it crosses a (mainly sodium-channel governed) threshold. By averaging over the local population and assuming Gaussianity, we obtain the firing rates

$$Q_V = 0.5Q_{Vmax}(1 + tanh(\frac{V - V_T}{\delta_V})), \tag{2.4}$$

$$Q_Z = 0.5Q_{Z\,max}(1 + tanh(\frac{Z - Z_T}{\delta_Z})), \tag{2.5}$$

where $Q_{V\,max}$ and $Q_{Z\,max}$ are the maximum firing rates of the excitatory and inhibitory neurons, respectively. The firing of each cell population feeds back onto the ensemble, thus raising or lowering the membrane potential accordingly.

Connections between the excitatory (*e*) and inhibitory (*i*) populations are modelled as additional inputs to the flow of ions across the membrane channels, weighted by synaptic factors a_{ei} and a_{ie}. *e-e* connections are modelled with greater physiological detail: The mean firing rate Q_V is assumed to trigger a proportional release of glutamate, which diffuses across the synapse on to AMPA-receptor sodium channels and NMDA-receptor voltage-gated calcium channels. Thus, the excitatory (V) and inhibitory (I) membrane potential is given by:

$$\begin{aligned} \frac{dV}{dt} = &-(g_{Ca} + r_{NMDA}a_{ee}Q_V)m_{Ca}(V - V_{Ca}) \\ &-(g_{Na}m_{Na} + a_{ee}Q_V)(V - V_{Na}) - g_K W(V - V_K) \\ &-g_L(V - V_L) + a_{ie}ZQ_Z + a_{ne}I_\delta, \end{aligned} \tag{2.6}$$

$$\frac{dZ}{dt} = b(a_{ni}I_\delta + a_{ei}VQ_V), \tag{2.7}$$

where r_{NMDA} denotes the number of NMDA recepter in relation to AMPA receptors, a_{ne} and a_{ni} are nonscpecific inputs, and a_{ee} parametrizes excitatory to excitatory synaptic strength. I_δ represents subcortical excitation of amplitude *I*, modulated by a random noise component of amplitude δ.

To model an array of populations with long-range connectivity between the same NMDA and AMPA receptor targets on pyramidal neurons, the following equation describes the mean membrane potential for pyramidal

neurons of node n:

$$\begin{aligned}\frac{dV^n}{dt} = &-(g_{Ca} + (1-C)r_{NMDA}a_{ee}Q_V^n \\ &+Cr_{NMDA}a_{ee}\langle Q_V\rangle)m_{Ca}(V^n - V_{Ca}) \\ &-g_K W(V^n - V_K) - g_L(V^n - V_L) \\ &-(g_{Na}m_{Na} + (1-C)a_{ee}Q_V^n + Ca_{ee}\langle Q_V\rangle)(V^n - V_{Na}) \\ &+a_{ie}ZQ_Z^n + a_{ne}I_\delta,\end{aligned} \tag{2.8}$$

where $\langle\ \rangle$ represents spatial averaging over cell assemblies, resulting in 'mean-field' variables. C weighs the strength of long-range excitatory couplings, so that, if $C > 0$, interdependencies and complex spontaneous activity patterns arise (Breakspear et al., 2003). In a large-scale brain model with realistic anatomical connectivity, C was set to a value which allowed for weakly stable synchronous dynamics. Switches between synchronous and desynchronous epochs arise from the nonlinear instabilities based on the chaotic dynamics of the nodes, linked by the complex structural connectivity. At this critical coupling, spontaneous activity patterns arise in the absence of noise or delays, and spontaneous patterns of coactivation rebuild RS FC patterns identified in empirical BOLD recordings both in the macaque (Honey et al., 2007) and human brain (Honey et al., 2009). This was the first study to show in a model how the large-scale anatomical structure of the primate cortex constrains the spatiotemporal characteristics of RS activity.

2.3.2. FitzHugh-Nagumo model

Another neural mass model, based on FitzHugh Nagumo units (FitzHugh, 1961; Nagumo et al., 1962), coupled in the space-time structure of a time-delayed connectivity matrix, was developed by Ghosh et al. (2008a,b). In the twodimensional simplification of the Hodgkin-Huxley model, dynamics are goverened by the evolution of the state variables u_i and v_i of neural population, indexed by i:

$$\dot{u}_i(t) = g(u_i, v_i) - c\sum_{j=1}^{N} f_{ij}u_j(t - \Delta t_{ij}) + n_u(t)$$
$$\dot{v}_i(t) = h(u_j, v_i) + n_v(t), \tag{2.9}$$

where $n_u(t)$ and $n_v(t)$ is added white Gaussian noise, and

$$g(u_i, v_i) = \tau v_i + \gamma u_i - \frac{u_i^3}{3}$$
$$h(u_i, v_i) = 1 - \frac{1}{\tau}[u_i - \alpha + \beta v_i],$$

with α= 1.05, β = 0.2, γ =1.0, τ =1.25. The equations for each node were coupled, and for a certain range of delays, calculated from Euclidean distances d_{ij} and propagation velocity v by $\Delta t_{ij} = \frac{d_{ij}}{v}$. While the nodes are damped oscillators when uncoupled, the authors observed increased instability in the ongoing dynamics in the coupled system if a sufficiently large coupling was combined with a certain realistic range of propagation velocity of 5-20m/s. They demonstrate that the tuning of the propagation velocity allows for the emergence of the resting state networks for biophysically realistic parameters.

The model is compared to functional imaging data by calculating simulated BOLD signal in form of the Balloon-Windkessel hemodynamic model (Friston et al., 2003). Even though the resulting BOLD signals are much slower, the delays on the scale of tens of seconds remain important for the stability of the system, as they shape the interactions of the underlying simulated neural signals. In contrast to the previous model of Honey et al. (2007), there are no chaotic local dynamics, and the BOLD RS patterns arise here from a combination of spatial and temporal connectivity patterns. The emergent slow BOLD fluctuations are caused by power variations in the 10 Hz oscillations of the underlying signal.

2.3.3. Wilson-Cowan model

Another 'mean-field' approach was taken by Deco et al. (2009) with noise driven Wilson-Cowan oscillators (Wilson & Cowan, 1972). This very simple neuron model is based on populations of homogenous model neurons, specifically the activity, i.e. the proportion of excitatory (*x(t)*) and inhibitory (*y(t)*) cells firing at any time *t*. In this model, the local dynamics of cortical regions are reduced to considering the interaction between these neuron population subtypes. While the model neurons are simple and thus only show elementary limit cycle behavior on their own, the global dynamics in a cortical model will depend on the interactions between the brain regions in addition to the local behavior. The local nodes were linked by time-delayed long-range excitatory connections in order to study how global slow oscillations could emerge from a network built from simple fast (gamma) oscillators, as which cortical regions have been described in the model by Wilson & Cowan (1973). In the coupled model, the activity (*z(t)*) of a pool is given by the decay of current activity plus added excitatory stimulation,

$$\tau \frac{\partial z(t)}{\partial t} = -z(t) + \Phi(z(t)), \tag{2.11}$$

with the nonlinear response function

$$\Phi(x) = \frac{c}{1 - exp - a(x - b)}, \tag{2.12}$$

which transforms the current into discharge rates, with membran time constant τ. Coupled together, the local populations of excitatory and inhibitory neurons are governed by:

$$\begin{aligned} \tau \frac{\partial x(t)}{\partial t} &= -x(t) + \Phi(I_b + w_+ x(t) - y(t)) + v(t), \\ \tau' \frac{\partial y(t)}{\partial t} &= -y(t) + \Phi(w_I X(t)) + v(t), \end{aligned} \tag{2.13}$$

where v is Gaussian noise with zero mean, and I_b is a diffuse spontaneous background input.

To model the network dynamics, the excitatory populations of 38 Wilson-Cowan units were coupled according to the CoCoMac macaque connectivity data (Stephan et al., 2000), using the connectivity matrix C_{ij} and the assumed delay matrix T_{ij}, so the global dynamics are given by

$$\tau \frac{\partial x_i(t)}{\partial t} = -x_i(t) + \Phi(I_b + \sum_j \alpha C_{ji} x_j(t - T_{ji}) - y_i(t)) + v_i(t), \quad (2.14)$$

$$\tau' \frac{\partial y_i(t)}{\partial t} = -y_i(t) + \Phi(w_I x_i(t)) + v_i(t), \quad (2.15)$$

where $C_{ij} = w_+/\alpha$ and α is the global coupling parameter. At $a{-}0.1, b = 40, c = 100, \tau = 1, \tau' = 0.2, w_i = 1.5$, single uncoupled nodes remain in a nonoscillatory low-activity state, while coupling (and thus increased mutual excitation shaped by the spatiotemporal connectivity matrix) led to noisy, self-sustained oscillations in the gamma-frequency range and the formation of two functional networks fluctuating slowly (~0.1 Hz) in their intranetwork synchronization. In line with empirical findings, these slow connectivity fluctuations showed to be in anticorrelation with each other (Fox et al., 2005).

2.3.4. Kuramoto model

Where Wilson-Cowan units can show either damped or self-sustaining oscillations, the model can further be simplified when assuming the local networks to be in the latter regime (as found to be the case for the network of Deco et al., 2009), and the inputs to the network perturb the system weakly enough to not throw it far off the vicinity of its limit cycle. In that case, the dynamics of the system can be closely approximated in one single dimension, which is the angle or phase of the oscillators on that cycle.

Cabral et al. (2011) approximated the reduction of the Wilson-Cowan system in one dimension by replacing the phase-difference function of how the nodes affect each other with a simpler sine function, resulting in a Kuramoto model of coupled phase oscillators. The Kuramoto model (Kuramoto, 1984; Strogatz, 2000; Yeung & Strogatz, 1999) has been used in an array of fields and topics including mathematical biology, statistical physics, and engineering, amongst others.

The model is noteworthy in that in a collection of simple oscillators, beyond a certain coupling threshold, clusters of synchronizing oscillators arise (as long as their natural frequencies are not too different). For same-frequency oscillators, the dynamics of the system in terms of each oscillator's phase $\theta_n(t)$ is governed by

$$\frac{d\theta_n}{dt} = \omega_n + k\sum_{p=1}^{N} C_{np} sin(\theta_p(t-\tau_{np}) - \theta_n(t)) + \eta_n(t), \qquad n = 1, ..., N, \tag{2.16}$$

where C_{np} is the relative coupling strength from node p to node n (i.e. C is the connectivity matrix), k is the global coupling strength parameter scaling all connections, τ_{np} are the delays between pairs of nodes calculated from propagation velocity v and the distance matrix L, expressed by mean delay $\langle v \rangle$. η_{n}(t) is white Gaussian noise representing local background input with zero mean and variance σ_n^2/T. $f_n = \omega_n/2\pi$ is the intrinsic frequency of node n, drawn from a fixed Gaussian distribution with mean $f_0 = 60Hz$.

Cabral et al. (2011) study the effect of the spatiotemporal coupling determined by $\langle \tau \rangle$ and k on the global synchrony of the system, given by the Kuramoto order parameter. This very generic oscillator model was then combined with an empirically obtained structural connectivity matrix of the human cortex and delays calculated from the spatial distance between nodes. The authors found that for large N, there exists a critical value k_c

for the global coupling where the synchrony jumps from zero (incoherence) to a positie value. Rising k increased synchrony, while rising $\langle\tau\rangle$ required a higher k for the same level of synchrony, therefore inhibiting global synchrony. The node dynamics at the critical coupling captured the empirical FC best at the level of critical coupling where clusters of strongly connected nodes are substantially synchronous with each other while the global network is still in a globally incoherent regime. Interestingly, while previous models found a key role for both the SC and noise (Ghosh et al., 2008a,b; Knock et al., 2009; Deco et al., 2009) or chaotic dynamics (Honey et al., 2007, 2009), this is not the case for the Kuramoto model. While there is some level of chaos in the incoherence regime (Popovych et al., 2005), and noise may influence cluster interactions and dynamical features of the system (Cabral et al., 2011; Deco et al., 2009), the presence of delays is the second parameter that played a major role in the establishment of well-fitting FC patterns, in that their inclusion prevented full synchronization of the network. This work showed in a lowdimensional model how delays are important to consider in the presence of oscillatory dynamics of the local nodes, a question we will revisit in Chapter 4 in a spiking-neuron network with oscillatory node dynamics.

2.3.5. Stefanescu-Jirsa model

A versatile mean-field model derived from Hindmarsh-Rose neurons (Hindmarsh & Rose, 1984), a threedimensional reduction of the Hodgkin-Huxley model capable of various spiking and bursting behaviors, was developed by Stefanescu & Jirsa (2008) (Stefanescu & Jirsa, 2011; Jirsa & Stefanescu, 2011; Ritter et al., 2013). Due to its additional dimension, the model is able to switch between a stable rest state and a limit cycle, giving rise to complex firing patterns such as synchronous and asynchronous firing, bursting and multicluster ermergence in a lowdimensional system.

In the model, describing an excitatory and an inhibitory population of

fully connected neurons, the three components, or modes, of the local dynamics are described by

$$\begin{aligned}
\dot{x}_{i1} &= y_{i1} - ax_{i1}^3 + b_{xi1}^2 - z_{i1} \\
&\quad + [K_{11}(X_1 - x_{i1}) - K_{12}(X_2 - x_{i1})] + I_{i1} \\
\dot{y}_{i1} &= c_i - dx_{i1}^2 - y_{i1} \\
\dot{z}_{i1} &= r[s(x_{i1} - x_{i0} - z_{i1}] \quad i_1 = 1, .., N_1 \\
\dot{w}_i &= v_i - aw_i^3 + bw_i^2 - u_i + K_{21}(X_i - w_i) + II_i \\
\dot{v}_i &= h_i - p_i w^2 - v_i \\
\dot{u}_i &= rsw_i - ru_i - n_i,
\end{aligned} \tag{2.17}$$

where, in the single-neuron formulation, the variables *x/w* encode the membrane potential, *y/v* the transport of fast sodium and potasium ions across the membrane, and *z/u*, the bursting variable, accounts for the inward current through slow ion channels. In the mean field reduction, whose terms take the form

$$X = \frac{1}{N}\sum_{i=1}^{N} x_i, \tag{2.18}$$

the mathematical structure of the single-neuron model is still reflected, and the three modes of the model (2.17) reflect different dynamical behaviors depending on the range of membrane excitabilities of the neuron cluster (Stefanescu & Jirsa, 2008).

In the coupled large-scale network, inputs from other nodes are added to local mean field potential x_i, so that the mean-field potential $x_i(t)$ of node i is goverened by

$$\begin{aligned}
x_i(t+1) &= x_i(t) + \int (x_i(t))dt \\
&\quad + c\sum_{j=1}^{N} w_{ij}x_j(t - \Delta t_{ij})dt + \eta(t),
\end{aligned} \tag{2.19}$$

where w_{ij} are the empirically obained coupling weights between node *i* and node *j*, scaled by a global coupling parameter *c*. The model also includes time delays, depending on distance matrix *D* and conduction speed *v*. $\eta(t)$ is an additive noise term.

This model, amongst others, was integrated into The Virtual Brain (TVB), a neuroinformatics platform and brain modeling framework that incorporates a brain simulator with several mean-field and spiking models, as well as statistical and visualization analysis tools (Sanz Leon et al., 2013). In this framework, the model was shown to be promising to study a broader range of dynamic features of the brain due to its range of parameters. At the same time, it is not too complex to interpret or to find sensible parameters due to a combination of statistical methods applicable with the TVB plattform, such as motif identification and dictionary lookups leading to dimensionality reduction, and crossmodal empirical model fitting (Ritter et al., 2013). The platform also makes it possible to compare model performance for different models on the same data, and thus inform model choices by pinpointing their strengths and limits in standardized, reproducible settings.

2.3.6. Spiking model

The spiking neuron model combines the large-scale network graph structure used in all full spatiotemporal resting state models with biophysically realistic populations of integrate-and-fire neurons on the microscopic scale. Figure 2.1 shows the basic network setup.

In this model, each node is represented by an excitatory and an inhibitory population of leaky integrate-and-fire neurons with AMPA and NMDA, or GABA-A synaptic receptor types, respectively (Brunel & Wang, 2001). This type of network of spiking neuron network tends to settle in stationary states, so called "attractors", typically characterized by a stable pattern of firing activity (Deco & Rolls, 2006; Deco et al., 2008), depending on

its input level. External or even intrinsic noise that appears in the form of finite size effects can provoke destabilization of an attractor inducing therefore transitions between different stable attractors. The spiking activity of the local network is determined by the dynamics of the membrane potentials $V(t)$, which are governed by a set of equations relating $V(t)$ to leakage and synaptic activity I_{syn} (including a noise term).

For the spiking model, each neuron's membrane voltage below threshold V_{thr} is governed by:

$$C_m \frac{dV(t)}{dt} = -g_m(V(t) - V_L) - I_{syn}(t), \tag{2.20}$$

with membrane capacitance C_m, leak conductance g_m, resting potential V_L and synaptic input current I_{syn}, where

$$I_{syn} = I_{AMPA,ext} + I_{AMPA,rec} + I_{NMDA} + I_{GABA} \tag{2.21}$$

,

$$I_{AMPA,ext}(t) = g_{AMPA,ext}(V(t) - V_E) \sum_{j=1}^{N_{ext}} s_j^{AMPA,ext}(t), \tag{2.22}$$

$$\frac{ds^{AMPA,ext}(t)}{dt} = \frac{s_j^{AMPA,ext}(t)}{\tau_{AMPA}} + \sum_k \delta(t - t_j^k), \tag{2.23}$$

$$I_{AMPA,rec}(t) = g_{AMPA,rec}(V(t) - V_E) \sum_{j=1}^{N_E} w_j s_j^{AMPA,rec}(t), \tag{2.24}$$

$$\frac{ds^{AMPA,rec}(t)}{dt} = \frac{s_j^{AMPA,rec}(t)}{\tau_{AMPA}} + \sum_k \delta(t - t_j^k), \tag{2.25}$$

$$I_{NMDA}(t) = \frac{g_{NMDA}(V(t) - V_E)}{1 + \lambda e^{-\beta V(t)}} \sum_{j=1}^{N_E} w_j s_j^{NMDA}(t), \tag{2.26}$$

$$\frac{ds^{NMDA}(t)}{dt} = -\frac{s_j^{NMDA}(t)}{\tau_{NMDA,decay}} + \alpha x_j(t)(1 - s_j^{NMDA}(t)), \tag{2.27}$$

$$\frac{dx^{NMDA}(t)}{dt} = -\frac{x_j^{NMDA}(t)}{\tau_{NMDA,rise}} + \sum_k \delta(t - t_j^k), \tag{2.28}$$

$$I_{GABA}(t) = g_{GABA}(V(t) - V_I) \sum_{j=1}^{N_I} w_j s_j^{GABA}(t), \tag{2.29}$$

$$\frac{ds^{GABA}(t)}{dt} = \frac{s_j^{GABA}(t)}{\tau_{GABA}} + \sum_k \delta(t - t_j^k), \tag{2.30}$$

with synaptic conductances g, excitatory and inhibitory reversal potantials V_E and V_I, respectively, the Dirac-delta function δ, and synaptic weight parameter w_j (determining the connection strengths between and within neural populations). The gating variables s_j are the fractions of open ion channels of the neurons. Connections between excitatory and inhibitory pools were set to 1, and recurrent self-excitation to /w+/=1.5. Synaptic parameters were V_E = 0mV, V_I = -70mV, τ_{AMPA} = 2ms, $\tau_{NMDA,rise} = 2ms$, $\tau_{NMDA,decay}$ = 100ms, τ_{GABA} = 10ms, α = 0.5kHz, β = 0.062, γ = 0.28. Once a neuron crosses V_{thr}, a spike is transmitted to connected neurons, and its membrane potential is reset to, and maintained at V_{reset} for refractory period τ_{ref}.

All neurons in the network received an external background input from $N_{ext} = 800$ external AMPA signaling excitatory neurons injecting uncorrelated poisson-distributed spike trains, representing the noisy fluctuations that are typically observed *in vivo*. Specifically, for all neurons inside a given population p, the rate v_{ext}^p of the resulting global spike train is described by:

$$\tau_n \frac{dv_{ext}^p(t)}{dt} = -(v_{ext}^p(t) - v_0) + \sigma_v \sqrt[2]{2\tau_n} n^p(t), \tag{2.31}$$

where τ_n = 300ms, v_0 = 2.4kHz, σ_v is the standard deviation of $v_{ext}^p(t)$, and $n^p(t)$ is normalized Gaussian white noise. Negative values of $v_{ext}^p(t)$, that could arise due to the noise term, are rectified to zero.

After applying the mean field reduction to the above spiking model (Deco et al., 2013b), the activity is governed by:

$$\frac{dS_i(t)}{dt} = -\frac{S_i}{\tau_S} + (1 - S_i)\gamma H(x_i) + \sigma \upsilon_i(t), \tag{2.32}$$

$$H(x_i) = \frac{ax_i - b}{1 - exp(-d(ax_i - b))}, \tag{2.33}$$

$$x_i = wJ_N S_i + GJ_N \sum_j C_{ij} S_j + I_0, p \tag{2.34}$$

where $H(x_i)$ and S_i denote the population rate and the average synaptic gating variable for each local cortical area, C_{ij} is the structural connectivity matrix containing the link strengths between brain areas i and j, and local excitatory recurrence w is 0.9. Parameter values for the input–output function are /a/=270 (VnC), /b/=108 (Hz), and /d/=0.154 (s). The kinetic parameters are γ =0.641/1000. (The factor 1000 is for expressing everything in ms), τ_S =100 (ms). The synaptic couplings are J_N =0.2609 (nA) and the overall effective external input is I_0 =0.3 (nA). In equation (2.32), υ_i is uncorrelated standard Gaussian noise and the effective noise amplitude at each node is σ =0.001(nA).

This model is very detailed, but due to the large number of equations computationally costly. In order to simplify the model and make simulations for different connectivity structures and multiple runs and parameters feasible, the model can be reduced to a neural mass model under certain assumptions. Based on the mean field model of (Brunel & Wang, 2001), the dynamic mean field (Wong & Wang, 2006) simplifies the original spiking model by replacing the synaptic gating variables by a DC component and a Gaussian fluctuation term dependent only on external synaptic gating variables, reducing the latency of the dynamics to the slow NMDA component, and linearizing the input-output relation of the inhibitory interneurons and integrating them into the excitatory dynamical equation.

BOLD fMRI signal was simulated by means of the Balloon-Windkessel hemodynamic model of Friston et al. (2000, 2003) and all parameters are taken from there. The model describes the perfusion changes based on

neural activity (S_i in the reduced model) in each brain region causing a vasodilatatory signal with autoregulatory feedback. The BOLD signal is then modeled as a static nonlinear function of volume and deoxyhemoglobin that comprises a volume-weighted sum of extra- and intravascular signals. In the context of the present simulations, the BOLD signal is vastly dominated by the linear contributions of the hemodynamic model and the nonlinearities do not impact the results.

While the model is restricted to modeling spontaneous low-rate activity below the stabilization of high-activity states due to the linearizations and reduction to slow dynamics, the reduced model captures both the bifurcation properties of the underlying spiking model and the empirical functional connectivity patterns at the critical working point (Figure 2.1 e; Deco et al. 2013b). This, and the closeness of the working point to the bifurcation, indicate that Resting State Dynamics do not fully explore the whole state space of possible configurations available to the brain, but rather a lowerdimensional subspace of possible states consisting of "ghost" attractors, regions of state space at the edge of the bifurcation (Deco & Jirsa, 2012). In this perspective, RSN dynamics are equivalent to the brain wandering around in the atrium of our cognitive architecture. The criticality of the dynamics can be likened to the flexibility of movement within this architecture: below the working point, the system remains near the entrance and does not visit any functional states (no functional connectivity), whereas supercritical dynamics keep it located in specific sections. The situation at the critical point allows the system to move most freely, to efficiently access more specific building compartments (functional states) when prompted (by specific inputs). If this analogy holds true, explicit analysis of the model time course pattern dynamics and quantification with high-order moments such as variance or entropy can help us shed light on the detailed underlying computations at rest by making model performance comparable on more dimensions. The temporal dynamics between resting state patterns such as sequence orders of activation patterns or coexpression and responses to external stimulations or network damage should be evident also in the complexity and

variability of the simulated time series, and provide empirically testable measures and predictions to understanding the brain's criticality.

In the following Chapter [3] [1], we will illustrate how dynamical biophysical markers such as complexity (described in detail in section 3.3) can provide an excellent comparison measure for model and empirical resting state dynamics. In this ongoing work, we show first results relating empirical observations of decreasing spontaneous MSE in senescence to criticality and model dynamics, and demonstrate how dynamical markers provide quantifiable access to network dynamics beyond spatial pattern analysis.

2.3.7. Conclusion from models

From the number of RS models that studied the spontaneous dynamics of the brain at a large scale, the conclusion arises that the connectome carries a key role in shaping the spatial pattern of functional states, reflected by the occurrence of slow oscillations and the emergence of networks of cofluctuating brain areas. Each model requires some intrinsic dynamics together with a global scaling of couplings from the connectivity matrix to push the regime into a state where nodes interact and form complex patterns without being caught in constant high-activity states or rigid oscillatory behavior. This finding is fairly independent of the specific model, and indicates that some aspects of brain dynamics are guided by general principles which are shared in many complex systems. These include network properties treated in Chapter 1.3.2, and the notion of criticality, discussed in Chapter 2.2. Essentially, the underlying structure (responsible for integrating and communicating functional modules) is critical in shaping the concrete patterns potentially emerging from the system, but the emergence of a dynamical regime depends on a location of the system at a critical working point between rigidity and chaos.

[1] 'section' in the published paper

The different models have implemented this dynamic regime differently, with the local model corresponding to a fixed-point (e.g. Deco & Jirsa, 2012; Ghosh et al., 2008b), limit cycle (e.g. Deco et al., 2009; Cabral et al., 2011), or chaotic oscillators (Honey et al., 2007, 2009), although some models may be able to enter different regimes (Stefanescu & Jirsa, 2011, 2008). As to whether noise importantly shapes the intrinsic system dynamics depends on the existence or nonexistence of instabilities of dynamics at the local node level. Multistability can occur in the absence of noise when intrinsically chaotic local dynamics are given (Honey et al., 2007, 2009), and in this case neither delays nor noise are essential. In other models, transitions between stable regimes may depend on noise fluctuations (Deco et al., 2009). On the other hand, a complex spatiotemporal network structure can be enough to create basic mean FC patterns and slow RS fluctuations also with simple physical oscillators (Cabral et al., 2011). These large differences in which of the parameters importantly shape the dynamics of the system depend on the fundamental differene in conceptualization of brain areas. However, in the brain, noise and delays are naturally present and one must carefully consider the question under study and the conclusions that can be drawn by building a model on specific local dynamics.

If brain dynamics are essentially asynchronous, with neurons firing noisily at low rates as in Deco & Jirsa (2012), time delays can essentially be neglected as they do not substantially alter the stationary asynchronous state of the system, save for reducing the stability of the oscillatory network states (Jirsa & Ding, 2004; Jirsa, 2009). However, if we consider brain areas as phase-interacting oscillators at time scales in the range of the estimated delays, the latter are critical to consider as they shape the phase interactions and configuration patterns between nodes (Ghosh et al., 2008b; Cabral et al., 2011).

In the following chapter, we study the effects of structural disconnectivity in an asynchronous model based on Deco & Jirsa (2012). In Chapter 4, we will explore the role of delays in a spiking-neuron network model of rest-

ing state dynamics, developed from the asynchronous model. There, we aim to represent oscillatory neuron populations as frequently measured with neurophysiology. As discussed, in this case, delays are expected to play an important role. They indeed shape the model FC in a way that gives best results in a range of propagation velocities that are also physiologically realistic, confirming that the presence or absence of oscillation is important to determine whether delays shape system interaction and FC patterns.

3. Modeling complexity in Aging

This chapter reproduces the second part of the paper[1] referenced in Chapter 2. Here, we utilize an asynchronous spiking model (described in Section 2.3.6) to simulate BOLD signal for two scenarios of decreasing structural connectivity as a model of changing brain structure and dynamics in the healthy aging brain.

3.1. Brain structure changes in aging

Above, we have laid out how there is an important, yet complex relation between structural and functional brain connectivity, and that computational models find a certain regime of critical connectivity and network interactions optimize the dynamical properties and functional connectivities. This view implies that in the real brain, some mechanisms regulate effective brain connectivity to establish and maintain this regime. Failure of the system to do so should result in dysfunctional states. In line with this notion, brain connectivity is known or suspected to be altered in psychopathology (Bullmore & Sporns, 2009; Whitfield-Gabrieli & Ford, 2012). In fact, observable changes in brain connectivity (Alstott et al., 2009; Honey & Sporns, 2008) and their functional consequences (Lynall et al., 2010; Supekar et al., 2008) allow us to further probe and improve our models, and, in turn, to better characterize neurological diseases and lesions (Cabral et al., 2012) in terms of their principal mechanisms. To better understand how changes in connectivity affect the brain dynamics, and to what extent the brain can adapt to those changes, we can use computational models.

[1] Nakagawa et al. (2013)

This approach is not limited to the study of pathological states. Our brain network naturally changes over our lifespan, with maturation-related changes in childhood and both gray and white matter decreases in healthy, nonpathological aging. Many structural, cellular, and physiological mechanisms appear to tune our brain during its maturation to maximize its complexity and cognitive performance (Tononi et al., 1994; Lippé et al., 2009; McIntosh et al., 2008; Vakorin et al., 2011). In contrast, senescence is primarily associated with involuntary anatomical decline and decreasing complexity. Structural changes in adult aging have recently been mapped out in some detail with advances in high-resolution structural MR, DTI/DSI, tractography, and derived measures. Results still vary in the specifics, in part due to the still developing methodologies (Galluzzi et al., 2008; Sullivan & Pfefferbaum, 2007; Giorgio et al., 2010; Gunning-Dixon et al., 2009). In general, though, both gray and white matter are found to decrease with age, with an anterior-posterior gradient in white matter (Ardekani et al., 2007; Grieve et al., 2007; Head et al., 2004; Pfefferbaum & Sullivan, 2003; Salat et al., 2005). Over time, gray matter decreases approximately linearly, while measurements of white matter changes are more heterogeneous: volume increases up to ages 30-40 and volume decreases occur only from around age 50 in most areas (Pfefferbaum A, 1994; Ge et al., 2002; Giorgio et al., 2010), but diffusion measures show linear decay at this age already (Giorgio et al., 2010; Salat et al., 2005).

These changes in structure and structural connectivity with age are associated with decreases in cognitive performance: older adults show decreases in many aspects of cognition attributed to loss of processing speed (e.g. Salthouse, 1996), and aspects of executive functions including task switching and working memory seem especially vulnerable (Park et al., 2002). In trying to link cognitive decline with structural changes, some studies have found associations between gray matter volume and memory or cognitive performance in some areas (Salat et al., 2002; Rosen et al., 2003; Rodrigue & Raz, 2004), but see Tisserand et al. (2000); Gunning-Dixon & Raz (2003) for contrary results. Decreases in white matter vol-

ume are related to executive function and memory decline (Brickman et al., 2006; Guttmann et al., 1998; Resnick et al., 2003), and microstructural damage (white matter hyperintensities, WMH), have been linked to decreased processing speed and executive functions (DeCarli et al., 1995; Gunning-Dixon & Raz, 2003, 2000; Madden et al., 2009; Oosterman et al., 2004; Prins et al., 2005). Finally, processing speed and age have also been linked to lower brain signal complexity in recent studies (Garrett et al., 2011a,b, 2012; McIntosh et al., 2008, 2010, 2013; Yang et al., 2012).

Here, we investigated how structural connectivity pruning (representing white matter losses) affects complexity in a large-scale computer model of resting state dynamics. To this end, we created connectomes with different levels of connectivity with two pruning algorithms (detailed in the methods section), and simulated resting state dynamics with a dynamic mean field model. We then calculated MSE from the time series, to test whether or not complexity can serve as a marker to distinguish different structural decline scenarios.

3.2. Model network structure

The global network structure determining the connectivity between the 74 nodes of the model was comprised of a combination of long-range and short-range connections. For the long-range connections, high resolution diffusion tensor images were downsampled and parcellated into 74 areas to construct a coarse-grained connectivity matrix. These connections were extracted from a combination of diffusion spectrum MRI tractography and a mapping of the macaque connectome (*CoCoMac* database) onto the human brain (for details see (Knock et al., 2009).

As DTI measures directionality of water diffusion in white matter tissue (Beaulieu, 2002), the more diffuse lateral connections along the corti-

cal sheet are not detected by DTI measuring, and are here considered by short-range connectivity matrices.

These matrices used here were constructed from a Gaussian decaying connectivity on a triangulated cortical surface 'Cortex_reg13.mat' that is included in The Virtual Brain software package, available at http://thevirtualbrain.org/app/. The triangulated mesh that describes an individual cortical surface is based on a set of anatomical MRI scans. The mesh was obtained by extracting a high resolution surface from MRI and sampling down the high resolution surface, while balancing between curvature preservation and mesh regularity. The resulting surface composes the cortical geometry of 16,384 vertices and 32,760 triangles. Each vertex covers nearly 16 mm^2 of the cortical sheet. Periodic boundaries conditioned the two hemispheres composed of 8,192 vertices each. To obtain the connectivity of each vertex with its neighborhood on the triangulated mesh, the edge lengths (with the mean of 3.9761 mm) were considered for sampling the short-range connectivity function (Spiegler & Jirsa, 2013). The short-range connectivity matrices used here differ in spatial decay of connectivity between vertices, with standard deviations of the gaussian spatial filter ranging between 10 mm and 40 mm. Each vertex of the cortical surface was then assigned to 1 of the 74 brain regions (37 per hemisphere), and the sum of the weighted lateral connections between vertices belonging to two different brain regions was taken as the short-range connectivity between those two regions.

To capture white matter decreases, we studied the effects of long-range pruning by repeatedly decreasing the coupling weight of randomly selected node pairs of the long-range connectivities, and to capture decreasing lateral connections, we used short-range connectivity with increasingly faster spatial decay in steps of 10 mm. Matrices were combined in both cases, with pruning affecting selectively the short-range or the long-range contributions of the combined matrix (Figure 3.1).

Simulations were run for four different connectivity levels, with a 16%

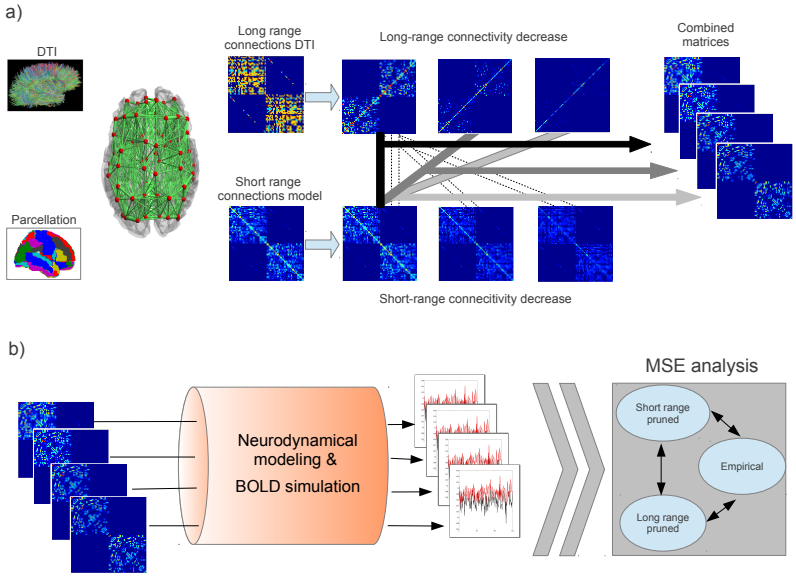

Figure 3.1: *Methods: a) Construction of matrices representing connectivity decreases found in aging. A brain graph (second to left) is constructed from DTI fiber estimations between brain areas. Each node on the graph (red) represents a brain area, and connection strengths (green) determine the values in the connectivity matrices. To determine if there are differential effects, short-range and long-range connections are pruned separately, and matrices are then combined (shown for long-range pruning). b) Simulation and analysis pipeline. Dynamic mean field simulations are run for different levels of connectivity decrease for both scenarios, and BOLD time series are simulated for complexity (MSE) analysis.*

connectivity decrease for every step, for both long-range pruning and short-range pruning.

To locate the system at Resting State dynamics, we here set the global coupling weight between nodes w to 3.50, where the original, unpruned

matrix was at its critical point just below bifurcation. and simulations remained in an asynchronous low-firing regime.

3.3. Complexity and Multiscale Entropy

"Complexity" is a dynamic neurophysiological marker of efficient processing, cognitive performance and age, representing the richness of information in a system. For time series, it can be quantified by entropy-related measures such as MSE (Costa et al., 2005, 2002) or Permutation Entropy (Richman & Moorman, 2000). Complexity has been linked to behavioral stability and task performance (McIntosh et al., 2008, 2010; Yang et al., 2012) as well as knowledge (Heisz et al., 2012). It increases in the early years of life (Lippé et al., 2009; McIntosh et al., 2008) as processing shifts from local to more distributed processing (Vakorin et al., 2011). This tuning process reflects the increasing functional differentiation with development. In older adults, less complex dynamics are observed at rest (Yang et al., 2012), and a smaller increase in complexity is observed in task (Garrett et al., 2012) or photic stimulation (Takahashi et al., 2009). These findings suggest that MSE can serve as a neurophysiological marker between underlying structure and functional network integrity or efficiency. Healthy, young brains are generally described by more complex time series, and the findings of Yang et al. (2012) suggest that this relation can even be found in relatively short, resting fMRI data sets.

Many physiological systems produce irregular, complex time series, so highly regular states often mark dysfunction and disease (Pincus & Goldberger, 1994; Goldberger et al., 2002). However, an increase in irregularity does not always mean an increase in complexity: noise signals are highly irregular and maximize entropy on the first temporal scale, but lose complexity quickly towards larger time scales (Goldberger et al., 2002): over longer periods, noise is deterministic, as it has one single

expected mean value. To address this multiscale nature of truly complex time series, Costa et al. (2002, 2005) developed the MSE measure, which estimates sample entropy (Richman & Moorman, 2000) on the original time series as well as on downsampled versions, revealing variability of the signal across different time scales. Given a time series x of length t, a downsampled time series x_s is calculated for every scale factor s by constructing t/s non-overlapping windows of x, and taking the mean of all x in the window as new value for x_t, shortening x_s by the scale factor. Sample entropy is then calculated for each scale. It is defined as the negative natural logarithm of the conditional probability that sequences in a dataset that are similar for m data points (within similarity tolerance r, given as fraction of the standard deviation of the dataset) will remain similar adding another data point. We calculated MSE using the physionet (Goldberger et al., 2000) MSE algorithm (available at `http://www.physionet.org/physiotools/mse/`) both on the neuronal activity and the virtual BOLD signal for all simulations. For the BOLD signal, biophysical parameters were taken as in Friston et al. (2003), and sampling rate = 2500ms and lowpass filtering (at 0.08 Hz) were set equal to the values in Yang et al. (2012) for comparability. To be able to calculate MSE for five time scales for the BOLD time series to and compare the results to empirical data, we used pattern length m = 1 and similarity factor r = 0.35 (varied between 0.05 and 0.5 without changes in the results patterns). MSE was calculated from the neuronal time series at sampling resolution of 125 ms and from the BOLD signal at 2500 ms over scales 1:5 (2.5-12.5 s).

3.4. Complexity declines in aging

Results are presented from simulations of the dynamical mean field model for decreasing levels of structural connectivity, imitating the decreasing connectivity in the adult human brain. Network structure was derived from a combined anatomical connectome of long-range and short-range

connections between brain areas, and the lower-connected matrices were constructed by pruning at one of the two ranges. For each pruning level and method, MSE was then calculated for both the neuronal time series and an fMRI BOLD model. For the rate model, both short-range and long-range pruning led to lower complexity values over all scales. As visible in Figure 3.2, MSE decrease was strongest for the first pruning step. Entropy decreases with respect to the baseline were significant in all cases (all p-values < 0.001), resembling the difference between younger and older subjects in the empirical data, with no differences between short-range and long-range pruning (largest $t(18) = 1.60$, $p = 0.13$).

MSE curves from the BOLD model time series are shown in Fig 3.3. For all simulations using the BOLD model, there was an increase in entropy from scale one to two, after which it gradually declined. This initial increase was not visible in the empirical data of Yang et al. (2012), where the entropy values decreased gradually by about 0.1 from scales one to five. The difference in the shape of the MSE curve appeared in spite of the fact that the same BOLD sampling, lowpass filtering, and MSE calculation parameters were used. On the second to fifth scales, the entropy values were quite similar in shape and amplitude to the empirical data, though with a steeper drop in complexity across scales. The increase in entropy in the model from the time scale of about 2.5 to 5-10 seconds indicates that the network dynamics are more regular on the fastest timescale, and that network interactions are therefore mainly shaped on the slower time scales. This is in line with the non-oscillatory network dynamics and slow NMDA component, producing slow BOLD fluctuations. The difference between model and empirical data on the fastest time scale may have various possible reasons,though. On the empirical side, scanner, movement or physiological artifacts may appear. Concerning neural dynamics, the model is in a low-firing regime producing slow BOLD fluctuations of several seconds (for detail, see Deco & Jirsa, 2012). At faster time scales, neural oscillations and local dynamics may modulate the dynamics of each node in a way that would not be captured by the model. However, if this were the case, the same pattern should be visible in rate-

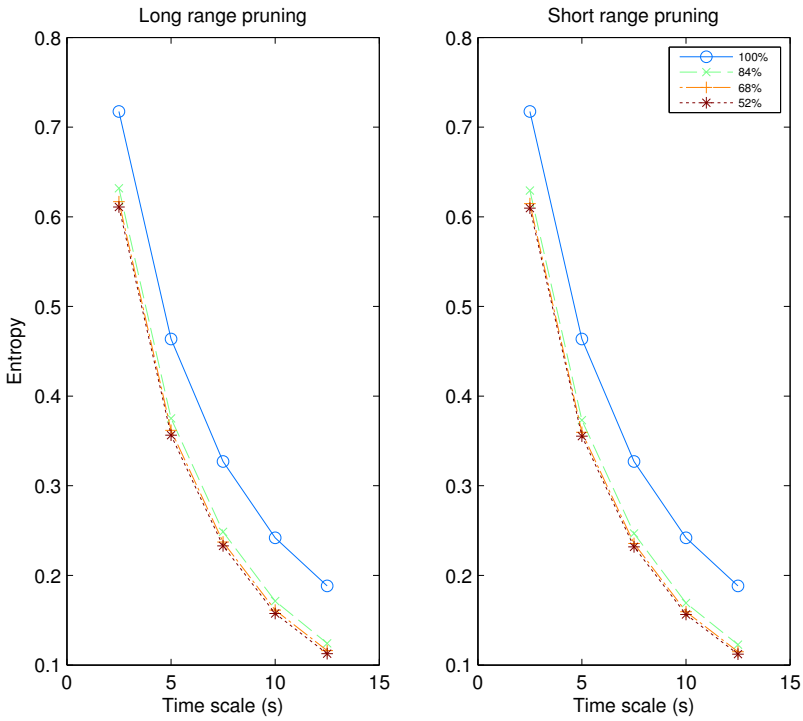

Figure 3.2: MSE
in a model for aging]*Rate MSE: MSE curves calculated from the down-sampled time series of the dynamic mean field model for time scales from 2.5s to 12.5s.*

derived MSE measures. As the origin of this difference is unresolved and manifests on the fastest scale, we focus in the following on the slower time scales 3-5 (7.5-12.5s) for the BOLD signal.

The effect of pruning was much smaller than for the neuronal rate (Figure 3.4). There were no differences between the two pruning methods on any of the scales (largest $t(18) = 0.94$, $p=n.s.$), and the effect of decreasing the density of the connectome became apparent as an inter-

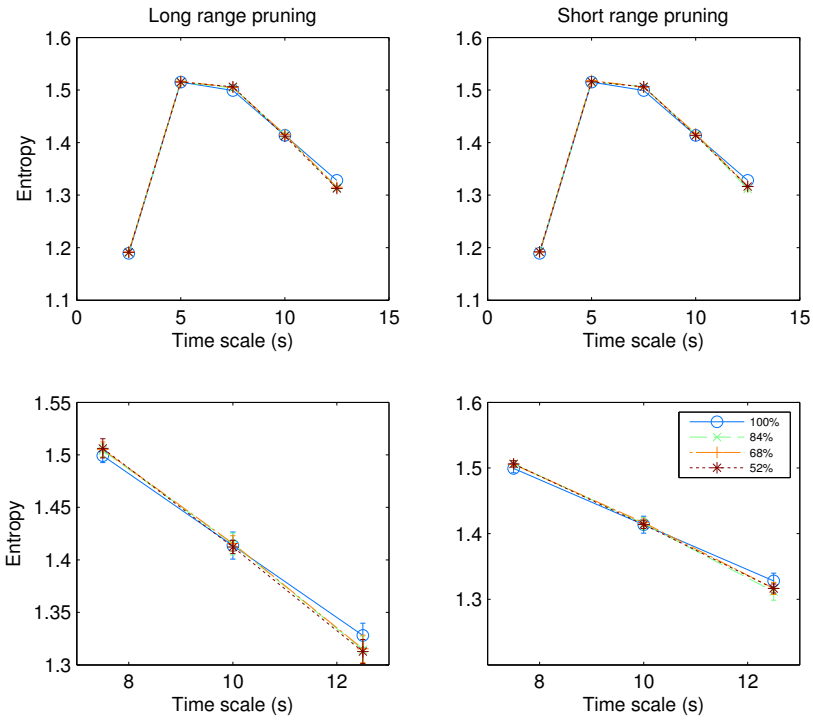

Figure 3.3: Multiscale Entropy
in aging - simulated BOLD signal]*BOLD MSE: MSE curves calculated from the simulated BOLD time series of the model. Top row: BOLD scales 2.5s-12.5s, bottom row: closeup of top row at the slowest scales. Error bars in lower panels depict standard deviations.*

action of pruning and scales. The tendentially higher complexity of the pruned cases at the third scale (highest $t(9) = -2.67$, $p < .05$ for short range pruning; p-values for long-range pruning between 0.05 and 0.10, their difference n.s.) inverted to lower complexity at the slowest time scale ($t(9)=$3.14, $p <.05$)) for all lower-connected cases (Figure 3.3, top right panel). On this scale, the pruned case reached lower entropy values due to its steeper slope over lower scales (lowest $t(9) = -3.14$,

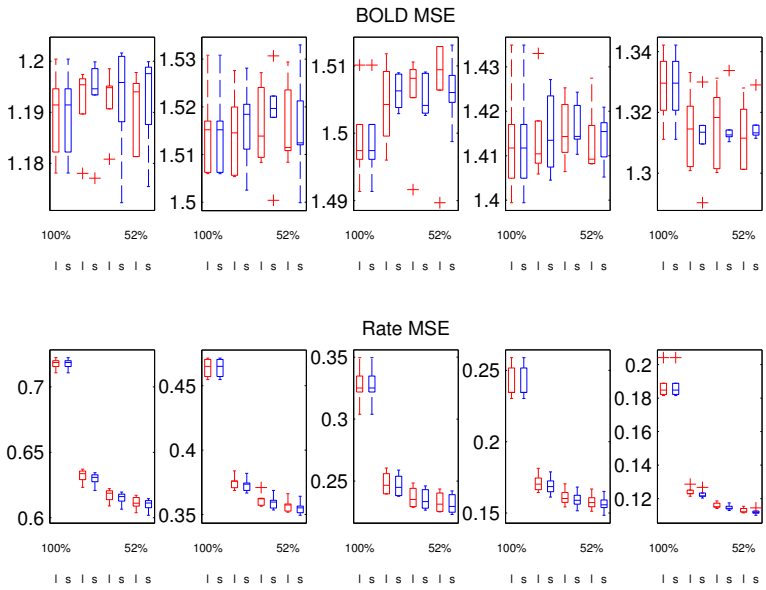

Figure 3.4: MSE
in aging - boxplots for scales and trial]*MSE Boxplots: Boxplots of MSE values from ten trials for all scales, for BOLD (top row) and for rate (bottom row) MSE. Each panel shows one boxplot for each connectivity density (100%, 84%, 68%, 52%) for long-range pruning (red, 'l') and short-range pruning (blue, 's'). Boxplots are centered on the median and are limited by the quartiles, and whiskers extend by a factor of 1.5. Outliers are marked by '+'.*

$p < .05$). In summary, rate based measures showed concordance with empirical fMRI-BOLD MSE decreases with weakening connectivity. Model BOLD complexity showed lower entropy for lower connectivities on the largest scale only.

Here, we investigated the changes in dynamical complexity of a model of spontaneous large scale activity with decreasing connectivity. Connectome pruning was implemented by two different algorithms targeting

diffuse lateral short-range connections along the cortical sheet and DTI-based white fiber tract long-range connections, respectively. MSE complexity measures were calculated from simulated neuronal and BOLD dynamics based on a large scale computational model of cortical resting state dynamics. From the model perspective, the decrease in complexity observed in the neuronal time series corresponded best to an increasing distance from the model working point at which the model best reproduces healthy resting state functional connectivity (Deco & Jirsa, 2012). This point lays just below the bifurcation from a global low activity state to the appearance of high firing states and multistability in the system. From this point, as a consequence of pruning, mutual communication between the nodes becomes weaker and dynamics modulations from large-scale connectivity quickly decreased on large time scales.

The fact that the largest difference in entropy was caused by the first 16% of connectivity decline suggests that the resulting complexity of the model is most strongly affected near the dynamical working point of the model. Once the system is not near its dynamical working point anymore, the spontaneous dynamics of the nodes will be largely dominated by their internal dynamics. This may also be the reason why short-range and long-range pruning did not show differential effects on complexity: while the increasingly different connectomes may give rise to different network structures and attractor landscapes in high activity states, the main effect of connectivity reduction will be similar in the low-activity regime. In analogy, one would expect a similarly lower complexity in older brains due to structural decline and synaptic efficacy loss independent of the specific hypoconnection structure, while the form of the functional changes would depend on the specifics of the connectivity losses. For comparison, We show MSE curves for very high and low couplings in Inline Supplementary Figures 3.5 and 3.6. In line with our interpretation, MSE is highest for optimal coupling, and lower for both high and low-connected cases, with lowest MSE for low coupling strength. Note, however, that, the very high coupling state is not straightforward to interpret as it leaves the low activity regime for which the dynamic mean field is well defined.

The interpretation of these results is limited by the fact that, while pruning resulted in lower rate entropy over most scales as expected from the model, complexity of the simulated BOLD signal was affected much less clearly than expected. Here, the model did not reproduce the empirical pattern of steady decline and lower entropy for decreased connectivity occuring in old age over most scales. There may be various reasons for this. Surely, a network of similar nodes may only produce such effects that lay in the model dynamics and connectivity itself, and not those that may be due to changes in the local dynamics. This should, in principle, not only affect the BOLD dynamics differentially, but differences in sampling, filtering, and the BOLD conversion model itself introduce factors that may shape both signals differently.

In summary, both BOLD and rate signals did point towards lower complexity caused by structural connectivity decline on large scales. This effect may well be connected to the large proportion of cognitive performance decrease explained by processing speed changes in aging (Salthouse, 1996), as the system needs higher overall activation and provides lower communication efficiency. A more in depth comparison of pruning with and without compensatory shifting of the global or specific couplings, and pruning-related changes in graph properties are worthwhile topics for further investigation, e.g. in the context of stroke recovery.

3.5. Conclusions

So far, the major focus has been on the spatial components of resting state networks and their alteration due to external or internal factors. We are only beginning to understand the spatiotemporal dynamics of RSN and their interactions. This is of particular interest to resting state research, as complexity measures can be used as a biomarker of the network dynamics independent of external stimuli, and how the system is affected by different consciousness states and diseases. We suggest that scrutiniz-

ing complexity in models may contribute to a better understanding of the time scales of network interactions and allow for comparison of different models in terms of their ability to recreate observable complexity patterns across different scales.

We conclude that structural connectivity decrease led to lower complexity on slow time scales in a biophysically based computational large-scale model mainly in the rate dynamics. From the perspective of model, decreased MSE in older adults' resting fMRI time recordings can best be explained as a displacement of the system from its optimal dynamical working point. Multiscale complexity measures can be powerful tools to link the structural connectome to functional brain dynamics on various temporal scales and, as this study shows, can serve as functional biomarkers to link the dynamics and performance of virtual brain models to the richness of brain network activity.

3.6. Acknowledgements

The authors declare to have no conflicts of Interest. GD was supported by the ERC Advanced Grant: DYSTRUCTURE (n. 295129), by the Spanish Research Project SAF2010-16085 and by the CONSOLIDER-INGENIO 2010 Programme CSD2007-00012, and the FP7-ICT BrainScales. The research reported herein was supported by the Brain Network Recovery Group through the James S. McDonnell Foundation. TTN was supported by the SUR of the DEC of the Catalan Government and by the FSE. We thank Mohit Adhikari and Sven Hilbert for helpful comments on earlier versions of the manuscript.

3.7. Supplementary Figures

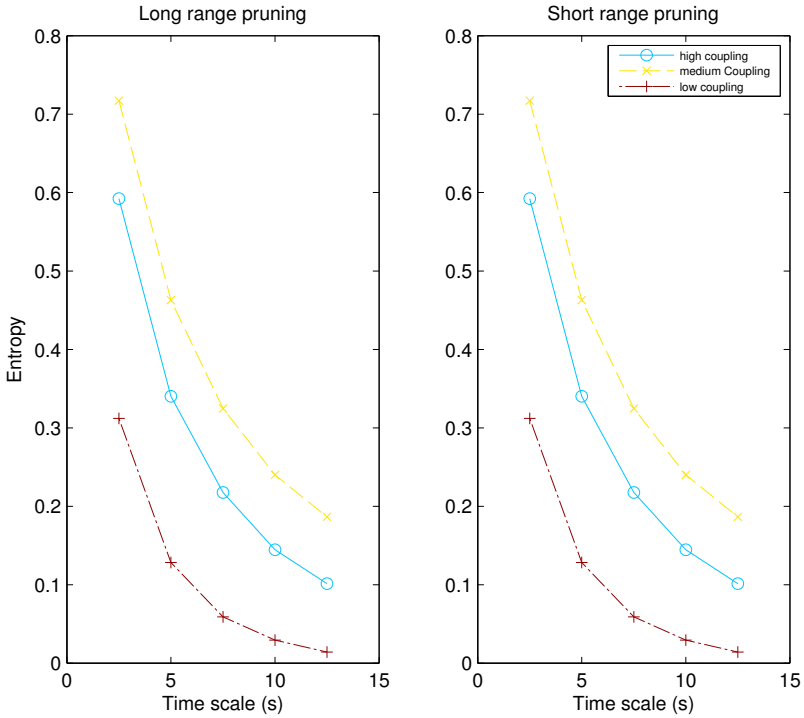

Figure 3.5: MSE
in aging - MSE-coupling rate]*(Supplemenary) Rate MSE: MSE curves for high (w=10.00), medium (w=3.50) and low (w=0.01) global couplings for unpruned connectivity matrices; calculated from the down-sampled time series of the dynamic mean field model for time scales from 2.5s to 12.5s.*

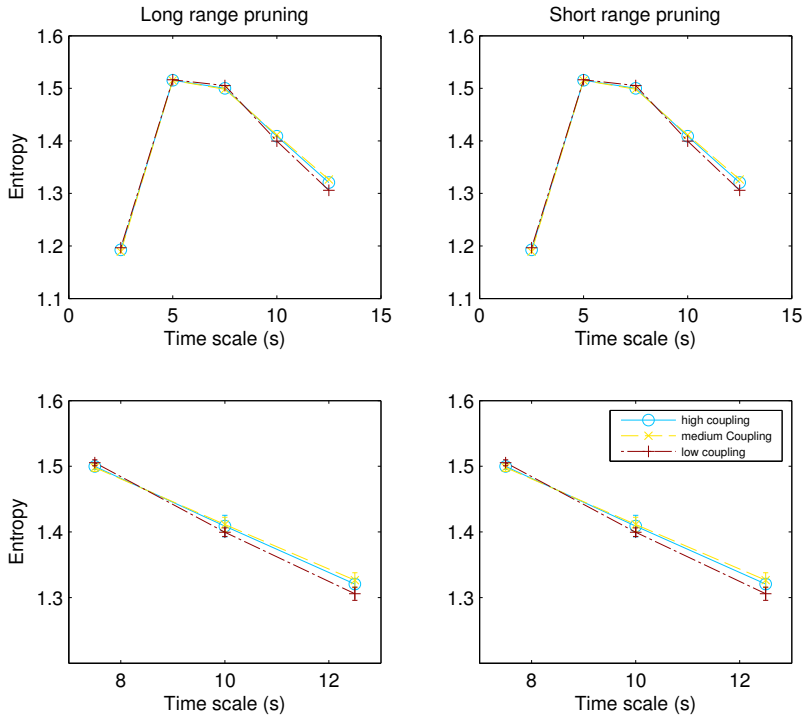

Figure 3.6: MSE
in aging - MSE-coupling simulated BOLD]*(Supplemenary) BOLD MSE: MSE curves for high (w=10.00), medium (w=3.50) and low (w=0.01) global couplings for unpruned connectivity matrices. Top row: BOLD scales 2.5s-12.5s, bottom row: closeup of top row at the slowest scales. Error bars in lower panels depict standard deviations.*

4. Resting State Rhythms: oscillations and delays

So far, we have introduced empirical findings of RSNs and RS activity in Chapter 1, as well as the rationale for modeling this activity in large-scale computational models in Chapter 2. In Chapter 3, we investigated the influence of increasing distance from the optimal working point near the bifurcation of an attractor network, finding that structural disconnection may thus decrease ongoing brain signal complexity. Prompted by the increasing number of electrophysiological recordings of RS activity, we will next turn to the question how oscillatory dynamics influence the behavior and parameter interactions of the model. To achieve this, we use a modified spiking-neuron network model with the same structural setup, but added input-dependent oscillatory dynamics on the local level.

This chapter reproduces a paper with the title: "How delays matter in an oscillatory whole brain spiking-neuron network model for MEG alpha-rhythms at rest".[1] The work was published in NeuroImage (NeuroImage 87 (2014) 383-394) by Nakagawa T. T., Woolrich M., Luckhoo H., Joensson M., Mohseni H., Kringelbach M. L., Jirsa V. K., and Deco G. The abstract reads:

> In recent years the study of the intrinsic brain dynamics in a relaxed awake state in the absence of any specific task has gained increasing attention, as spontaneous neural activity has been found to be highly structured at a large scale. This so called resting state activity has been found to be comprised by nonrandom spatiotemporal patterns and fluctuations, and

[1] Nakagawa et al. (2014)

several Resting State Networks (RSN) have been found in BOLD-fMRI as well as in MEG signal power envelope correlations. The underlying anatomical connectivity structure between areas of the brain has been identified as being a key to the observed functional network connectivity, but the mechanisms behind this are still underdetermined. Theoretical large-scale brain models for fMRI data have corroborated the importance of the connectome in shaping network dynamics, while the importance of delays and noise differ between studies and depend on the models' specific dynamics. In the current study, we present a spiking neuron network model that is able to produce noisy, distributed alpha-oscillations, matching the power peak in the spectrum of group resting state MEG recordings. We studied how well the model captured the inter-node correlation structure of the alpha-band power envelopes for different delays between brain areas, and found that the model performs best for propagation delays inside the physiological range (5-10m/s). Delays also shift the transition from noisy to bursting oscillations to higher global coupling values in the model. Thus, in contrast to the asynchronous fMRI state, delays are important to consider in the presence of oscillation.

4.1. Introduction

It is an astonishingly hard task to do, think, and attend nothing; thoughts, observations, and feelings naturally arise from within us, more or less at random. Without any specific external stimulation, we fluctuate in our mental states as the brain fluctuates between different activity patterns. While in the study of cognitive tasks, these fluctuations seem to be a nuisance that necessitate averaging over many trials, they are themselves structured and informative in many ways. fMRI and, more recently,

neurophysiological imaging studies have found that the brain's spontaneous activity patterns decompose into networks of brain areas, defined primarily not by their mean activity level but by the functional connectivity between them (Mazoyer et al., 2001). This way, several Resting State Networks (RSN) with known task-related functional importance such as sensorimotor, visual and attentional areas and networks, have been identified in spontaneous brain activity in the absence of tasks (Biswal et al., 1995, 1997; Cordes et al., 2000, 2002; Damoiseaux et al., 2006; De Luca et al., 2005, 2006; Lowe et al., 1998). A specific 'Default Mode Network' (Gusnard & Raichle, 2001; Greicius et al., 2003; Damoiseaux et al., 2006; van den Heuvel et al., 2008; Buckner et al., 2008b), an RSN which shows higher activity during the resting state than during various task conditions, has also been identified. These functional networks and their dynamics are determined both by the underlying anatomical connectivity and the local neuronal dynamics and interactions, leading to spatiotemporal patterns and oscillations at different time scales. To understand them is of key value to understanding the brain's cognitive machinery and its ability to flexibly control mental states. So, it is of prime interest to gain deeper insight into the origins and mechanisms of spontaneous functional connectivity (FC) patterns, and we can apply theoretical models and numerical simulations of resting state activity to study these dynamics.

resting state models take advantage of recent technical advances capable of tracking white fiber tracts noninvasively via DTI/DSI in humans (Cabral et al., 2011; Deco & Jirsa, 2012; Honey et al., 2009, 2010; Izhikevich & Edelman, 2008; Senden et al., 2012) to combine realistic neuroanatomical long-range connections between brain areas with the models' local dynamics (oscillators, neural masses, or explicitly modeled neurons) in order to construct a dynamical cortical model for the human cortex. The simulated activity patterns from the freely interacting network have successfully reproduced resting state dynamics: Anticorrelated functional networks such as found by Fox et al. (2005) in cortex have been observed to emerge in models with different local dynamics (e.g. Honey et al. (2007): chaotic oscillators; Deco et al. (2009): Wilson-

Cowan oscillators). Slow fMRI rhythms below 1 Hz observed by several authors in fMRI resting state recordings (Biswal et al., 1995; Cordes et al., 2001; Fransson, 2005; Damoiseaux et al., 2006; De Luca et al., 2006) can also be found in Wilson-Cowan (Deco et al., 2009), Kuramoto oscillator (Cabral et al., 2011), neural mass (Honey et al., 2007), and spiking neuron models (Deco & Jirsa, 2012). In all these models, the underlying network structure is crucial in shaping the network dynamics and maintaining the system close to criticality (see Deco et al., 2013a). Further, delays were found to shape the emerging spatial patterns and modes in oscillatory networks much more in directed graphs (Ghosh et al., 2008b,a) than in undirected graphs (Knock et al., 2009). In general, the extent to which delays (and noise) critically influence the global dynamics and interactions, depends also on the nature of local network dynamics (Deco et al., 2009; Deco & Corbetta, 2011). Consequently, the choice of local dynamics depends on various factors and goals that are pursued by the studies, as for example, the desired level of abstraction/physiological realism, the time- and spatial scales, and the network mechanisms to be investigated.

While modeling studies have so far been mostly focused on fMRI FC and slow oscillations that were empirically observed, recent neurophysiological studies have investigated the resting state with increasing temporal resolution. Using combined EEG/fMRI and source-reconstructed MEG recordings to increase spatial resolution, these studies have found that alpha and beta bandlimited power (BLP) envelopes retrace fMRI based FC patterns and slow fMRI rhythms (Mantini et al., 2007; de Pasquale et al., 2010; Liu et al., 2010; Brookes et al., 2011a,c; Hipp et al., 2012). So far, the various anatomically informed, oscillatory dynamics network models have been limited to fMRI, and have not yet been validated with empirical neurophysiological data, which can capture faster oscillations. In MEG recordings, for example, alpha-oscillations are especially predominant in, and have always been associated with the resting state. They are readily identifiable and robustly found in electrophysiological recordings since the first human EEG studies by Hans Berger a century ago (for a historical overview, see Shaw, 2003). The origin of this typical alpha-

acitivity is not comprehensively determined yet, though self-sustaining sources have been identified both in cortex (Lopes da Silva, 1991) and in the thalamocortical loop (Lopes da Silva et al., 1974). In fact, alpha-activity is most likely a collection of rhythms from several sources (Ben-Simon et al., 2008; Freyer et al., 2011, 2012; Neymotin et al., 2011; Shaw, 2003) which may contribute to the variability of alpha-rhythm characteristics (e.g. peak frequency, amplitude, topography) found in the brain both over time (Freyer et al., 2011, 2012) and between subjects (Chiang et al., 2011).

In the present study, we focused on the influence of noisy oscillations on bandlimited connectivity patterns in a biophysical setting. As the integrity of a model always depends on the spatial connectivity structure, but not in all cases on the temporal structure (e.g. in the case of chaotic oscillators, (Honey et al., 2007, 2009); or in the asynchronous state (Deco & Jirsa, 2012)), it is unclear to what extent the brain's effective connectivity is affected by, and sensitive to the delays introduced by long fibers and limited transmission velocities in the brain, when considering complex neuronal population dynamics (Knock et al., 2009). We here aimed to study the effect of delays on the FC structure and model performance in a neurophysiologically detailed model by recreating the irregular oscillations evident in MEG recordings in the alpha-band and relating the numerical simulations for different delays and the empirical data. For this, we employed a leaky-integrate-and-fire (LIF) spiking neuron model with realistic NMDA, AMPA and GABA synapses (Deco & Jirsa, 2012), and an oscillation-inducing calcium-dependent hyperpolarization current (triggering spike-frequency adaptation SFA; e.g. Fuhrmann et al., 2002; Liu & Wang, 2001; Meech, 1978). In the following, we will show that the presented model exhibits network oscillations in the alpha-range when the model nodes are coupled, and that it successfully captures alpha-band FC. It does so most robustly in the presence of delayed large scale connectivity, suggesting a functional importance for long-range delays in sustaining interaction patterns between areas and resting state networks in the healthy brain.

4.2. Methods

4.2.1. Neuroanatomical connectivity matrix

Weighted neuroanatomical connectivity matrices were extracted from the diffusion tensor imaging (DTI) data of 21 healthy, normal participants (11 males, aged 22-45 years). Extraction methods were based on Gong et al. (2009). Diffusion MRI was acquired by using a single-shot echo planar imaging-based sequence with coverage of the whole brain; repetition time (TR), 9390 ms; echo time (TE), 65 ms. DTI images utilized 32 optimal nonlinear diffusion weighting directions (b = 1200 s/mm2) and 2 non-diffusion weighted volumes; reconstructed matrix = 128x128x45; reconstructed voxel size 2.0mm x 2.0mm x 2.0mm. We also acquired T1-weighted structural images with a threedimensional 'FLASH' sequence (TR = 12 ms, TE = 5.6 ms, flip angle = 19°, with elliptical sampling of k-space, giving a voxel size of 1x1x1 mm in 5.05 mins). All scans were performed on the same Philips Achieva 1.5 Tesla Magnet. Weighted brain networks were constructed by first parcellating the brain, and then extracting the network from interregional connectivity analysis. Brain parcellation was constructed using the automated anatomical labeling (AAL, Tzourio-Mazoyer et al., 2002) template. The brain was parsed into 45 regions per hemisphere (90 in total), each region representing a node of the brain network. For each participant, parcellation was conducted in the diffusion MRI native space, and the b0 image was coregistered linearly to the T1-weighted structural image with the Flirt Tool (FMRIB, Oxford, Jenkinson et al., 2002). The transformed T1-weighted image was next mapped to the T1 template of ICBM152 in Montreal Neurological Institute (MNI) space (Collins et al., 1994), inversed, and further applied to warp the AAL mask from MNI space to the diffusion MRI native space, where interpolation using nearest-neighbor method ensured that the discrete labeling values were preserved. For the analysis of interregional connectivity (via Fdt toolbox in FSL, Oxford), diffusion MRI

data was preprocessed by coregistering the diffusion-weighted images to a reference volume using an affine transformation for the correction of head motion as well as eddy current induced image distortion.

The local probability distribution of fiber direction and voxel connectivity probability were estimated via probabilistic tractography (Behrens et al., 2007), and the procedure was then extended to the level of each region. The seed regions selected for each of the parcellated brain regions and the connectivity probability to each of the other 89 regions was calculated. It must be noted that because of the dependence of tractography on the seeding location, the probability from *i* to *j* is not necessarily equivalent to that from *j* to *i*. However, these two probabilities are highly correlated across the brain for all subjects (the least Pearson $r = 0.70, p < 10^{-50}$). Therefore, the undirectional connectivity probability P_{ij} between region *i* and *j* was defined by averaging these two probabilities. Calculations of regional connectivity probability were implemented using in-house Perl scripts.

Finally, a weighted network graph was constructed by defining a distance and weight associated with each edge. The high connectivity probability between brain regions were taken here to be short distances in a graph. Specifically, $W_{ij} = 1 - P_{ij}$ was computed as the distance/weight between brain region *i* and *j*, as used in previous literature (Achard & Bullmore, 2007). Note that the distance here does not correspond to the physical length of the white matter pathway linking the brain regions. For each subject, a 90×90 weighted cortical network/graph *W* was constructed, representing the anatomical organization of cerebral cortex.

4.2.2. MEG Data Collection and Analysis

MEG data were recorded from 10 healthy participants who underwent a five minutes resting state scan with their eyes closed. Recordings were performed at 1000 Hz sampling frequency on an Elekta Neuromag (Elekta

Neuromag Oy, Helsinki, Finland) with 102 magnetometers and 102 pairs of orthogonal radial gradiometers. Subjects' head shape was recorded using a Polhemus Isotrack system, and four head position indicator (HPI) coils allowed for the head to be localized in the scanner. Data preprocessing included signal space separation (Taulu et al., 2005), denoising with independent component analysis, source reconstruction and bandpass filtering of the MEG signal. Signal space separation compensates for external interference and sensor artifacts by projecting the MEG data onto a basis set of spherical harmonics. Harmonics corresponding to sources originating from within the sensor array are preserved whilst interfering sources from outside the environment surrounding the sensor array are rejected. The sensor space MEG data were denoised using temporal independent component analysis (ICA) to remove cardiac, 50 Hz mains and, in some subjects, eye movement artifacts.

Each dataset was then coregistered into the MNI space by registering the canonical MNI template to the Polhemus head shape data. A local spheres forward model (Huang et al., 1999) was then estimated using the subject's head shape. Both coregistration and forward model estimation were performed with the Matlab SPM8 package (FIL,UCL). The MEG data were then bandpass filtered into delta (1-5 Hz), theta (4-8 Hz), alpha (8-13 Hz), beta (13-30 Hz), low gamma (30-48Hz) and high gamma (52-80 Hz) bands. An LCMV beamformer was used to transform the original sensor time series for each frequency band into source space time series, that is, to reconstruct the activity at the 90 locations defined by the AAL brain parcellation.

Functional connectivity scores between node pairs were estimated by taking the bandlimited power envelopes of a pair of nodes, regressing one out from the other to orthogonalize the time series and thereby removing any zerolag correlations. We then calculated the Pearson correlation between the orthogonalized time series. Since the orthogonalization can be performed in both directions (X from Y and Y from X), the mean of both resulting correlation values was taken as the final correlation value. The

full approach is described in detail and discussed in Brookes et al. (2012) and is the same as in Hipp et al. (2012). Functional connectivity scores between node pairs were estimated in the following way. For a given frequency band, a pair of nodes was selected. The first node of the pair was regressed from the second to orthogonalize the two time series, removing any zerolag correlations induced by field spread. The correlation between the low pass filtered envelopes of the two orthogonalized time series was estimated, and a correlation matrix computed (Figure 4.1 a).

This procedure was repeated but instead regressing the second voxel from the first and estimating the envelope correlation (Brookes et al., 2012; Hipp et al., 2012). The two different correlation values were then averaged to give a single correlation score. Here, we consider mainly the MEG signal's alpha BLP based on findings that, along with beta, it best captures the functional connectivity of RSN in MEG data Brookes et al. (2011b); Hipp et al. (2012); Luckhoo et al. (2012)

4.2.3. Global cortical model

The global model consists of 90 model nodes, each comprising an inhibitory and an excitatory pool of neurons, whose properties are described in detail below. Each node of the model represents one brain area, and the connections between any two nodes are implemented by interconnecting the respective neurons between the excitatory pools via NMDA and AMPA synapses. Transmission strengths are weighted by the corresponding value in the neuroanatomical connectivity matrix described above. As the DTI measure used to extract the structural connectivity is symmetrical, so are the connectivities in the model. Connections between nodes are limited to act between excitatory pools as they are here considered to represent long-range axons of pyramidal neurons. These connections are weighted by a global coupling factor W, which determines the overall connectivity strength in the resulting network. W, and the propagation velocity v are the main parameters to be varied in the simulations to find

an area of parameter space where the correspondence between empirical and model data becomes maximal. In the brain, delays depend on axonal transmission times, which are determined by axon diameter, myelinization, and distance. The delay between two brain areas in the model was determined by their euclidean distance in MNI-templated source space (max=160mm) divided by v, with propagation speed v in m/s and inter-area distance D in mm. The Euclidean distances are necessarily a lower bound estimate of fiber tract lengths, therefore propagation speeds would here be somewhat underestimated.

1. Local dynamics

   Each node's local dynamics are modeled with 200 spiking neurons, featuring a biophysically realistic neural network model, consisting of leaky-integrate-and-fire (LIF) spiking neurons with NMDA, AMPA, and GABA$_A$ receptors (Brunel & Wang, 2001). The model was first adapted for modeling resting state dynamics by, and is described in detail in Deco & Jirsa (2012). Their detailed global attractor model combines a realistic mechanistic model at the level of each single brain area with the large-scale cortical network structure. In the model, every node consists of an excitatory (index E,N_E =160) and an inhibitory pool (index I,N_I =40). The local dynamics are described by combining the dynamical equations of each neuron and the synaptic variables with all connected neurons. Excitatory/inhibitory neuron ratio and conductivities were balanced to reflect empirically realistic values and low spontaneous firing rates (DeFelipe, 1993; Destexhe et al., 1998) in each node (Figure 4.3, inlay).

   Neurons inside a node were all-to-all connected in order to keep neuron numbers low and simulations feasible. There were N_E excitatory and N_I inhibitory presynaptic connections for every neuron, in addition to the excitatory inputs from long-range connections from pyramidal cells of other nodes and background input from 800 external neurons as described at the end of this paragraph.

The neurons are modeled as LIF units that are characterized by the dynamics of their membrane potential. When the membrane voltage crosses a threshold V_{thr}, the neuron generates a spike, which is transmitted to connected neurons via its AMPA and NMDA or GABA synapses, and the membrane voltage is set to V_{reset}, where it is held fixed for the neuron's refractory period τ_{ref}. The subthreshold equation for the membrane potential is given by:

$$C_m^{E,I}\frac{dV(t)}{dt} = -g_m(V(t) - V_L) + I_{total}(t), \tag{4.1}$$

describing a basic RC-circuit with the cell membrane capacitance C_m in parallel with membrane resistance R_m, leak conductance g_m = $1/R_m$, resting potential $V_L = -70mV$, and synaptic and afterhyperpolarization (AHP) currents. Membrane time constants are given in Table 4.1. The total current I_{total} is the sum of synaptic external excitatory AMPA currents, AMPA and NMDA recurrent excitatory currents, GABAergic inhibitory currents and an afterhyperpolarization current

$$I_{total}(t) = I_{AMPA,ext}(t)+I_{AMPA}(t)+I_{NMDA}(t)+I_{GABA}(t)+I_{AHP}(t). \tag{4.2}$$

The synaptic currents and their mediation through gating variables $s_i^j(t)$ are described by:

$$I_{AMPA,ext}(t) = g_{AMPA,ext}(V(t) - V_E)\sum_{j=1}^{N_{ext}} s^j_{AMPA,ext}(t), \tag{4.3}$$

$$\frac{ds^j_{AMPA,ext}(t)}{dt} = \frac{s^j_{AMPA,ext}(t)}{\tau_{AMPA}} + \sum_k \delta(t - t_k^j), \tag{4.4}$$

$$I_{AMPA,rec}(t) = g_{AMPA,rec}(V(t) - V_E)\sum_{j=1}^{N_E} w_j s^j_{AMPA,ext}(t), \tag{4.5}$$

Table 4.1: Membrane and synaptic parameters

Parameter	Excitatory (N_E = 160)	Inhibitory (N_I = 40)
C_m	0.5 nF	0.2 nF
g_m	25 nS	20 nS
V_L	-70 mV	-70 mV
V_{thr}	-50 mV	-50 mV
V_{reset}	-55 mV	-55 mV
τ_{ref}	2 ms	1 ms
$g_{AMPA,ext}$	2.496 nS	1.944 nS
$g_{AMPA,rec}$	0.104 nS	0.081 nS
$g_{NMDA,rec}$	0.327 nS	0.258 nS
g_{GABA}	4.375 nS	3.4055 nS

$$\frac{ds^j_{AMPA,rec}(t)}{dt} = \frac{s^j_{AMPA,rec}(t)}{\tau_{AMPA}} + \sum_k \delta(t - t^j_k), \tag{4.6}$$

$$I_{NMDA,rec}(t) = \frac{g_{NMDA,rec}(V(t) - V_E)}{1 + \gamma e^{-\beta V(t)}} \sum_{j=1}^{N_E} w_j s^j_{NMDA,rec}(t), \tag{4.7}$$

$$\frac{ds^j_{NMDA,rec}(t)}{dt} = \frac{s^j_{NMDA,rec}(t)}{\tau_{NMDA,decay}} + \alpha x_j(t)(1 - s^j_{NMDA,rec}(t)), \tag{4.8}$$

$$\frac{dx^j_{NMDA,rec}(t)}{dt} = \frac{x^j_{NMDA,rec}(t)}{\tau_{NMDA,rise}} + \sum_k \delta(t - t^j_k), \tag{4.9}$$

$$I_{GABA}(t) = g_{GABA}(V(t) - V_I) \sum_{j=1}^{N_I} w_j s^j_{GABA}(t), \tag{4.10}$$

$$\frac{ds^j_{GABA}(t)}{dt} = \frac{s^j_{GABA}(t)}{\tau_{GABA}} + \sum_k \delta(t - t^j_k), \tag{4.11}$$

with indices over neurons j, synaptic conductances g, excitatory and inhibitory reversal potantials V_E and V_I, respectively, the Dirac-delta function δ, and synaptic weight parameter w_j (determining

the connection strengths between and within neural populations). NMDA currents are voltage dependent and modulated by intracellular calcium concentrations (equation 4.7). Connections between excitatory and inhibitory pools were set to 1, and recurrent self-excitation to w_+ = 1.5. Synaptic parameters were V_E = 0 mV, V_I = -70 mV, τ_{AMPA} = 2 ms, $\tau_{NMDA,rise}$ = 2 ms, $\tau_{NMDA,decay}$ = 100 ms, τ_{GABA} = 10 ms, α = 0.5 kHz, β = 0.062, γ = 0.28. The remaining constant neural parameters are given in table 4.1.

The adaptation-inducing calcium-dependent AHP current I_{AHP} is given by:

$$I_{AHP}(t) = -g_{AHP}Ca(t)(V(t) - V_K), \tag{4.12}$$

$$\frac{dCa(t)}{dt} = -\frac{Ca(t)}{\tau_{Ca}} + \alpha_{CA}\sum_i \delta(t - t_i), \tag{4.13}$$

where $\alpha_{Ca} = 0.2$, $\tau_{Ca} = 70$ ms, $g_{AHP} = 100$ nS, and were chosen to induce alpha-range oscillations in the presence of network input. For a more detailed discussion on the dependency of adaptation-induced oscillations on the input and the time constant, see (Augustin et al., 2013). Note that we here focused on the implementation of noisy oscillations as opposed to fixed frequency oscillators or to the asynchronous state, and manually adjusted the SFA values to introduce heterogenous alpha-activity into the model. Parameters were based on previously established values (Brunel & Wang, 2001; Ermentrout et al., 2001) guided by physiological measurements (Helmchen et al., 1996; Svoboda et al., 1997; Ahmed et al., 1998).

All neurons in the network received an external background input from N_{ext} = 800 external AMPA signaling excitatory neurons injecting uncorrelated poisson-distributed spike trains, representing the noisy fluctuations that are typically observed *in vivo*. Specifically, for all neurons inside a given population p, the rate v^p_{ext} of the

resulting global spike train is described by:

$$\tau_n \frac{dv_{ext}^p(t)}{dt} = -(v_{ext}^p(t) - v_0) + \sigma_v \sqrt[2]{2\tau_n} n^p(t) \tag{4.14}$$

where t_n = 300 ms, v_0 = 2.4 kHz, σ_v is the standard deviation of $v_{ext}^p(t)$, and $n^p(t)$ is normalized Gaussian white noise. Negative values of $v_{ext}^p(t)$ that could arise due to the noise term are rectified to zero. The resulting simulated time series was calculated by summing up all synaptic input currents (AMPA, GABA and NMDA). This signal more directly corresponds to a simulated LFP signal (as in e.g. Mazzoni et al., 2008) than to the dendritic currents the MEG signal originates in, but some evidence from simultaneous intracortical recordings and MEG during tactile stimulation suggests good correspondence between LFP and MEG signals (Zhu et al., 2009). This may be due to the fact that though dendritic integration of synaptic input may be highly nonlinear due to dendrite shape, this effect may be balanced by ion channel distribution and synaptic properties, which can cancel dendritic signal distortion (Magee, 2000). Power envelopes were calculated analogously to those of MEG recordings (Figure 4.1 b).

4.3. Results

We present a theoretical model of spontaneous brain activity that specifically considers the noisy oscillatory nature evident in MEG resting state recordings. The model is based on local LIF-neuronal dynamics of populations of inhibitory and excitatory neurons, combined with a structural connectivity matrix that determines inter-areal connection strengths. Oscillations emerge in the model from the recurrent input between nodes, paired with neural adaptation in each node. Considering the noisy oscillations of the empirical data and the model, we show in the following that the model captures the network connectivity of the MEG resting state data

in an optimal limited range of global coupling strenghts. The inclusion of neurophysiologically realistic delays shifts the working point to higher mean coupling values and increases the concordance between model and empirical data.

4.3.1. MEG data

In the literature, resting state activity has been associated primarily with BLP in the alpha- and beta-bands (Brookes et al., 2011b,a; Mantini et al., 2007). In line with these findings, the power spectrum of the MEG data set from the present study had a peak around 10 (8-12) Hz (Figure 4.2, first panel). Though typically the characteristics (e.g. peak location, frequency differences between areas, peak amplitude) vary across persons, age and sex groups, its appearance is a very robust finding (Chiang et al., 2011). In our group of 10 healthy adult subjects, the mean power spectral peak was centered at 8.7 Hz ($\pm$ 2.25). The data was lowpassed filtered and freed from artifacts as described in detail in the methods section. When filtering the time series in 15 bands of 4 Hz width from 0 to 60 Hz, the alpha-band also carries the highest mean BLP connectivity between nodes.

Brookes et al. (2011c) showed resting state networks resembling those previously found in fMRI studies for these MEG recordings. Using ICA, they independently identified eight RSN in the MEG alpha- and beta-band power envelopes closely coinciding with RSN also found in fMRI recordings (their Figure 1: a) DMN in alpha; b) left lateral frontoparietal, c) right lateral frontoparietal, d) sensorimotor, e) medial parietal, f) visual, g) frontal and anterior cingulate, and h) cerebellar networks). Focussing here on the oscillatory data component and studying the effect of long-range delays on the model FC structure over a range of coupling and delay paramaters, we directly fitted the model FC to the empirical alpha power FC structure. Graph measures for the empirical FC matrix are shown in Supplementary Figure 4.7.

4.3.2. Model data

The model consisted of local nodes connected to each other by long-range connections. The structure of these long-range connections was fixed as it was based on neuroanatomical DTI measurements. Additionally, two free parameters shaped the spatiotemporal network structure. Connectivity strength between nodes was varied systematically with coupling parameter W, and the spatiotemporal pattern of the connectivity was modulated by introducing global propagation velocity parameter v, which changed the temporal dynamics of the network. W is unitless and unknown and was the main free parameter in the model, and we varied v from Infinity (no delays) across a physiological range of delays (5,10 m/s) to very large delays (1 m/s).

In the model, isolated nodes did not oscillate autonomously or from the background activity only. Increasing input from other nodes triggered activity-dependent SFA, leading itself to noisy oscillations in the alpha-band (Figure 4.2). The shape of the model frequency spectrum thus depended on the global coupling parameter W: increasing the coupling between brain areas caused the network nodes to start oscillating at around 10 Hz, at a similar frequency as the alpha-peak evident in the MEG data. When coupling was further increased, the network oscillations became more and more regular. The transition from the low asynchronous state over noisy oscillations with irregular spiking across all pools of neurons to the highly regular population spikes for high W can be seen for one brain area example time series in Figure 4.3. Oscillatory power and peak frequency further depended on the mean input (Figure 4.2), bottom panels).

4.3.3. Model Fit

For each simulation in parameter space of W and v, we extracted the BL alpha-power and calculated the FC from each node to each other node (Figure 4.4). To judge the model's performance and find the optimal working point, we systematically varied W and v, and compared the resulting model FC matrices between model nodes with the corresponding MEG derived FC. After applying a Fisher-Z transform to the FC measures (due to the nonadditivity of correlation coefficients, Zimmerman et al., 2003), the matrices unique triangular parts were vectorized and the performance of the model was then calculated from the Pearson correlation between MEG data and model.

Figure 4.5 shows the model performance defined by alpha range power envelope correlations for a range of W and v parameters. The ability of the model to capture the empirical functional connectivity depends on the coupling strength and propagation speed. For weak couplings, there is no connection between the model nodes, and all nodes have independent activity. For intermediate couplings, the network nodes couple dynamically and trigger the SFA. A performance peak of the model in predicting the empirical FC in the alpha-BLP can be found with this intermediate coupling range for all delay levels, the maximal fit being reached at lower coupling levels for smaller delays, and the performance curve flattening out for very large delays (1 m/s) (remaining low for higher couplings, not shown). Also note that delays increase the region of global coupling values for which the model yields a good prediction of the empirical FC: the range of global coupling values for which the fit is systematically rising beyond 0.10 (orange/yellow in figure 4.5, bottom) is much wider for intermediate delays at 5 m/s than for v=Inf. See Supplementary Figure 4.8 (for model performance and correlation distances for frequency bands from delta to high gamma-bands, which shows highest maximal fits for the alpha range, decreasing both towards lower and higher frequency bands.

Figure 4.6 shows the FC pattern of two brain areas pertaining to distinct

networks: the left posterior cingulate (DMN) and left dorsomedial frontal cortex (associated with task control). The functional differences of the regions are reflected by their embedding in different networks at rest, and functional connections between nodes without direct structural links can be observed both in the MEG data and in the model.

The here presented model is quite different from simpler oscillator models such as presented by Cabral et al. (2011) and Deco et al. (2009) where delays play a critical role in maintaining phase heterogeneity between the nodes. In the spiking model, complete synchronization is prevented for most of parameter space by the heterogeneity and size of the network, through background noise and a wider distribution in time of individual spike times. Therefore, delays are not critically necessary for a good model fit. They do, however, change the spatiotemporal connectivity pattern. As a result, strong connection inputs are more evenly distributed in time and mean firing rate is reduced, and with it SFA. Without delays, all inputs into a pool arrive at the same time, and therefore sum up to higher momentary inputs. With delays, time differences between the arrival of inputs from other brain areas are introduced. In theory, in spontaneous activity, this change in temporal connectivity may also lead to synchronizing strong inputs in some cases. Effectively, though, the introduction of delays distributes inputs from different nodes in time. This leads on the one hand to higher required global coupling to effectuate changes in node activity in a nonlinear system where single weak activities may drown in the background noise. On the other hand, due to delays, there is also a less abrupt accumulation of the AHP-current and a later transition to regular oscillations for the delayed case (Figure 4.3, center row, left vs right column: while for $v = 5$, spiking is still quite irregular, the same global coupling without delays already shows population bursts). For even higher couplings, the system transitions to a high firing regular oscillation regime for all delays, as visible both in the spike rasterplots and the LFP time series in Figure 4.3.

4.4. Discussion

In this study, we investigated how spontaneous brain activity, oscillations and functional connectivity as recorded by MEG may be captured in a neurophysiological resting state model. To this aim, we equipped a local LIF-neuron population model (Deco & Jirsa, 2012) with SFA and implemented it on the nodes of a neuroanatomically based large-scale brain connectivity graph. Our results demonstrate that the model captures the network connectivity patterns in bandlimited alpha-power, and that it does so most robustly in the presence of cortical transmission delays.

Spatial patterns of fMRI resting state activity have been reproduced in the last years with a variety of models (Honey et al., 2007; Ghosh et al., 2008b,a; Honey et al., 2009; Deco et al., 2009; Cabral et al., 2011; Deco & Jirsa, 2012). In these models, network dynamics in resting state models are importantly shaped by three key factors: couplings, delays and noise (Deco et al., 2009). In all the models, the coupling matrix between the nodes plays a crucial role in shaping the spatial patterns of activity. The role of delays and noise, however, depend more on the specific local dynamics used to model neural activity. For example, neither delays nor external noise are necessary to keep the system dynamic and activated in the case of chaotic dynamics (Honey et al., 2007, 2009). In other cases, noise is essential to introduce transitions between multistable states (Ghosh et al., 2008b; Deco et al., 2009; Deco & Jirsa, 2012). Noise can be neglected also in a complex network arrangement of Kuramoto oscillators with delays, which may show ongoing dynamics and transient couplings (so called Chimera states) (Cabral et al., 2011). Delays, in general, do not influence slow asynchronous dynamics (Deco & Jirsa, 2012), but become essential in the case of underlying oscillatory dynamics on the time scale of the delays (Jirsa & Ding, 2004; Jirsa, 2009). When assuming intrinsic nonchaotic oscillatory dynamics in the local nodes (Deco et al., 2009; Cabral et al., 2011; Ghosh et al., 2008b,a), delays are necessary to prevent full synchronization of the network. In a FitzHugh-Nagumo os-

cillator model, Knock et al. (2009) showed that characteristics of the connectivity matrix matter for the importance of delays in shaping dynamics and found that the network structure is less affected by delay magnitude changes for symmetric than for asymmetric graphs. This is due to real symmetric matrices having real eigenvalues, so the networks equilibrium point may change with connectivity, but not the dynamics (though note that DSI matrices may also show asymmetries due to normalization of connectivity by brain area size, resulting in larger weights from larger areas to smaller ones than vice versa). This may, however, depend on the specific model, as e.g. in the model of Cabral et al. (2011), delays shape the spatiotemporal structure of the oscillators, whose phase interactions, and therefore clustering and frequency suppression, depend on the spatiotemporal layout in a DSI-derived SC network. In the here presented model, delays are important to consider as they shape network dynamics and increase the model fit in a physiological delay range.

We focused on alpha-band activity due to alpha being the most distinguished oscillatory rhythm during eyes-closed resting state, and to exemplarily address the question of how the spatiotemporal connectivity structure and presence of physiological, noisy oscillations interact to form network dynamics. Due to these dynamics occuring mainly in the alpha-range, this is also where the highest fits were found, followed by the beta- and theta-bands (Supplementary Figure 4.8). The advantage of this model is the spontaneous emergence of noisy oscillations in the network. Oscillations are important to consider when investigating RSN and resting state FC in the light of its neuronal dynamics and mechanisms, as we have seen from recent EEG/fMRI and MEG studies. Though the functions and details of origins of these oscillations are still undetermined, we can study their dynamics and properties with oscillatory models, where the critical settings and oscillatory dynamics depend on the specific model applied. In the Kuramoto model, for example, oscillations emerge due to the tendency of coupled oscillators to synchronize, leading to clusters of nodes transiently synchronizing at reduced frequencies, and are based on the intrinsically (gamma-band) oscillatory nature of the nodes.

The here employed SFA mechanism parsimouneously creates alpha-oscillations based on an easily physiologically interpretable biological mechanism. Noisy oscillations emerge for the intermediate parameter range where the model best fits the data also in terms of functional connectivity, and naturally reproduces some details of empirically observable alpha-rhythms, such as the higher amplitude and frequency peaks for occipital nodes. This may be due to higher adaptation in visual areas, but also arises naturally in the model, as the oscillation frequency depends on the interplay of neural adaptation and recurrent excitatory input, and occipital nodes are more interconnected on average. As an outlook, the reduction of alpha-rhythms typically seen during tasks could be easily modulated by arousal-related ACh signaling (which reduces adaptation). We here focus on simulating the network in a full spiking model to consider the heterogenous spike times, and their stabilizing effect on the system's oscillatory response, as well as to allow for a direct physiological interpretation of the oscillatory source. This, however, makes it difficult to explore the stability of the network behavior over a large parameter space, and reduced models are needed to investigate regime bifurcations and to study parameter interactions in more detail. These relations (Deco et al., 2014; Jirsa, 2009) and the origins and dynamics of alpha activities (e.g. Freyer et al., 2011, 2012; Augustin et al., 2013) are under active investigation, and will help us in the future to further specify the oscillatory sources of models and study their impacts and influences on the network dynamics.

We here implemented SFA as an oscillation-generating mechanism in order to study the importance of delays in the presence of noisy network oscillations. The detailed origins, dynamics, and modulation of spontaneous oscillatory activity and causal role of adaptation in the brain in its different states, however, need to be studied in much more depth. In the brain, various types of adaptation currents in cortical neurons exist, differing in strength between layers. They are modulated by various factors such as polarization state (Connors et al., 1982; Llinas, 1988), cortical depth (Ahmed et al., 1998), and cholinergic signaling (Crook et al., 1998).

These interdependencies, and more systematic variation of adaptation parameters in (reduced) large-scale cortical models may be of great help to understand spontaneous brain dynamics and states in the future.

Though beyond the scope of this study, it is noteworthy that the bursting mode observed here for sufficiently strong adaptation and recurrency (Figure 4.3), while not resembling the oscillatory dynamics of the resting state, are much more reminiscent of up and down states in sleep dynamics (e.g. Steriade, 1997), though at different frequencies. The relation between acetylcholine signaling and cortical activation and cognitive states on one hand (Sarter & Bruno, 1999; Vazquez & Baghdoyan, 2001) and SFA on the other hand (Stiefel et al., 2009) may help us in the future to better understand spontaneous brain dynamics in wake and sleep. This transition was studied in a layered model of thalamus and portions of visual cortical areas by (Hill & Tononi, 2005), and by Deco et al. (2014) in a cortical model for slow waves. A key challenge for future work will be to consider these modulations, and to study the key responsible mechanisms, resulting network dynamics and interactions in whole brain models for different frequency bands.

In the presented data, maximal model fit was no higher than 0.4 for any delay condition, which leaves room for improvement. Of course, this may be related to dynamics and communications not captured by the model, such as, e.g., lateral connections (Spiegler & Jirsa, 2013), or directionality of fibers between brain areas. Results are also influenced by the quality of the DTI matrix, which is prone to miss interhemispheric connections (Hagmann et al., 2008). There is ongoing work in our lab to enhance the quality of the DTI by integrating FC and SC through a modeling approach. The DTI acquisition parameters from the used dataset at 1.5T and b=1200 may also have limited the SC precision. Another aspect to consider is the choice of brain parcellation and preprocessing, which may influence connectivity estimates (Cloutman & Lambon Ralph, 2012; Wang et al., 2009; Zalesky et al., 2010). Here, an AAL parcellation without volume normalization for the DTI was used. From a model and connectivity

perspective, smaller brain areas are favorable, although MEG signal leakage limits the spatial resolution. Importantly, though these issues need to be studied in more detail, they should not be critical in the main findings of the current study, as we focus on the relative changes and effects of including delays rather than the exact network structure.

In conclusion, brain connectivity and resting state FC investigation is becoming more and more important, both for understanding basic organization principles of brain networks as well as for investigating and potentially diagnosing medical conditions. With access to neurophysiological recordings of resting state activity at high temporal resolutions, we are now in the position to investigate the importance of oscillation in the brain for spontaneous network patterns. We here propose a model that offers an implementation of such noisy oscillations combined with large-scale resting state network connectivity. We demonstrate that in the presence of these oscillatory dynamics, the model best captures the bandlimited power connectivity patterns of the empirical data when considering delays.

4.4.1. Acknowledgements

The authors declare to have no conflicts of Interest. TTN was supported by the SUR of the DEC of the Catalan Government and by the FSE. GD was supported by the ERC Advanced Grant: DYSTRUCTURE (n. 295129), by the Spanish Research Project SAF2010-16085 and by the CONSOLIDER-INGENIO 2010 Programme CSD2007-00012, and the FP7-ICT BrainScales. The research reported herein was supported by the Brain Network Recovery Group through the James S. McDonnell Foundation. MJ was supported by the MINDLab Investment Capital for University Research Fund. MLK was supported by the TrygFonden Charitable Foundation. We thank Sven Hilbert and Katharina Glomb for useful discussions on the manuscript and two anonymous reviewers for their helpful comments

4.5. Supplementary Figures

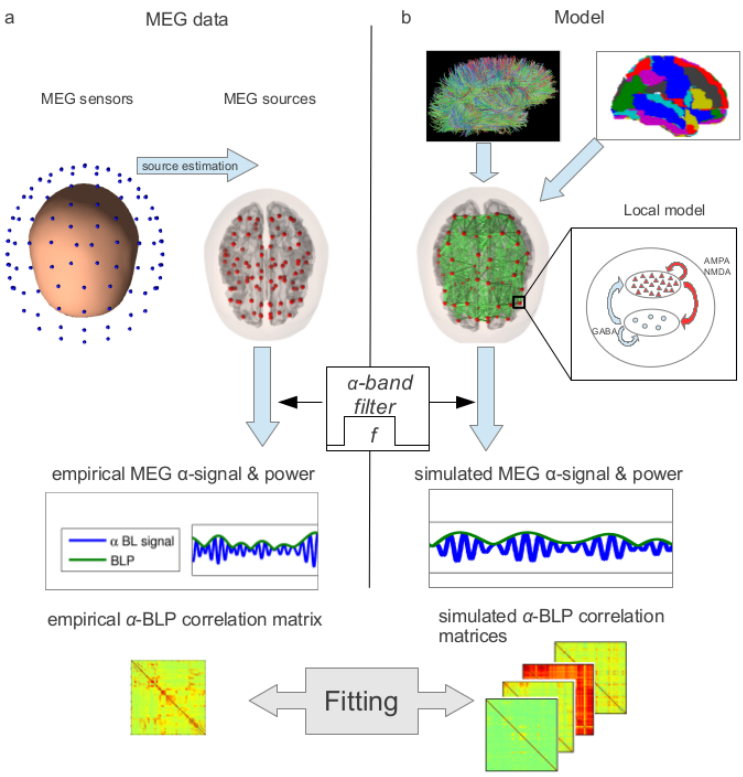

Figure 4.1: MEG
and model data processing and analysis]*Data processing and analysis: a) MEG time series were recorded by sensors and transformed into AAL source-space time series with a beamformer algorithm. The resulting time series for each brain area was then filtered in the alpha-band (8-12 Hz) and its BLP was extracted via Hilbert-envelope computation, resulting in 90 alpha-power time series. b) The model was constructed by taking the same AAL brain parcelation used for source-reconstruction of the MEG signal and putting a model node in the center of each brain area. LIF neuron populations determined local node dynamics and DTI-measurements determined the connection weights between nodes (see methods). The connected network was simulated for 5 mins, and resulting simulated LFP's band-pass filtered alpha-power envelopes were calculated the same way as for MEG recordings.*

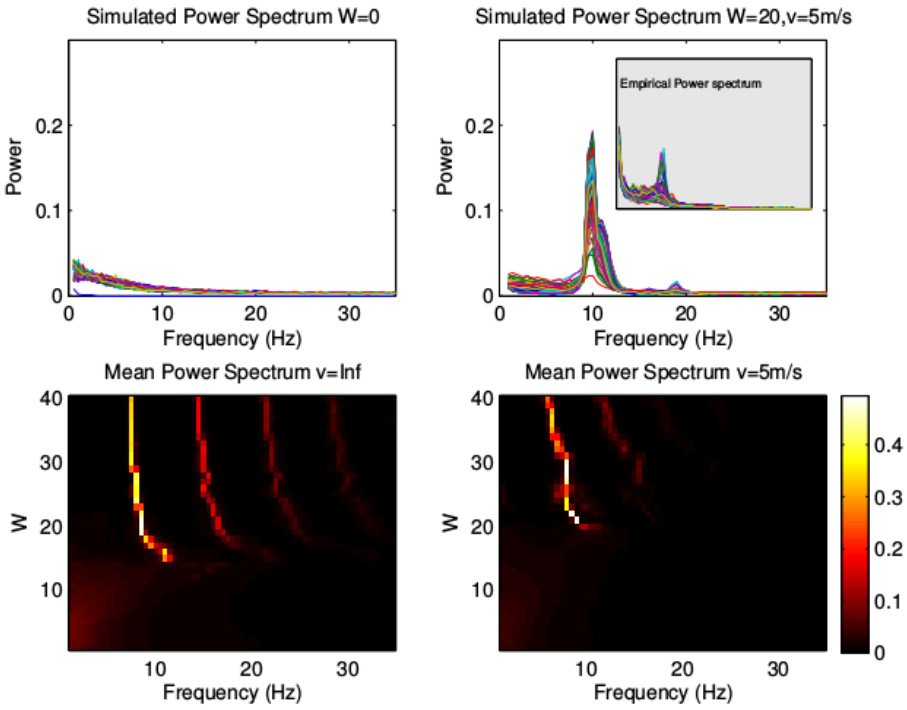

Figure 4.2: MEG

Power spectra]*Top: Power spectra for all brain areas / nodes for exemplary simulation with disconnected nodes (/*$W = 0$, top left) and at $W = 20$, $v = 5$ m/s (top right). The inlay shows the mean power spectrum for empirical MEG recordings. Bottom: Mean power spectra over all nodes for undelayed (left) and delayed (right) simulations./

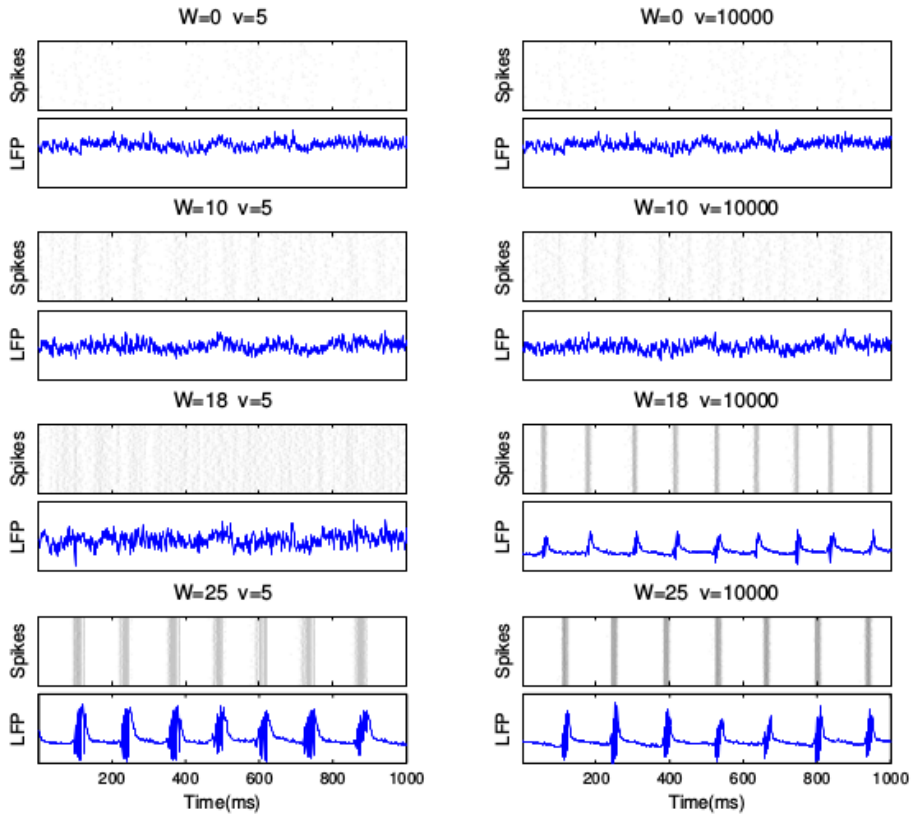

Figure 4.3: *Example raw time series for one brain area (PCC) over one second for different cortical conduction speed /v* (left column: 5 m/s, right column: No delays) and different global coupling values W/

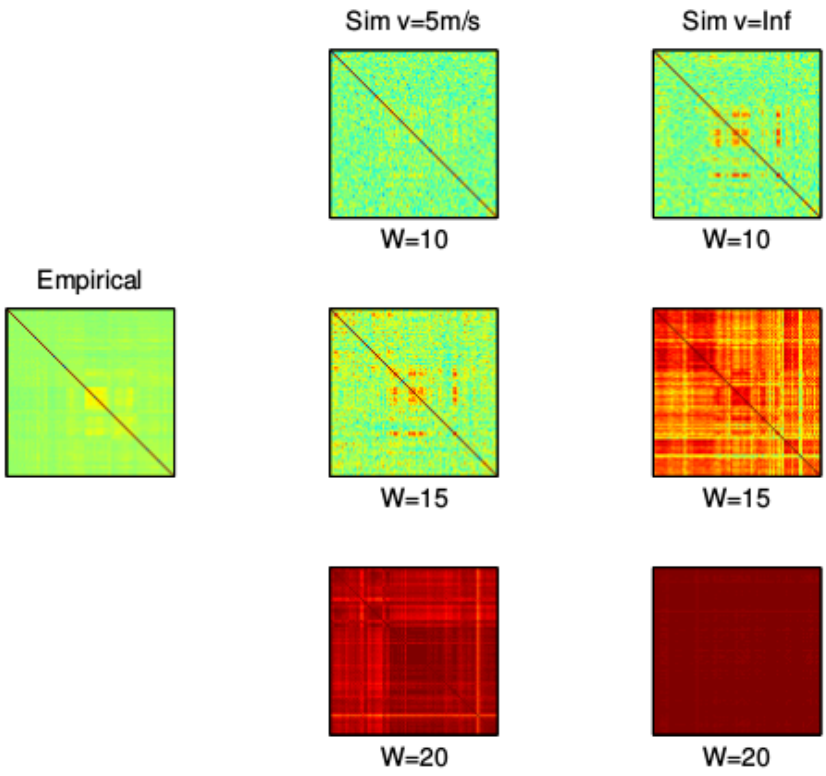

Figure 4.4: *FC matrices for empirical (first column) and simulated data at different delays and couplings (second and third column). High synchrony appears much earlier in the absence of delays (third column) as oscillations become more regular (see Fig 4.3).*

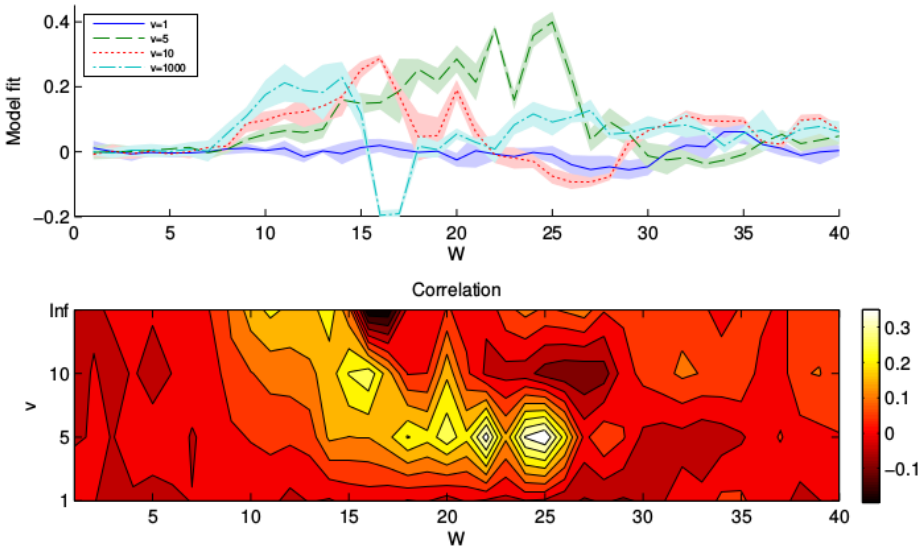

Figure 4.5: *Empirical Fit: Model performance as measured by Pearson correlation between empirical and model FC, based on alpha band-limited power correlations, with Error bars (standard deviation over 5 trials, top), and a color representation for mean over trials (bottom). Maximal fit of r=.40 is reached at W=25, v=5.*

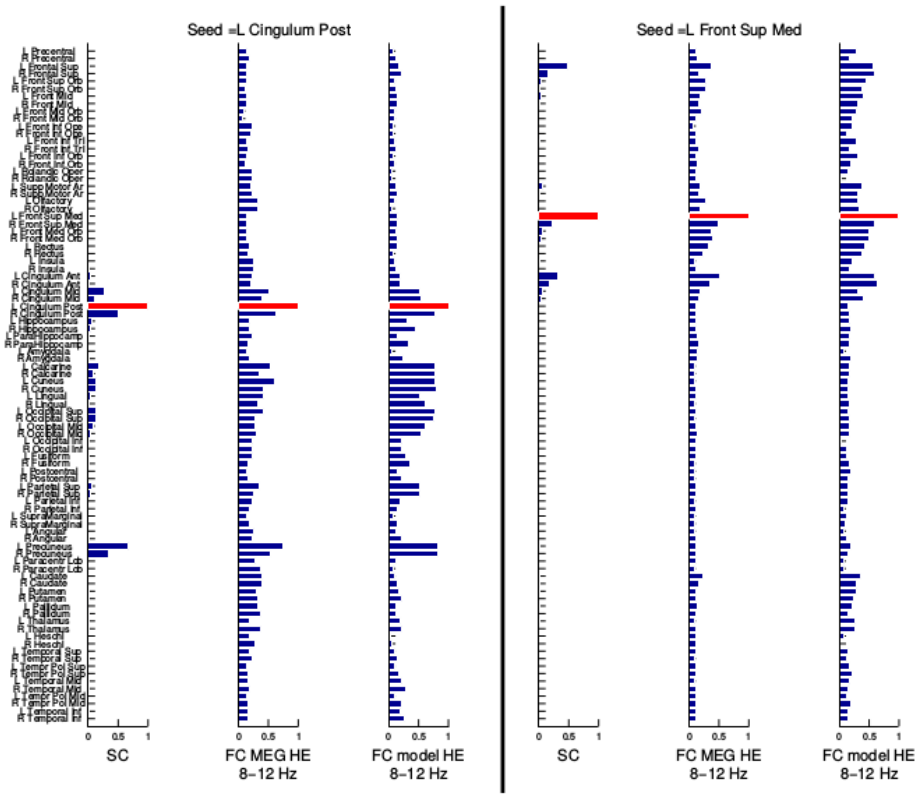

Figure 4.6: *SC, empirical FC and model FC of the alpha-band power envelopes (HE) for left posterior Cingulate Cortex (left) and left dorsomedial Frontal Cortex (right)*

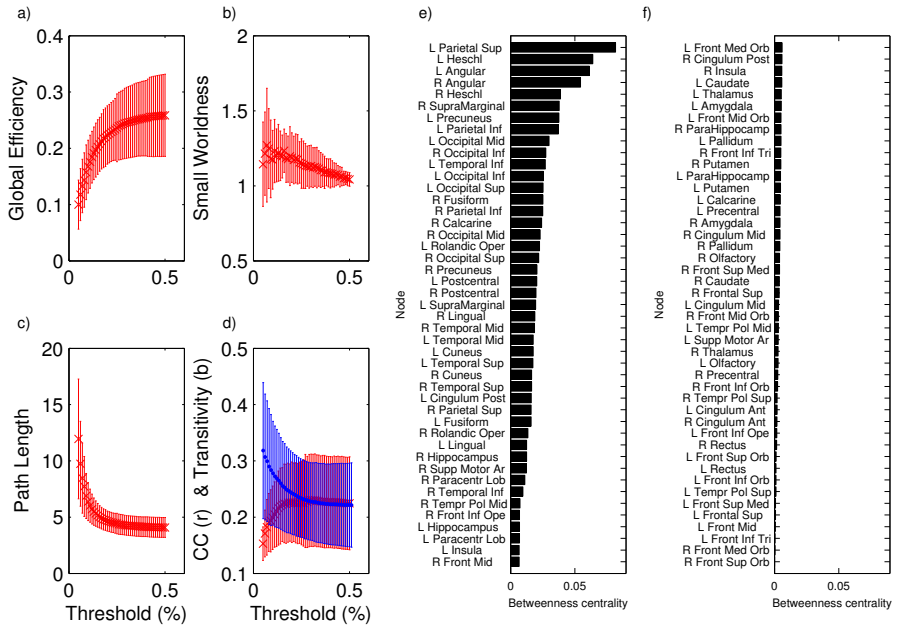

Figure 4.7: MEG data]*(Supplemenary) Graph analysis measures for the empirical alpha power (8-12 Hz) envelope FC matrix for thresholds from .05 to 0.5. Global measures: a) Global Efficiency, b) Small Worldness, c) Harmonic mean Path Length, d) Clustering Coefficient (red) and Transitivity (blue dotted) line. Betweenness Centrality for each node in decreasing order is shown in e) and f).*

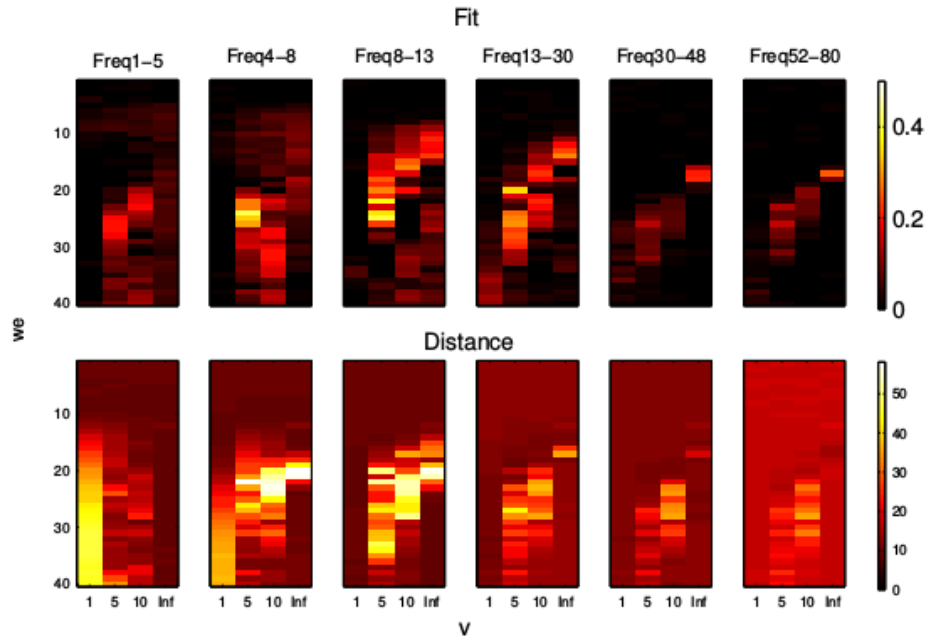

Figure 4.8: *(Supplementary) Empirical Fit (top) and distances (bottom) of simulated and empirial FC, over levels of empirical coupling and delays for different frequency bands from Delta to high Gamma.*

5. Decomposing resting state networks - new perspectives

So far, we have talked about how well models can reproduce FC patterns and their dynamics as a whole. In this chapter, we want to turn our attention towards the network compositions, or rather decompositions, of RS activity in the brain. We propose tensor factorization, specifically PARAFAC/CANDECOMP to be a viable alternative to the established approaches, and discuss the influence of constraints imposed on the data. The here presented results are explorative in nature, and an exhaustive specification of the methods and their applicability for this type of brain data and the necessary preprocessing for obtaining optimal results is still outstanding. Nonetheless, as we will discuss, these are promising methods potentially opening new doors to understanding and conceptualizing brain networks.

5.1. Introduction

5.1.1. Established methods: ICA in fMRI and M/EEG

To achieve a datadriven identification of RSNs, the most common approach after seed-based analysis (Fox et al., 2005) has been to apply PCA/ICA to the signal, mostly spatial ICA in the case of fMRI (e.g. Beckmann et al., 2005; De Luca et al., 2006; Chen et al., 2008; Biswal et al., 2010). Later, these RSNs have also been found in MEG (de Pasquale et al., 2010; Liu et al., 2010; Brookes et al., 2011a,c) and in EEG (Mantini et al., 2007; Jann et al., 2010). Slow RS networks and dynamics

comparable to fMRI data have primarily been found in the connectivity of band-limited power-envelopes in the slower, specifically the alpha- and beta- bands (Liu et al., 2010; Brookes et al., 2011a; de Pasquale et al., 2010). These findings did not only corroborate the existence and identities of structured spontaneous communities found in fMRI data, but opened up new possibilites to study the dynamics and mechanisms of how spatiotemporal structure in spontaneous brain activity emerges in time and across different frequencies. However, these studies were based on the fMRI spatial maps or had limited spatial resolution and matched a subset of similar, not equivalent components to fMRI RSNs. Also, as they stem from another modality, they are not conclusive with respect to how much of the signal is different due to differences in bandlimited neural activity as measured by M/EEG and fMRI BOLD, and how much is due to differences in the ICA modes. This matters, as spatial ICA maximizes the spatial independence of components while not constraining their temporal activity. This is optimal for fMRI data structure, as it typically combines many spatial datapoints with relatively few timepoints, but it is disadvantageous for identifying functionally distinct, potentially spatially overlapping components such as to be expected in hub-rich networks like the brain. Smith et al. (2012); Helwig & Hong (2013); Calhoun et al. (2012).

Smith et al. (2012) recently compared spatial and temporal ICs ('temporal functional modes, TFM') in fMRI data. The temporal decomposition yielded corresponding modes to the classical RSNs, but with somewhat distinct spatiotemporal signatures (e.g. more highly functionally segregated visual-subsystem TFM). Interestingly, they found the DMN to be not so much a single functional network but more of a time-averaged pattern of correlations and anticorrelations of different TFMs. The authors propose that cognition may occur in independent functional networks, and while not negating the DMN (which they reproduced in the time-average of both signal correlations and TFMs), they show how its prominence in RS research may in part be due to the choice of methods we apply to the data, including their own method, which imposes strong assumptions of temporal independence. ICA will maximize independence in space

or time (and, thus, assume independence), PCA aims to explain variance maximally in few dimensions and searches a low-dimensional representation explaining the maximal variance. Non-negative tensor factorization explains data by parts-based additive representations. Given these alternative, it is important to be aware of the assumptions we make about the data.

Accordingly, calls to rethink the modes and constraints with which we analyze brain network data have been increasing (Calhoun et al., 2012; Helwig & Hong, 2013). Different constraints imposed on the decomposition follow different application goals and determine the nature of the resulting components. Importantly, though, prior knowledge is needed to implement the appropriate constraints and to have confidence that the resulting components represent the data well. As emphasised by Cichocki (2009, p.8):

> "the successful and efficient use of such tools strongly depends on *a priori* knowledge, common sense, and appropriate use of the preprocessing and postprocessing tools. In other words, it is the preprocessing of data and postprocessing of models where expertise is truly needed in order to extract and identify physically significant and meaningful hidden components."

This becomes even more critical when stepping into higher dimensions. Multiway approaches are being used increasingly, and promise a datadriven and more easily interpretable decomposition of brain networks (Cichocki, 2013; Helwig & Hong, 2013). Especially in neurophysiological data, where frequency-specific activity adds a natural third data dimension, multiway decomposition methods offer a good way to explore brain networks in all dimensions simultaneously (Miwakeichi et al., 2004; Mørup et al., 2006; Martínez-Montes et al., 2008a,b; Wang et al., 2008).This way we can take into account spatial, temporal and spectral,

subject, group or trial information at once, and provide links between these data dimensions (Cichocki, 2013).

Beckmann and colleagues (Beckmann & Smith, 2004, 2005; Beckmann et al., 2005) introduced a probabilistic ICA (pICA) and a three-way extension in order to extract fMRI components in space, time, and session/subject domains. Comparing their approach with an unconstrained PARAFAC analysis, they show higher accuracy with less cross-talk in extracting (spatially independent) components from multi-subject datasets. However, Stegeman (2007); Helwig & Hong (2013) later showed that the robustness of tPICA depends on the chosen algorithm and iteration scheme, and produces biased results in the presence of deviations from the spatial independence assumption, and therefore recommend constrained PARAFAC (with orthogonality) or PARAFAC2 models.

These studies were performed on fMRI data, where multivariate techniques are used mostly to extract components across tasks or subjects (Sharma & Baron, 2013; Long et al., 2013). In neurophysiological data, frequency is an obvious third dimension of the datasets. At first, component and connectivity analyses were mostly repeated over frequency bands (e.g. Brookes et al., 2011c; de Pasquale et al., 2010; Tagliazucchi et al., 2012b; Hillebrand et al., 2012), but recently, multi-variate frequency interactions are increasingly proposed to play an important functional role in brain dynamics. Marzetti et al. (2013) introduced a multivariate interaction measure (MIM), quantifying lagged interaction between a seed in the DAN and other areas across frequency bands. Similarly, Brookes et al. (2012) took a multivariate, seed-based approach to measure MEG power envelope FC across frequency bands, which, in its extension (Brookes et al., 2014), allows for the construction of signal-leakage corrected, seed-based, time-frequency connectivity plots in a framework accounting for temporal non-stationarity.

In light of the abovementioned discussion on model assumptions, PARAFAC / Candecomp (CP) is a promising tool to understanding brain networks: unique solutions are readily obtained with minimal constraints, and *a pri-*

ori independence and orthogonality assumptions are therefore not always necessary. Remaining assumptions are that the data are variable, as well as roughly trilinear and additive (Murphy et al., 2013).

Computerized tensor decomposition methods have been developed decades ago (Hitchcock, 1927; Carroll & Chang, 1970; Harshman, 1970), but have advanced since then with the development of new algorithms (Cichocki et al., 2008; Bader & Kolda, 2007; Friedlander & Hatz, 2008; Kim & Park, 2011; Phan et al., 2012; Kim et al., 2013), and they have become more readily available to a wider audience in recent years with tutorials and toolboxes (Bader & Kolda, 2007; Friedlander & Hatz, 2008; Cichocki, 2009; Kolda & Bader, 2009; Murphy et al., 2013). While the reader is referred to these methodological papers for an in-depth discussion, in the following we will give a short overview of the PARAFAC method and important considerations regarding its applications.

5.1.2. Tensor factorization

PARAFAC/Candecomp is one of many tensor decomposition methods, and represents a generalization of a matrix singular value decomposition (Kolda & Bader, 2009). Given a data array/tensor $\underline{Y}$, CP decomposes it into a sum of component rank-one tensors, where rank-one tensors are tensors that can be written as an outer product of N vectors (N being the tensors dimensionality). It follows that a third-order, rank-one tensor $\underline{X}$ of size I is given by the outer product of its constituent vectors, $\underline{X} = a \circ b \circ c$, and element $x_{i,t,q}$ is given by $a_i b_t c_q$. This relation is illustrated for $\underline{Y}$ by vector arrows in Figure **??** (left). However, as not all three-dimensional tensors are rank-one already, a three-dimensional PARAFAC model decomposes a given tensor into a sum of multi-trilinear terms, and returns three-component ('loading') matrices (Cichocki, 2009), which can be written as:

$$y_{itq} = \sum_{j=1}^{J} a_{ij} b_{tj} c_{qj} + e_{itq}, \tag{5.1}$$

in matrix form:

$$\underline{Y} = a_j \circ b_t \circ c_q + \underline{E} = [[A, B, C]] + \underline{E}, \tag{5.2}$$

where $\underline{Y}$ is the tensor, *A*,/B/ and *C* are the three factor matrices and $\underline{E}$ is the error. The factor matrices are a combination of the vectors from the rank-one components.

#+CAPTION[PARAFAC Matrix and vector representation]:*Representation of Matrix (uppercase) and vector (lowercase) PARAFAC representation of three-*

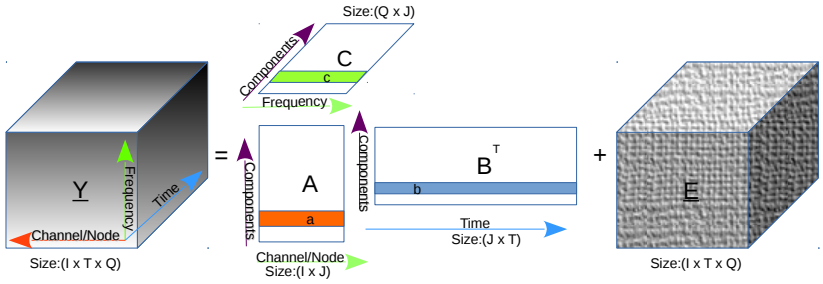

dimensional Tensor Y

Every component matrix stores the weight of each dimensional element (e.g. timepoints, frequency bands, or nodes) on each component. This way, several components can be active at the same time. For a given component, all values are linked across dimensions, i.e. the 'activity' of a component is simultaneously fixed on all three dimensions. The interactions between components are set to zero, that is, all but the superdiagonal of the core-tensor, which holds interactions in the more general TUCKER decomposition (not depicted), is zero. This mostly prohibits a perfect reconstruction of the data (and hence TUCKER is better used for data compression), but permits easier interpretation of the components. As

the optimal decomposition is typically not determinable analytically, the best decomposition is determined iteratively to maximize variance explanation. The original alternating least squares (ALS) algorithm does this by repeatedly fixing two of the three component matrices to solve for the remaining one. (Kolda & Bader, 2009).

In general, the PARAFAC model does not suffer from lack of rotational uniqueness, meaning that most PARAFAC solutions have one unique best solution. This is considered a major advantage of this model over factor analysis solutions (Kruskal, 1989). However, a model without any constraints that best represents the input data numerically may not always be unique nor optimal in terms of interpretability of the factors. Also, a best-fitting decomposition may not exist for every data array, and diverging components with nearly linearly dependent columns in A, B, C may appear (Stegeman, 2014). To avoid these problems and to increase the physcial meaningfulness of the decomposition, constraints such as non-negativity, unimodality or orthogonality can be imposed for each mode individually in PARAFAC. Of course, these constraints have to actually be present in the data structure to result in a meaningful decomposition. For the frequency domain for example, a non-negativity constraint can naturally be used, while unimodality may be meaningful depending on the underlying processes. For both the time and the spatial domains, further constraints can be made. We here applied two- and threedimensional decompositions with 1. no constraints, 2. orthogonality, and 3. non-negativity constraints.

Furthermore, it is important to note, and reflect upon, the limitations of the model in terms of what kind of data it can represent. As it uses the same number of components/columns J, components are tied together in all modes. Unlike in other decompositions such as PARAFAC2 or TUCKER3, interactions between the modes cannot be represented, and the model cannot meaningfully represent the data in such a case. While there is no direct test for data trilinearity, the Core Consistency diagnosis (CorCondia, CC) can be used as an indicator for 3-way tensors. Being the similarity (from 0 to 1) between a PARAFAC and a TUCKER decomposition of the same data, a high CC of 0.8 or 0.9 indicates few interactions between the components, and hence a good model fit, while a low value of e.g. 0.5 indicates that the data cannot be presented well by a PARAFAC model (Cichocki, 2009).

5.1.3. Motivation

Here, we use PARAFAC to decompose MEG RS recordings in space, time, and frequency bands. We explore alternative decomposition methods on a preprocessed source space MEG RS recording. Using the previously established ICA approach and two- and threedimensional PARAFAC, we set out to identify RS networks both in time, space, and frequency bands in order to study if the PARAFAC model can give a meaningful representation. We compare decomposition results of spatial and temporal ICA as well as PARAFAC with different constraints in order to visualize the different interpretations of the data, and discuss the importance of choice and future application potential of these analysis methods.

5.2. Methods

5.2.1. MEG Data Collection and Analysis

The study included data from 7 healthy participants taken from a larger data set including 12 subjects (6 males, age range 19-27) with no history of neurological disorders. MEG was recorded with a CTF-151 system (CTF Systems Inc., Vancouver, Canada) on two separate days. Both days included the following recording paradigm: 5 minutes of rest with open eyes, 5 minutes of rest with closed eyes, a task, ~90 minutes attempted sleep, a re-run of the task. The sleep recordings were scored by an expert sleep technician according to the principles given by Rechtschaffen & Kales (1968) in 30-seconds windows with each window being assigned to one of the following 6 state categories: 'wakefulness', 'NREM sleep stage 1', 'NREM sleep stage 2', 'NREM sleep stage 3', 'NREM sleep stage 4', 'REM sleep'. Written informed consent was given by all participants, and the protocol was in accordance with the Declaration of Helsinki and accepted by the medical ethics committee of the VU University Medical Center, Amsterdam, the Netherlands. The data subset from 7 out of 12 participants for the study at hand was chosen on the grounds that each of these 7 participants

showed sleep scores indicating epochs of at least 270 seconds of undisrupted wakefulness (S0), NREM sleep stage 2 (S2), and Deep NREM sleep (SWS). SWS was defined as epochs of data scored as NREM sleep stage 3, NREM sleep stage 4, or a combination of the two. For this study, only the 'wakefulness' state recordings were used.

All pre-processing steps were performed in MATLAB (The MathWorks, Inc.) employing software developed at Oxford Centre for Human Brain Activity (OHBA). OHBA's Software Library (OSL) is borrowing functions from other software packages, such as SPM8 (Litvak et al., 2011), FieldTrip (Oostenveld et al., 2011), and FSL (Jenkinson et al., 2012). Each recording (~45 minutes) was preprocessed as one continuous piece. The raw CTF-151 data was high-pass filtered at 0.1 Hz, and single channels with excessive noise levels were removed from further analyses. Data was then submitted to Blind Source Separation by temporal Independent Component Analysis (ICA) using the FastICA algorithm (Hyvärinen & Oja, 2000; Vigário et al., 2000) as implemented in the FastICA toolbox for MATLAB. Each independent component (IC) was represented by an independent time-course and a topological map describing each of the MEG sensors' contribution to the given IC. All ICs were reviewed manually and categorized as either neural or artifact. Artifactual ICs included cardiac, ocular (Mantini et al., 2008; Vigário et al., 2000) or facial muscle-interference (Muthukumaraswamy, 2013) and were removed by subtracting them from the full-rank data (Mantini et al., 2011). The artifact-corrected data was band-pass filtered into 4 frequency bands of interest: delta (0.25-4 Hz), theta (4-8 Hz), alpha (8-13 Hz), and beta (13-30 Hz), and submitted to source reconstruction.

In order to estimate the sources of neural activity leading to the signals measured at the sensors of the MEG array, the data was spatially filtered using a Linearly Constrained Minimum Variance (LCMV) beamformer (Hillebrand & Barnes, 2005; Van Veen et al., 1997). More specifically, an overlapping-spheres forward model was implemented using a quasi-static approximation of Maxwell's equations with a sphere fitted to each of the 151 MEG sensors (Huang et al., 1999), upon which a scalar LCMV beamformer (Sekihara et al., 2001; Woolrich et al., 2011) was employed. A prerequisite for successful source-reconstruction in MEG is co-registration. Since no individual structural scans were obtained for the participants studied here, a template average structure in Montreal Neurological Institute (MNI) coordinates was used. For one participant, the dimensions

of this average template were in conflict with his/her position in the scanner (i.e. bulging outside of the helmet) when co-registered to the MEG device coordinate system. In order not to lose the data from this participant, a structural MRI from another data set with suitable dimensions was used (Holliday et al., 2003). An affine registration was applied between this substitute MRI and the MNI template brain, used for the rest of the participants, to make later group comparisons possible. One of the main advantages of using beamformers, compared to other strategies of source-reconstruction, is the fact that projection of source activity at any given location is independent from prior or later projection to other locations (Barnes & Hillebrand, 2003). Hence, it was possible to focus the beamformer at 90 center-of-gravity locations derived from the AAL template (Tzourio-Mazoyer et al., 2002), yielding 90 time-courses for each of the participants' three vigilance states in each of the four frequency bands.

Power envelopes were extracted separately for each frequency band, downsampled to 25 Hz, normalized to zero mean and unit variance, and concatenated over subjects. Both 2D (temporal and spatial ICA) and 3D decomposition methods were then applied to the data via the TDALAB (Zhou & Cichocki, 2013; Cichocki et al., 2014) Matlab Toolbox.

1. Temporal ICA (PMFefica2): Based on previous work finding RSNs in MEG power envelopes via temporal ICA (Brookes et al., 2011c), we expected to find core RSN networks also in the present dataset based on 90 nodes. The analysis was confined to the AAL regions, and spatial components were extracted by calculating the correlation of the nodes' envelope time courses with each of the components.

2. Spatial ICA (PMFefica1): At 90 spatial nodes, the data did not meet conditions for spatial ICA, but we included it to compare visually the method results in the same parcellation space.

3. 2D PARAFAC: For twodimensional CP, different constraints were chosen, identified by one numeric digit on the dimensions space and time, respectively: constraints: 0 = none, 1 = orthogonality, 2 = nonnegativity, 3 = unimodality and nonnegativity. bi = binarized data. hence, '*CP02bi*' denotes CP decomposition with no spatial constraint, nonnegativity in time, on binarized data.

4. 3D PARAFAC: For 3D-CP, the third dimension is frequency, which is naturally constrained to positive values, so the nonnegativity constraint was applied.

5.3. Results

5.3.1. 2D decomposition

To gain an overview over the different methods, we first compared the different methods in terms of variance they explained, for each band separately (Figure 5.1).

For binarized data (*CP02bi* and *CP20bi*), less variance was explained than for continuous CP and ICA (*PMFefica*). Temporal ICA (*PMFefica1*) and CP performed equally well, both with slightly higher values than spatial ICA, especially over lower numbers of components. Only in the gamma band, spatial ICA quickly surpassed the other methods. The gradual increase and similarity for *CP20* and *PMFefica1* suggested there is no clear cutoff or preferred method. In general increasing the number of components beyond the first five or six tends to fragment existing components, but not to uncover structurally different, competing factors.

Temporal ICA clearly showed the existence of established networks in the dataset, specifically a visual network, a frontopolar network, and a sensorimotor network, together with left and right lateral temporal networks, visible in Figure 5.2 for alpha and beta band. These networks tend to decompose into left- and right-hemispheric subnetworks as number of components increase (see Supplementary Figures 5.12 and 5.13).

In the different frequency bands, component structure only slightly changes (5.2): A stronger widespread component with occipital focus and a ventral visual stream component are most prominent in delta, while theta, beta and gamma profiles are quite similar to the alpha pattern.

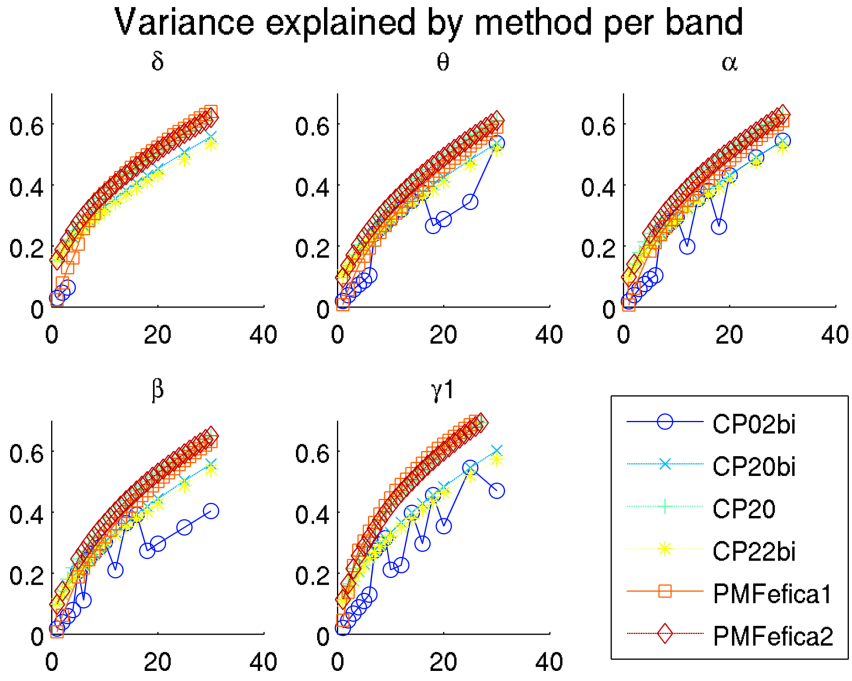

Figure 5.1: ICA & Parafac methods comparison]*Subplots 1-5: Variance explained for different methods by frequency band (legend subplot 6), and 3-D PARAFAC/CP decomposition with different constraints. CP constraints: 0 = none, 1 = orthogonality, 2 = nonnegativity, 3 = unimodality and nonnegativity. bi = binarized data. PMFefica1 = spatial ICA, PMFefica2 = temporal ICA.*

The differences between ICA and CP are shown in 5.3. All methods similarly show a lobular structure. In CP, the first component with strongest activation in occipital cortex is also the most widespread one, extending to include areas from most of the rest of the brain also. The remaining components however are similar to the ones extracted by ICA, marking the sensorimotor, medial frontal, and left and right temporal cortices. The Supplementary Figures (5.8 to 5.15) show how the component structure nontrivially depends on method, constraints, preprocessing and number of components extracted.

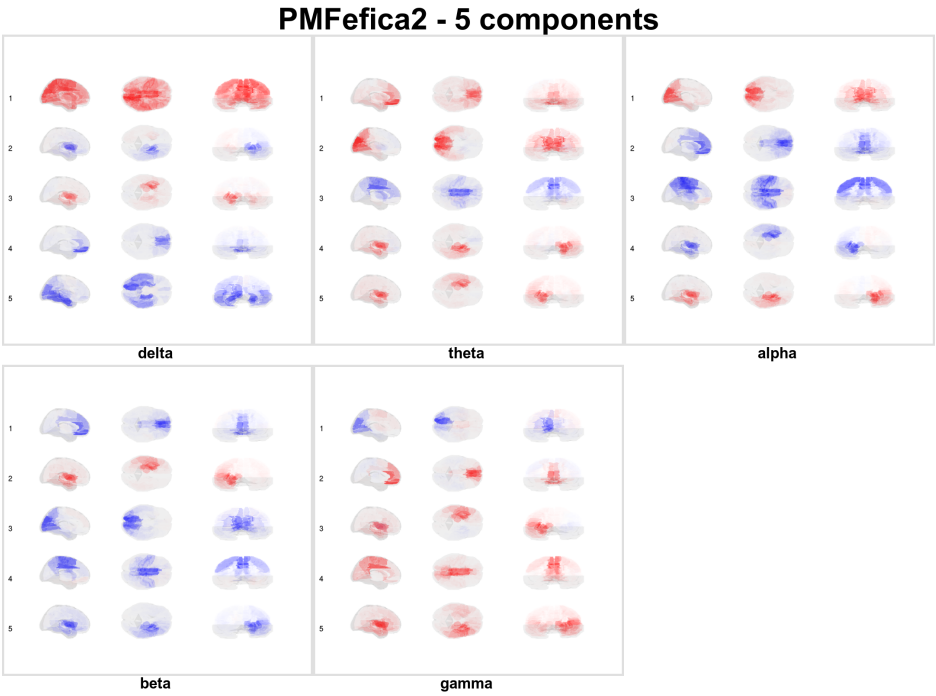

Figure 5.2: ICA 5 Components]*Temporal ICA networks in the delta- (left) and theta-band (right), with negative (blue) and positive (red) weights. Here, 5 Components are shown seperately for each frequency band.*

5.3.2. 3D decomposition

In three dimensions, we used CP002 and CP202, taking advantage of the natural non-negativity in the frequency domain. In many instances, highly collinear components were extracted, leading to low CC values. Using both CC and fit values for determining the optimal number of components, no satisfactory level of explained variance and consistency could be found. The crossover between CC and fit at 13 components leaves us with CC at 0.49 and the fit at 0.19. By comparing with 6 components, it is visible that there is one robust widespread, strong delta component, losing importance with increasing number of compo-

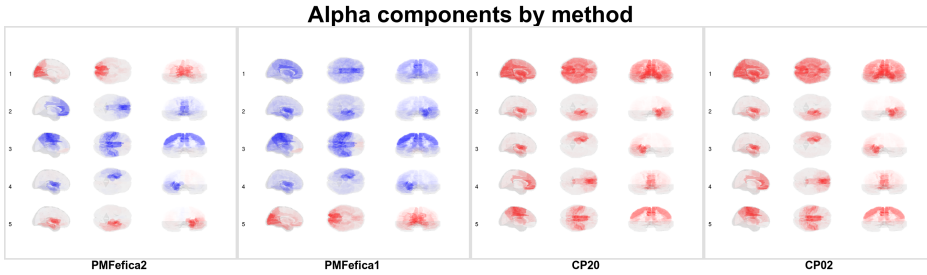

Figure 5.3: *Five component decompositions in the alpha band, for temporal and spatial ICA (PMFefica1,2), and CP with nonnegativity contraint in the spatial and temporal dimension, respectively.*

nents and slow, intermittent activity (Component No. 4 in Figure 5.4 / No. 7 in Figure 5.5, No. 5 in Figure 5.6 and No. 11 in Figure 5.7). Furthermore it is apparent that gamma components double from two to four components, so that most new components appear in the theta to beta range. In CP002, most of these components appear negative (blue), compared to a global positive alpha component, but the pattern matches with the one from CP202 in Figure 5.7: These are mostly components arising around cortical hubs in the cingulate cortex, superior/medial frontal areas, together with basal ganglia, hippocampus and amygdala, with varying involvement of these and other participating areas.

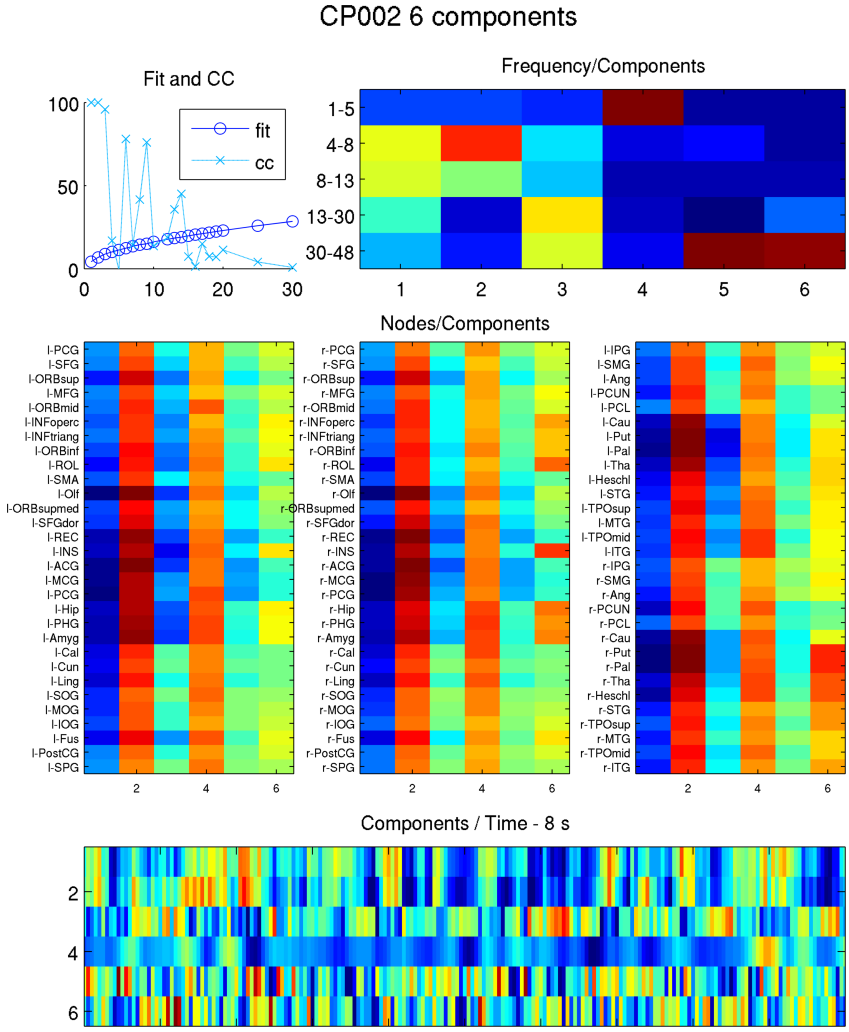

Figure 5.4: *CP002 decomposition with nonnegativity constraint in the third (frequency) mode - 6 Components. Panel 1 shows the quality of the decomposition, the rest of the panels the score of each element on the components. In accordance with the panel titles, a column is a component for panels 2-5, and for the last panel, a row is a component*

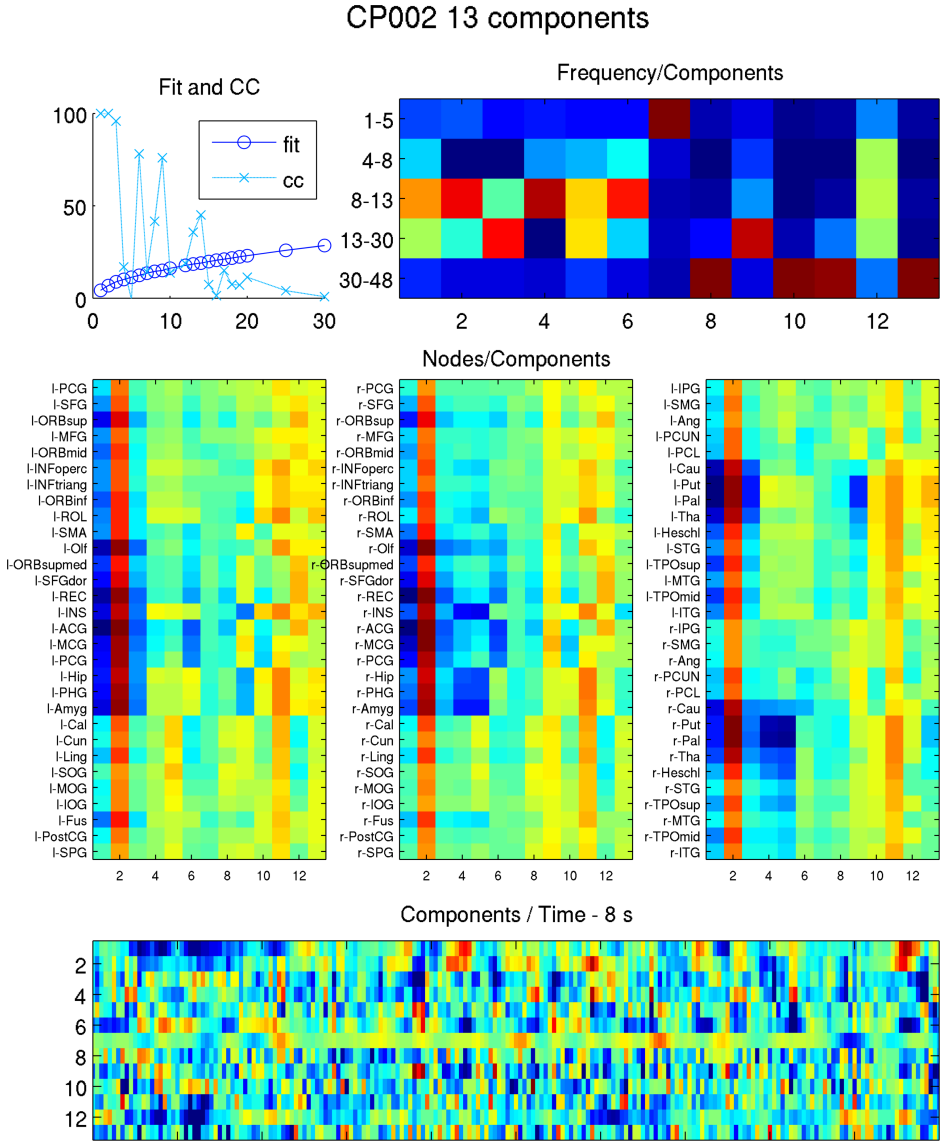

Figure 5.5: *CP002 decomposition with nonnegativity constraint in the third (frequency) mode - 13 Components.*

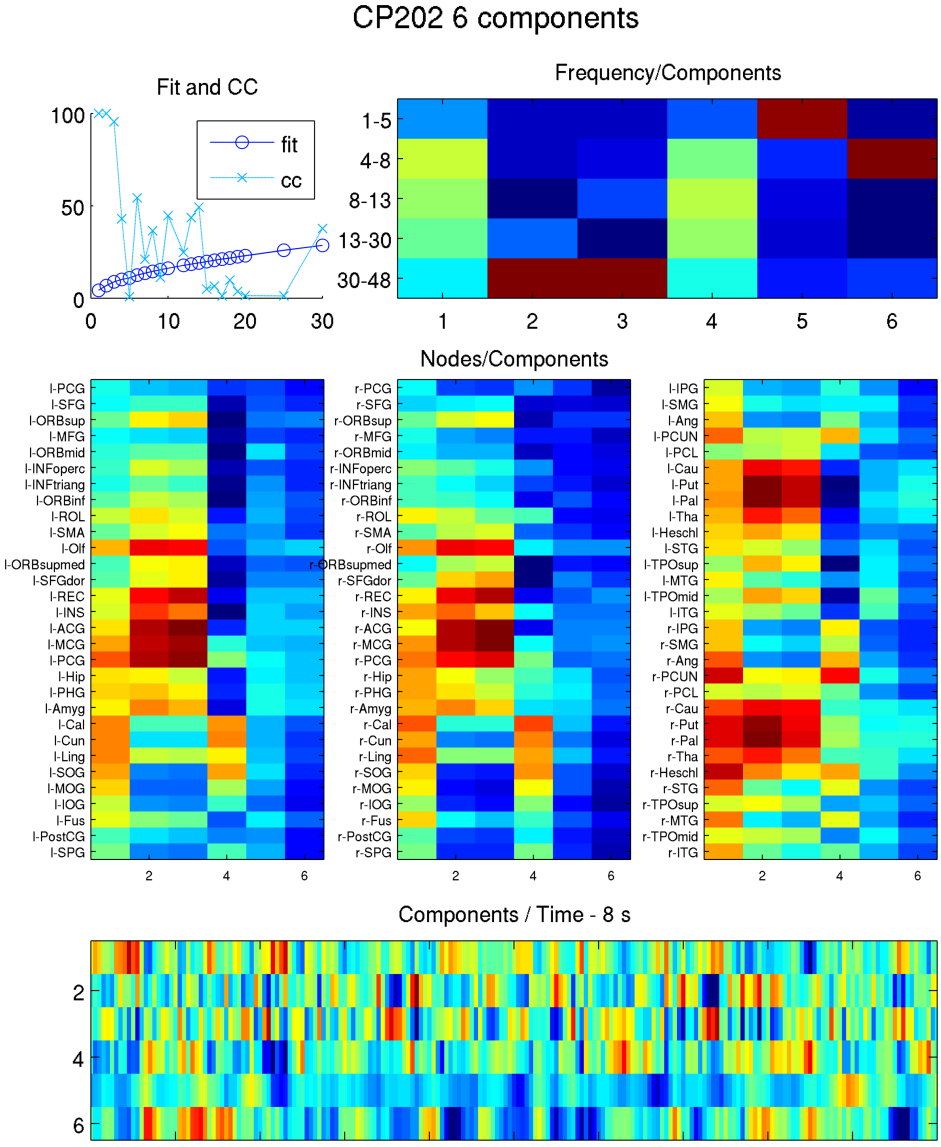

Figure 5.6: *CP202 decomposition with nonnegativity constraint in the first (space) and third (frequency) mode - 6 Components.*

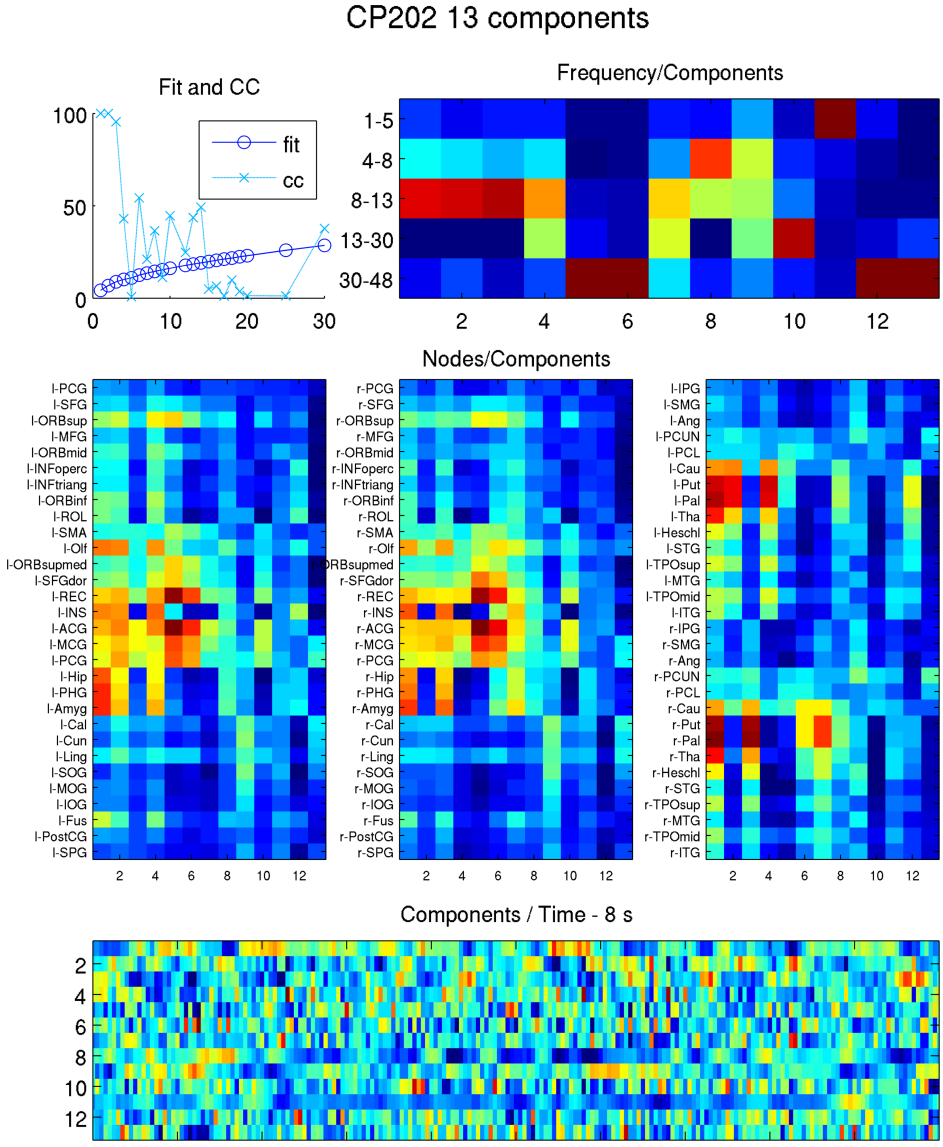

Figure 5.7: *CP202 decomposition with nonnegativity constraint in the first (space) and third (frequency) mode - 13 Components.*

5.4. Discussion

In this chapter, we presented an alternative approach to using ICA, the to-date standard method of decomposing whole brain activity into distinguishable networks of brain activity. In an AAL-parcellated RS-MEG dataset, ICA and twodimensional CP decompositions explain similar amounts of variance. ICA decomposition showed a principally lobular delineation, with an occipital component, a frontal component, a parietal component, and a left and a right temporal component (Figure 5.3 far left). The first three of these coincide with the visual, frontopolar, and sensorimotor functional networks previously identified (e.g. Figure 1.3 F,D,G).

The results show that the methods match in the strongest components but differ in spatial extent and overlap. Temporal ICA showed the most isolated components while the other methods tended to have one widespread, strongest component.

Taken together, our results show that twodimensional CP methods are capable of reproducing some of the strongest functional RS networks. Due to the limited spatial resolution and purely datadriven approach, with no manual selection of components, the decomposition only reproduces some of the established RSNs, which are the least distributed ones. Especially the DMN does not appear as a component in any of the decompositions, but it was also not necessarily expected after the study of Smith et al. (2012). The strong fragmentation into single brain areas/lobes is likely also due to the combination of constraints and spatial resolution. It appears that the RSNs extracted by ICA emerge due to the independence maximization of the method, but that they are not the strongest components signal-wise in the data. We speculate that the CP methods pick up the strongest components signal-wise, which are more spatially modular in the concatenated band-limited power-envelope datasets.

This is just a first glimpse into the potentials and caveats of tensor decomposition approaches for extracting meaningful data components and their profiles and interactions accross multiple modes. Here, we extracted a lobular structure from a spatially coarse-grained parcellation. We did not find clear evidence for higher sensitivity of CP methods over more traditional ICA measures in detecting functional networks, but we did show that CP can extract similar components. The

variations of constraints in space and time remained inconclusive, and a more comprehensive investigation of their effects on synthetic data is warranted.

For detailed specifications of what kind of features can or cannot be extracted with CP, and how multivariate, large-scale neurophysiological signals are best preprocessed and decomposed, further study will be necessary. With the increasing availability of ressources such as toolboxes and introductory articles (Cichocki et al., 2014), this is an active field promising to yield highly interesting results in the near future.

5.5. Supplementary Figures and Tables

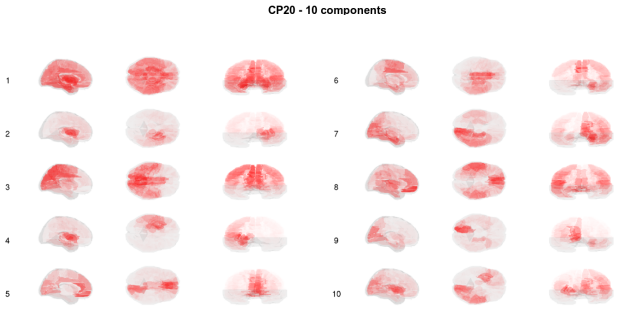

Figure 5.8: *CP20 in the beta-band - 10 components*

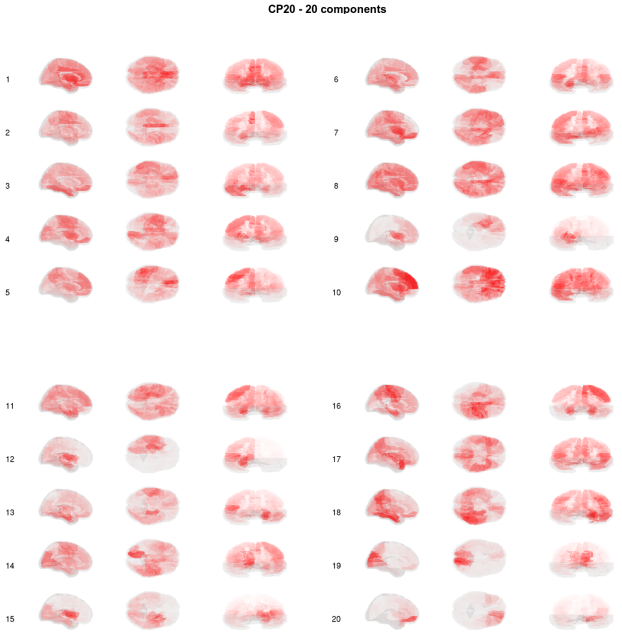

Figure 5.9: *CP20 in the beta-band - 20 components*

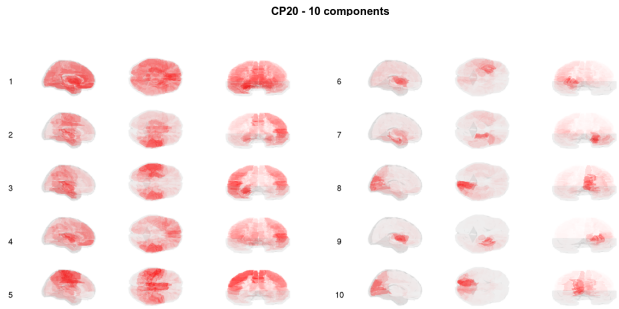

Figure 5.10: *CP20 in the beta-band, binarized - 10 components*

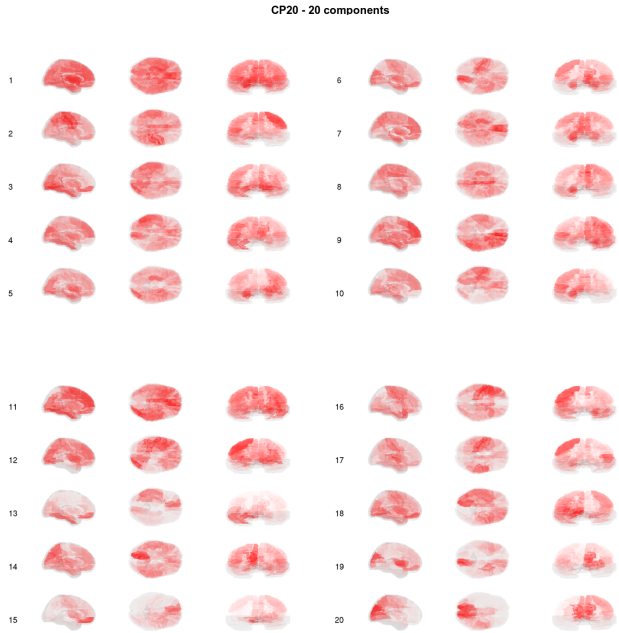

Figure 5.11: *CP20 in the beta-band, binarized - 20 components*

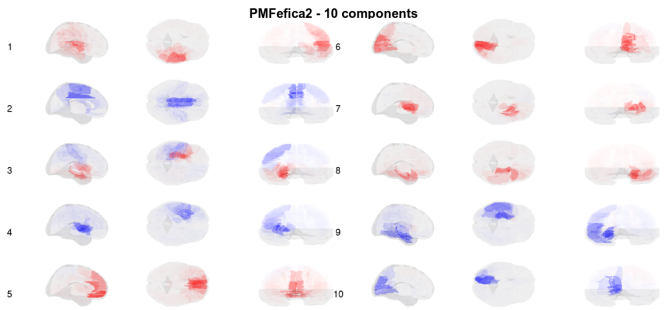

Figure 5.12: ICA
- 10 components]*Temporal ICA in the beta-band - 10 components*

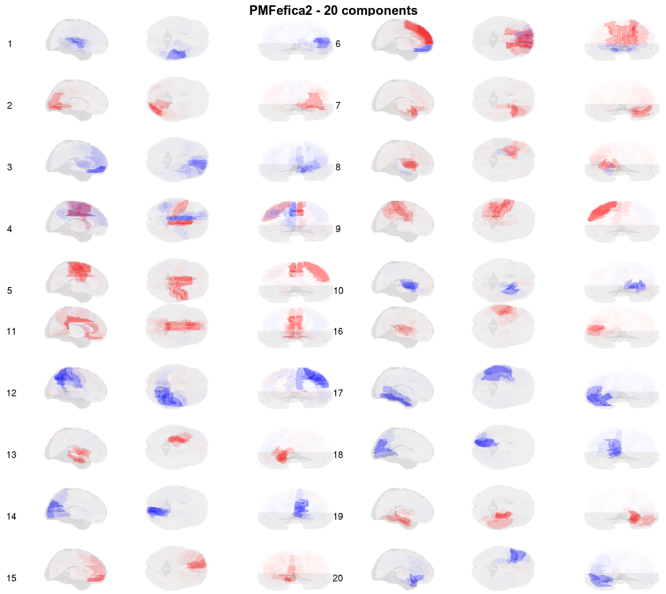

Figure 5.13: ICA
- 20 components]*Temporal ICA in the beta-band - 20 components*

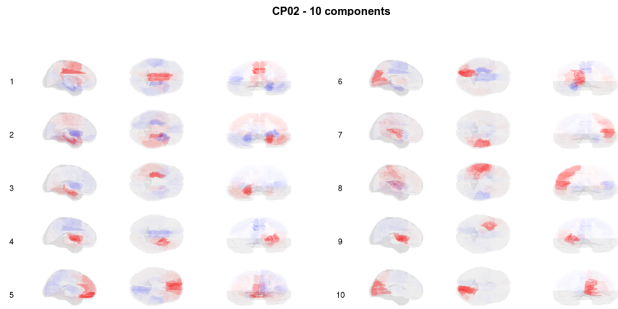

Figure 5.14: *CP02 in the beta-band, binarized - 10 components*

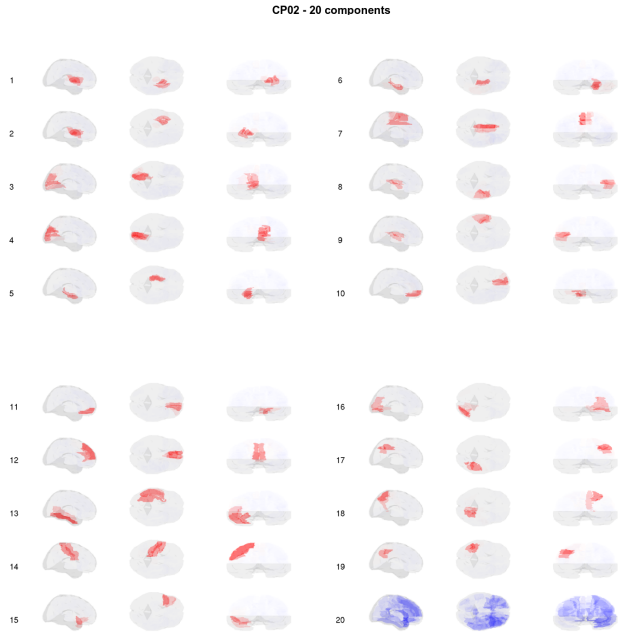

Figure 5.15: *CP02 in the beta-band, binarized - 20 components*

Table 5.1: AAL region abbreviations]*AAL regions ans abbreviations, as in Tagliazucchi et al. (2012b). Region numbers in the first column are for for left-right, correspondingly.*

Nr	Region Name	Abbreviation
1-2	Precentral Gyrus	PCG
3-4	Superior frontal gyrus	SFG
5-6	Superior frontal gyrus, orbital part	ORBsup
7-8	Middle frontal gyrus	MFG
9-10	Middle frontal gyrus, orbital	ORBmid
11-12	Inferior frontal gyrus, opercular	INFoperc
13-14	Inferior frontal gyrus, triangular	INFtriang
15-16	Inferior frontal gyrus, orbital	ORBinf
17-18	Rolandic operculum	ROL
19-20	Supplementary motor area	SMA
21-22	Olfactory cortex	Olf
23-24	Superior frontal gyrus, medial	ORBsupmed
25-26	Superior frontal gyrus, dorsal	SFGdor
27-28	Rectus gyrus	REC
29-30	Insula	INS
31-32	Anterior cingulate gyrus	ACG
33-34	Middle cingulate gyrus	MCG
35-36	Posterior cingulate gyrus	PCG
37-38	Hippocampus	Hip
39-40	Parahippocampal gyrus	PHG
41-42	Amygdala	Amyg
43-44	Calcarine cortex	Cal

Nr	Region Name	Abbreviation
45-46	Cuneus	Cun
47-48	Lingual gyrus	Ling
49-50	Superior occipital gyrus	SOG
51-52	Middle occipital gyrus	MOG
53-54	Inferior occipital gyrus	IOG
55-56	Fusiform gyrus	Fus
57-58	Postcentral gyrus	PostCG
59-60	Superior parietal gyrus	SPG
61-62	Inferior parietal gyrus	IPG
63-64	Supramarginal gyrus	SMG
65-66	Angular gyrus	Ang
67-68	Precuneus	PCUN
69-70	Paracentral lobule	PCL
71-72	Caudate	Cau
73-74	Putamen	Put
75-76	Pallidum	Pal
77-78	Thalamus	Tha
79-80	Heschl's gyrus	Heschl
81-82	Superior temporal gyrus	STG
83-84	Temporal pole, superior	TPOsup
85-86	Middle temporal gyrus	MTG
87-88	Temporal pole, middle	TPOmid
89-90	Inferior temporal gyrus	ITG

6. General discussion

In the preceeding chapters, we laid out our work focussing on the complex spatiotemporal activity patterns that occur in the brain intrinsically, that is, in the absence of experimental tasks or stimulations. We applied a biophysically realistic computational model of brain dynamics in order to study critical network parameters and contingent changes in the spatiotemporal network setup of RS brain dynamics. We set out to demonstrate how both the interaction of the complex structural connectivity patterns and their temporal embedding in the presence of oscillations shape RSN dynamics and functional connectivity patterns. In order to do so, we applied a large-scale brain model with integrate-and-fire neurons and anatomically derived connectivity patterns. With this model, we studied the connectivity patterns resulting from its internal dynamics in relation to key parameter settings. In the following, we will discuss the implications of our findings in context of the existing literature, as well as the present and future of RSN- and brain dynamics research in general.

As we have seen in Section 2.3, there is a wealth of models for brain dynamics that have been used in large-scale brain simulations, with varying degrees of complexity, biological realism, and different underlying dynamics. Unavoidably, all brain simulations are to some degree reductions, usually by many, many degrees. But even the most ambitious projects in terms of realism, such as the HBP, face challenges: of how to handle, analyze, summarize and, most importantly, understand and extract the important features of the immense quantities of data produced. As such, there is no one 'correct' model of the brain, and the choice of model optimally depends on the objective and the nature of the dynamics in question. Abstract models may suffice for studying population-behaviour in order to generalize beyond the specific implementation of a function, to find similarities in different systems or conclude about the global configuration of the system. More detailed models, however, are needed to study the mechanisms by which these global dynamics are instantiated in the microscopic scales of the system. Recently, it has been shown that the global configurations and a variety of dynamics can be implemented in highly reduced models of simple oscilla-

tors (e.g. Cabral et al., 2011, 2014) and even analytical derivations of statistical moments (Deco et al., 2013b).

In the present work, we have mainly been interested in the macroscopic network configurations in relation to both global and local parameters and mechanisms. We studied the effects of gradually decreasing global and local connectivity strengths (Chapter 3), and local oscillatory dynamics and inter-area signal propagation delays (Chapter 4). We worked with the versatile model of Deco & Jirsa (2012), which in its basic form comprises a network of biophysiologically realistic integrate-and-fire neurons. In consideration to computational cost this network, too, is reduced in many ways such as the limited number of 18.000 neurons and 90 brain areas. Our choice of this model was based on that it allows both for further reduction and for the inclusion of biophysically meaningful mechanisms. One such mechanism is SFA through AHP, which we used to introduce oscillatory dynamics in the connected network.

In relation with fMRI data, we applied an asynchronous model in the low activity regime to simulate BOLD data. We had found before that, in the absence of oscillations on the same time scale, introduction of delays does not change the global network configuration. In that case, the time scale of the accumulation of the incoming activity is such that the phase delay does not substantially change the interaction patterns between the nodes. Notably, both in oscillatory and nonoscillatory systems, a critical dynamical region was identified, in which the empirical FC and the model configuration coincide best, and fit decreases again beyond a certain coupling strength (see Figure 2.1 h). This optimal working point is near a bifurcation (Deco & Jirsa, 2012; Deco et al., 2013a), which corresponds to a metastable region between high and low activity states in the spiking attractor network. Critical dynamics are increasingly studied and found in neural networks (Beggs, 2008; Haken, 1996; Rabinovich et al., 2001, 2008), and evidence accumulates that criticality is a key organizing principle in the brain as a whole (Bassett et al., 2006; Deco et al., 2013a; Kitzbichler et al., 2009; Poil et al., 2008, 2012; Tagliazucchi et al., 2012a). In this perspective, RS brain dynamics are far from random, noisy fluctuations of activity around main structural pathways, but a key base from which to access the array of cognitive architectures the brain has available. A functional setting of the system at this working point thus maximizes its flexibility and ability to explore various functional states without fully activating sensory and cognitive goal-focused processing.

Our main contribution lies within showing how the critical model parameters and behaviour depend on the underlying system. In the asynchronous model, we showed how brain signal complexity is affected by increasing distance from the critical working point. Also, we demonstrated that, while the SC is critical for the dynamics in all cases, it starts interacting with delays in the presence of noisy oscillations on a similar timescale. With this, we were able to expand the model to consider oscillatory activity as recorded by electrophysiology. By combining coupling and delay parameters, we were able to identify a best-fit region for the model. We concluded that delays matter in this case, and that propagation velocities in the range of what is neurologically realistic stabilize the system. They increase both the maximum and range of good fit over the coupling by preventing precipitated global synchronization in the system.

In this scenario, strength of the oscillation is input-dependent, meaning that neurons transition from a low-input asynchronous state to noisy oscillatory activity and later to a synchronous bursting regime. The frequency depends somewhat on the input strength, whereby input actually decreases the frequency (see Figure 4.2). This seems contrary to empirical findings of cortical activity at first sight, but one must consider that higher input also most probably leads to decrease in the oscillation-generating SFA (discussed in detail below). In our model, the oscillation frequency of the whole system behaves quite similar to that of a single, unconnected node in that it primarily depends on the strength and timescale of the AHP current. In contrast, Cabral and colleagues (Cabral et al., 2011; Cabral, 2012) observe a substantial frequency reduction in a coupled system of weakly coupled gamma-band Kuramoto oscillators. Both models can result in clusters of nodes at different frequencies. This is due to the input-dependency in our case, where a densely connected cluster would show lower frequency than a weakly connected cluster, and due to the different sizes and delays of transiently emerging clusters in the Kuramoto system. As these two cases build upon two distinct principles, it is desirable to disentangle these two scenarios. To do so, we will have to study with scrutiny the emerging cluster dynamics in time, both empirically and in the proposed models. It would also be worthwhile to see if a more complex large-scale model, e.g. of firing neurons, can reproduce reduced-frequency synchronization of gamma-oscillating units such as found in the Kuramoto oscillators.

In our model, delays play a critical role in distributing the mutual inputs in the

network, so that inputs do not acumulate to cause activity bursts with a following refractory periods in all neurons at the same time. The oscillatory dynamics in the model were introduced by SFA of the excitatory neuron populations of all cortical nodes. This of course does not mean that these are the only possible, actual mechanisms by which the alpha/beta oscillations observed ubiquously in electrophysiological RS recordings are generated in the human brain. Other simulation studies have proposed different underlying oscillatory dynamics. For example, intrinsic local gamma dynamics that lead to slower oscillations in the coupled system (Deco et al., 2009; Cabral et al., 2011) have also been proposed as underlying generator. Different oscillator types actually lead to similar results (Ghosh et al., 2008b), and the cortex also responds to oscillatory thalamic inputs (Freyer et al., 2009, 2011; Roy et al., 2014). In fact, the neural origin and propagation of spontaneous cortical oscillations in wakefulness and sleep is multifaceted, and interesting works are being conducted on the topic (Ladenbauer et al., 2012; Augustin et al., 2013; Hindriks et al., 2014). It is quite fascinating that we have known of different frequency brain oscillations from the very first eletrophysiological recordings in the early 19th century, and yet we still have such little integrated knowledge about their function or the mechanisms behind their appearance and modulation between different mental states. In the course of this project, by studying SFA effects on spiking behavior (see Figure 4.3) and reviewing the literature, we have embraced the notion that SFA may be a key mechanism in modulating mental state and lower-than-gamma oscillation occurence in the human brain. Different types of SFA have already been identified and found in cortex (Lopes da Silva et al., 1980), but their role in controling cognitive states are only now being studied with large-scale models (e.g. Deco et al., 2014). In this view, the cortex, without further input, would be largely governed by global waves induced by slow scale SFA, such as we can see in up and down states in human sleep. We already know that ACh signaling decreases SFA, so reticular activation would decrease synchrony in global waves, allow for weaker, faster time scale adaptation to occur, which may elicit the typical resting inactivity alpha-rhythm. This, again, may be shut down by further ACh signaling in some or all networks, and high-rate neural computations and local inhibitory-excitatory loop oscillation in the gamma range would occur. Of course, this is only a very rough image, and many specific functions may use certain frequency ranges independently. Yet, different functionally associated rhythms, such as the posterior alpha or the rolandic alpha, fit well in this concept in that they are ac-

tually 'idling' rhythms (Ritter et al., 2009), that is, in a low-power standby state, quickly activable but not busily processing yet.

Many empiricical and computational questions arise from this possible general principle of brain states. Are the different rhythms based on different neural mechanics, or are they distinguishable because they are separated into clusters by the spatiotemporal cortical connectivity? How many neurons feature SFA, and are different adaptation time scales (from bursty supersecond global oscillations to shallow noisy beta rhythms) implemented in different neuron populations? How much of the oscillations are induced by the thalamocortical loop and is resonance-related? How far are interneurons involved in these dynamics? Some pieces of these and other questions are known (e.g. bursty versus regular spiking cells). Their further study, however, is still outstanding (e.g., do bursty and regular spiking cells form a continuum or two cluster?), and indispensable if we want to profoundly comprehend brain states, mental states (including the concepts of wakefulness and sleep stages themselves), and, by extension, important aspects of neuropsychological diseases.

Ultimately, when modeling RS activity, it would be desirable to combine and study both fMRI BOLD and EEG/MEG data in one model, so being able to include rhythmic neural activity is important. Recently, several studies have combined tract imaging, as well as fMRI and EEG/MEG in the same or several recording sessions, so that individual data can be obtained in different modalities (e.g. Sato et al., 2010; Tagliazucchi et al., 2012b; Schölvinck et al., 2010). With these new possibilities, we also have to think about how to represent and explain various data features in one model. This is in no sense trivial, and the knowledge of how different models behave with respect to one or two parameters is an invaluable basis to move towards more comprehensive models. As more data aspects are integrated and compared, though, we also need a new level of standardization and reproducibility. For this necessary development, well-standardized open source model platforms such as TVB (Sanz Leon et al., 2013) open up new possibilities in large-scale brain simulation.

Computational studies are also increasingly concerned with brain network dynamics, in the sense of spatiotemporal fingerprints and interactions of functional networks. In Chapter 5, we explored a new approach to decomposing RS activity into networks, and the nature and assumptions underlying their extraction.

Smith et al. (2012) showed differences in spatial and temporal ICA in fMRI data. By comparing the commonly applied ICA approach with tensor decomposition approaches (CP/PARAFAC) with different underlying assumptions about the nature of the underlying data, we found similar components and variance explained for some conditions, and showed that CP may be a valid an valuable approach. Many caveats remain and many factors (such as the most appropriate preprocessing steps and data simplifications) to lead to a more automatic network decomposition method, are still to be determined. A more detailed scrutinization of these methods on synthetic and brain data, however, promises to give us powerful tools to reliably extract meaningful components.

7. Conclusions

In this thesis, we have studied the connectivity patterns emerging in a biophysically realistic large-scale model of spontaneous dynamics of the human brain in a state of wakeful rest. We built the model upon an empirically derived structural connectome, and used MEG recordings to judge model performance. First, we demonstrated the impact of the just strength of connectivity in order to maintain variability and complexity. The model suggests that a dislocation from the optimal working point at the edge of criticality may explain the changes of brain dynamics in aging. Then we expanded the model in order to study if the presence of oscillations, integrated into a spiking-neuron network, would cause the consideration of propagation delays to be important for network configuration. We were able to show that delays are important to consider in the presence of oscillations of a similar timescale. We found that physiologically realistic delays result in best concordance between the model and empirical data. Our results suggest highest robusticity in the presence of delays, and the model is readily adjustable to include different dynamic regimes such as slow bursty activity or high rate firing. To better define and unmingle different functional components in the data, we proposed the use of tensor factorization methods, and showed their potential to extract meaningful subnetworks from RS brain recordings.

To conclude, we expect that the findings and explanations we have here presented contribute to the advancement of the field of RS and brain dynamics research. We anticipate that the herein discussed concepts and caveats carry inspiration and impetus for further advancing our understanding of intrinsic dynamics underlying RS brain activity.

Bibliography

Achard, S. & Bullmore, E. (2007). Efficiency and Cost of Economical Brain Functional Networks. *PLoS Comput Biol*, 3(2), e17, doi:10.1371/journal.pcbi.0030017. http://dx.plos.org/10.1371/journal.pcbi.0030017.

Ahmed, B., Anderson, J. C., Douglas, R. J., Martin, K. A., & Whitteridge, D. (1998). Estimates of the net excitatory currents evoked by visual stimulation of identified neurons in cat visual cortex. *Cerebral Cortex*, 8(5), 462 – 476, doi:10.1093/cercor/8.5.462. http://cercor.oxfordjournals.org/content/8/5/462.abstract.

Alstott, J., Breakspear, M., Hagmann, P., Cammoun, L., & Sporns, O. (2009). Modeling the Impact of Lesions in the Human Brain. *PLoS Comput Biol*, 5(6), e1000408, doi:10.1371/journal.pcbi.1000408. http://dx.doi.org/10.1371/journal.pcbi.1000408.

Ardekani, S., Kumar, A., Bartzokis, G., & Sinha, U. (2007). Exploratory voxel-based analysis of diffusion indices and hemispheric asymmetry in normal aging. *Magn Reson Imaging*, 25(2), 154–167, doi:10.1016/j.mri.2006.09.045. http://www.sciencedirect.com/science/article/pii/S0730725X06003365.

Arieli, A., Sterkin, A., Grinvald, A., & Aertsen, A. (1996). Dynamics of Ongoing Activity: Explanation of the Large Variability in Evoked Cortical Responses. *Science*, 273(5283), 1868–1871, doi:10.1126/science.273.5283.1868. http://www.sciencemag.org/content/273/5283/1868.

Augustin, M., Ladenbauer, J., & Obermayer, K. (2013). How adaptation shapes spike rate oscillations in recurrent neuronal networks. *Front. Comput. Neurosci*, 7, 9, doi:10.3389/fncom.2013.00009. http://www.frontiersin.org/Computational_Neuroscience/10.3389/fncom.2013.00009/abstract.

Bader, B. W. & Kolda, T. G. (2007). Efficient MATLAB computations with sparse and factored tensors. *SIAM Journal on Scientific Computing*, 30(1), 205–231. http://epubs.siam.org/doi/abs/10.1137/060676489.

Bakker, R., Wachtler, T., & Diesmann, M. (2012). CoCoMac 2.0 and the future of tract-tracing databases. *Front Neuroinform*, 6, doi:10.3389/fninf.2012.00030. http://www.ncbi.nlm.nih.gov/pmc/articles/PMC3530798/.

Barnes, G. R. & Hillebrand, A. (2003). Statistical flattening of MEG beamformer images. *Hum. Brain Mapp.*, 18(1), 1–12, doi:10.1002/hbm.10072. http://onlinelibrary.wiley.com/doi/10.1002/hbm.10072/abstract.

Barry, R. J., Clarke, A. R., Johnstone, S. J., Magee, C. A., & Rushby, J. A. (2007). EEG differences between eyes-closed and eyes-open resting conditions. *Clinical Neurophysiology*, 118(12), 2765–2773, doi:10.1016/j.clinph.2007.07.028. http://www.sciencedirect.com/science/article/pii/S1388245707004002.

Basser, P. J., Mattiello, J., & LeBihan, D. (1994). MR diffusion tensor spectroscopy and imaging. *Biophys J*, 66(1), 259–267. http://www.ncbi.nlm.nih.gov/pmc/articles/PMC1275686/.

Bassett, D. S., Meyer-Lindenberg, A., Achard, S., Duke, T., & Bullmore, E. (2006). Adaptive reconfiguration of fractal small-world human brain functional networks. *Proc Natl Acad Sci U S A*, 103(51), 19518–19523, doi:10.1073/pnas.0606005103.

Beaulieu, C. (2002). The basis of anisotropic water diffusion in the nervous system – a technical review. *NMR Biomed*, 15(7-8), 435–455, doi:10.1002/nbm.782. http://onlinelibrary.wiley.com/doi/10.1002/nbm.782/abstract.

Becker, R., Reinacher, M., Freyer, F., Villringer, A., & Ritter, P. (2011). How Ongoing Neuronal Oscillations Account for Evoked fMRI Variability. *J. Neurosci.*, 31(30), 11016–11027, doi:10.1523/JNEUROSCI.0210-11.2011.

Beckmann, C. & Smith, S. (2004). Probabilistic independent component analysis for functional magnetic resonance imaging. *IEEE Transactions on Medical Imaging*, 23(2), 137–152, doi:10.1109/TMI.2003.822821.

Beckmann, C. F., DeLuca, M., Devlin, J. T., & Smith, S. M. (2005). Investigations into resting-state connectivity using independent component analysis. *Philos Trans R Soc Lond B Biol Sci*, 360(1457), 1001–1013, doi:10.1098/rstb.2005.1634.

Beckmann, C. F. & Smith, S. M. (2005). Tensorial extensions of independent component analysis for multisubject FMRI analysis. *NeuroImage*, 25(1), 294–311, doi:10.1016/j.neuroimage.2004.10.043. http://www.sciencedirect.com/science/article/pii/S1053811904006378.

Beggs, J. M. (2008). The criticality hypothesis: how local cortical networks might optimize information processing. *Philos Transact A Math Phys Eng Sci*, 366(1864), 329–343, doi:10.1098/rsta.2007.2092. http://www.ncbi.nlm.nih.gov/pubmed/17673410.

Behrens, T., Berg, H. J., Jbabdi, S., Rushworth, M., & Woolrich, M. (2007). Probabilistic diffusion tractography with multiple fibre orientations: What can we gain? *NeuroImage*, 34(1), 144–155, doi:10.1016/j.neuroimage.2006.09.018. http://www.sciencedirect.com/science/article/pii/S1053811906009360.

Ben-Simon, E., Podlipsky, I., Arieli, A., Zhdanov, A., & Hendler, T. (2008). Never resting brain: simultaneous representation of two alpha related processes in humans. *PLoS ONE*, 3(12), e3984, doi:10.1371/journal.pone.0003984. http://www.ncbi.nlm.nih.gov/pubmed/19096714.

Berger, P. D. H. (1929). Über das Elektrenkephalogramm des Menschen. *Archiv f. Psychiatrie*, 87(1), 527–570, doi:10.1007/BF01797193. http://link.springer.com/article/10.1007/BF01797193.

Bernhardt, B. C., Chen, Z., He, Y., Evans, A. C., & Bernasconi, N. (2011). Graph-theoretical analysis reveals disrupted small-world organization of cortical thickness correlation networks in temporal lobe epilepsy. *Cereb. Cortex*, 21(9), 2147–2157, doi:10.1093/cercor/bhq291.

Bezgin, G., Vakorin, V. A., van Opstal, A. J., McIntosh, A. R., & Bakker, R. (2012). Hundreds of brain maps in one atlas: Registering coordinate-independent primate neuro-anatomical data to a standard brain. *NeuroImage*, 62(1), 67–76, doi:10.1016/j.neuroimage.2012.04.013. http://www.sciencedirect.com/science/article/pii/S1053811912003941.

Binder, J., Frost, J., Hammeke, T., Bellgowan, P., Rao, S., & Cox, R. (1999). Conceptual processing during the conscious resting state: A functional MRI study. *Journal of Cognitive Neuroscience*, 11(1), 80–93. http://apps.isiknowledge.com/full_record.do?product=WOS&search_mode=Refine&qid=3&SID=U2C5oj5eomiJdgADAlB&page=2&doc=16.

Birn, R. M. (2012). The role of physiological noise in resting-state functional connectivity. *Neuroimage*, 62(2), 864–870, doi:10.1016/j.neuroimage.2012.01.016.

Birn, R. M., Diamond, J. B., Smith, M. A., & Bandettini, P. A. (2006). Separating respiratory-variation-related fluctuations from neuronal-activity-related fluctuations in fMRI. *NeuroImage*, 31(4), 1536–1548, doi:10.1016/j.neuroimage.2006.02.048. http://www.sciencedirect.com/science/article/pii/S1053811906001248.

Biswal, B., Yetkin, F. Z., Haughton, V. M., & Hyde, J. S. (1995). Functional connectivity in the motor cortex of resting human brain using echo-planar MRI. *Magn Reson Med*, 34(4), 537–541. http://www.ncbi.nlm.nih.gov/pubmed/8524021.

Biswal, B. B., Kylen, J. V., & Hyde, J. S. (1997). Simultaneous assessment of flow and BOLD signals in resting-state functional connectivity

maps. *NMR Biomed*, 10(4-5), 165–170, doi:10.1002/(SICI)1099-1492(199706/08)10:4/5<165::AID-NBM454>3.0.CO;2-7. http://onlinelibrary.wiley.com/doi/10.1002/(SICI)1099-1492(199706/08)10:4/5%3C165::AID-NBM454%3E3.0.CO;2-7/abstract.

Biswal, B. B., et al. (2010). Toward Discovery Science of Human Brain Function. *PNAS*, 107(10), 4734–4739, doi:10.1073/pnas.0911855107. http://www.pnas.org/content/107/10/4734.

Bohn, H. G. H. G. & Ray, J. (1855). *A hand-book of proverbs. Comprising an entire republication of Ray's collection of English proverbs, with his additions from foreign languages. And a complete alphabetical index; in which are introduced large additions, as well of proverbs as of sayings, sentences, maxims, and phrases*. London, H.G. Bohn. http://archive.org/details/ahandbookprover01raygoog.

Bonavita, S., et al. (2011). Distributed changes in default-mode resting-state connectivity in multiple sclerosis. *Mult. Scler.*, 17(4), 411–422, doi:10.1177/1352458510394609.

Breakspear, M. & Jirsa, V. K. (2007). Neuronal Dynamics and Brain Connectivity. In V. K. Jirsa & A. R. McIntosh (Eds.), *Handbook of Brain Connectivity*, Understanding Complex Systems (pp. 3–64). Springer Berlin Heidelberg. http://link.springer.com/chapter/10.1007/978-3-540-71512-2_1.

Breakspear, M., Terry, J. R., & Friston, K. J. (2003). Modulation of excitatory synaptic coupling facilitates synchronization and complex dynamics in a biophysical model of neuronal dynamics. *Network: Computation in Neural Systems*, 14, 703–732. http://informahealthcare.com/doi/abs/10.1088/0954-898X_14_4_305.

Brickman, A. M., et al. (2006). Regional white matter and neuropsychological functioning across the adult lifespan. *Biol Psychiatry*, 60(5), 444–453, doi:10.1016/j.biopsych.2006.01.011.

Brodmann, K. (1909). *Vergleichende Lokalisationslehre der Grosshirnrinde: in ihren Principien dargestellt auf Grund des Zellenbaues*. Leipzig: Johann Ambrosius Barth Verlag.

Brodmann, K. & Gary, L. J. (2006). *Brodmann's localization in the cerebral cortex the principles of comparative localisation in the cerebral cortex based on cytoarchitectonics*. [New York, NY]: Springer. http://site.ebrary.com/id/10160433.

Brookes, M. J., et al. (2011a). Measuring functional connectivity using MEG: Methodology and comparison with fcMRI. *NeuroImage*, 56(3), 1082–1104, doi:10.1016/j.neuroimage.2011.02.054. http://www.sciencedirect.com/science/article/pii/S1053811911002102.

Brookes, M. J., et al. (2014). Measuring temporal, spectral and spatial changes in electrophysiological brain network connectivity. *NeuroImage*, 91, 282–299, doi:10.1016/j.neuroimage.2013.12.066. http://www.sciencedirect.com/science/article/pii/S1053811914000123.

Brookes, M. J., Wood, J. R., Stevenson, C. M., Zumer, J. M., White, T. P., Liddle, P. F., & Morris, P. G. (2011b). Changes in brain network activity during working memory tasks: a magnetoencephalography study. *Neuroimage*, 55(4), 1804–1815, doi:10.1016/j.neuroimage.2010.10.074.

Brookes, M. J., et al. (2011c). Investigating the electrophysiological basis of resting state networks using magnetoencephalography. *Proc Natl Acad Sci U S A*, doi:10.1073/pnas.1112685108. http://www.pnas.org/content/early/2011/09/14/1112685108.abstract.

Brookes, M. J., Woolrich, M. W., & Barnes, G. R. (2012). Measuring functional connectivity in MEG: a multivariate approach insensitive to linear source leakage. *NeuroImage*, 63(2), 910–920, doi:10.1016/j.neuroimage.2012.03.048.

Brunel, N. & Wang, X.-J. (2001). Effects of neuromodulation in a cortical network model of object working memory dominated by recurrent inhibition. *J Comput Neurosci*, 11(1), 63–85.

Brunel, N. & Wang, X.-J. (2003). What Determines the Frequency of Fast Network Oscillations With Irregular Neural Discharges? I. Synaptic Dynamics and Excitation-Inhibition Balance. *Journal of Neurophysiology*, 90(1), 415 –430, doi:10.1152/jn.01095.2002. http://jn.physiology.org/content/90/1/415.abstract.

Buckner, R. L., Andrews-Hanna, J. R., & Schacter, D. L. (2008a). The Brain's Default Network. *Annals of the New York Academy of Sciences*, 1124(1), 1–38, doi:10.1196/annals.1440.011. http://onlinelibrary.wiley.com/doi/10.1196/annals.1440.011/abstract.

Buckner, R. L., Andrews-Hanna, J. R., & Schacter, D. L. (2008b). The Brain's Default Network. *Ann N Y Acad Sci*, 1124(1), 1–38, doi:10.1196/annals.1440.011. http://onlinelibrary.wiley.com/doi/10.1196/annals.1440.011/abstract.

Buckner, R. L. & Vincent, J. L. (2007). Unrest at rest: Default activity and spontaneous network correlations. *NeuroImage*, 37(4), 1091–1096, doi:16/j.neuroimage.2007.01.010. http://www.sciencedirect.com/science/article/pii/S1053811907000079.

Bullmore, E., Barnes, A., Bassett, D. S., Fornito, A., Kitzbichler, M., Meunier, D., & Suckling, J. (2009). Generic aspects of complexity in brain imaging data and other biological systems. *NeuroImage*, 47(3), 1125–1134, doi:10.1016/j.neuroimage.2009.05.032. http://www.sciencedirect.com/science/article/pii/S1053811909005242.

Bullmore, E. & Sporns, O. (2009). Complex brain networks: graph theoretical analysis of structural and functional systems. *Nat Rev Neurosci*, 10(3), 186–198, doi:10.1038/nrn2575. http://dx.doi.org/10.1038/nrn2575.

Bullmore, E. T. & Bassett, D. S. (2011). Brain Graphs: Graphical Models of the Human Brain Connectome. *Annu Rev Clin Psychol*, 7(1), 113–140, doi:10.1146/annurev-clinpsy-040510-143934. http://www.annualreviews.org/doi/abs/10.1146/annurev-clinpsy-040510-143934.

Burklund, L. J. & Lieberman, M. D. (2012). Advances in Functional Neuroimaging of Psychopathology. *Philosophy, Psychiatry, and Psychology*, 18(4), 333–337.

Cabeza, R., Dolcos, F., Graham, R., & Nyberg, L. (2002). Similarities and differences in the neural correlates of episodic memory retrieval and working memory. *Neuroimage*, 16(2), 317–330, doi:10.1006/nimg.2002.1063.

Cabeza, R. & Nyberg, L. (2000). Imaging cognition II: An empirical review of 275 PET and fMRI studies. *J Cogn Neurosci*, 12(1), 1–47.

Cabral, J. (2012). *Brain activity during rest*. PhD thesis.

Cabral, J., Hugues, E., Kringelbach, M. L., & Deco, G. (2012). Modeling the outcome of structural disconnection on resting-state functional connectivity. *NeuroImage*, 62(3), 1342–1353, doi:10.1016/j.neuroimage.2012.06.007. http://www.sciencedirect.com/science/article/pii/S1053811912005848.

Cabral, J., Hugues, E., Sporns, O., & Deco, G. (2011). Role of local network oscillations in resting-state functional connectivity. *NeuroImage*, doi:10.1016/j.neuroimage.2011.04.010. http://www.ncbi.nlm.nih.gov/pubmed/21511044.

Cabral, J., et al. (2014). Exploring mechanisms of spontaneous functional connectivity in MEG: How delayed network interactions lead to structured amplitude envelopes of band-pass filtered oscillations. *NeuroImage*, 90, 423–435, doi:10.1016/j.neuroimage.2013.11.047. http://www.sciencedirect.com/science/article/pii/S1053811913011968.

Calhoun, V. D., Eichele, T., Adalı, T., & Allen, E. A. (2012). Decomposing the brain: components and modes, networks and nodes. *Trends in Cognitive Sciences*, 16(5), 255–256, doi:10.1016/j.tics.2012.03.008. http://www.sciencedirect.com/science/article/pii/S1364661312000782.

Cammoun, L., et al. (2012). Mapping the human connectome at multiple scales with diffusion spectrum MRI. *Journal of Neuroscience*

Methods, 203(2), 386–397, doi:10.1016/j.jneumeth.2011.09.031. http://www.sciencedirect.com/science/article/pii/S0165027011005991.

Campbell, S. A. (2007). Time delays in neural systems. In A. R. McIntosh & V. K. Jirsa (Eds.), *Campbell, S.A., 2007. Time delays in neuHandbook of Brain Connectivity.* (pp. 65–90). Berlin: Springer-Verlag.

Carroll, J. D. & Chang, J.-J. (1970). Analysis of individual differences in multidimensional scaling via an n-way generalization of "Eckart-Young" decomposition. *Psychometrika*, 35(3), 283–319, doi:10.1007/BF02310791. http://link.springer.com/article/10.1007/BF02310791.

Chen, S., et al. (2008). Group independent component analysis reveals consistent resting-state networks across multiple sessions. *Brain Res.*, 1239, 141–151, doi:10.1016/j.brainres.2008.08.028.

Chiang, A. K. I., Rennie, C. J., Robinson, P. A., Van Albada, S. J., & Kerr, C. C. (2011). Age trends and sex differences of alpha rhythms including split alpha peaks. *Clin Neurophysiol*, 122(8), 1505–1517.

Cichocki, A. (2009). *Non-negative matrix and tensor factorizations applications to exploratory multiway data analysis and blind source separation*. Hoboken, NJ: John Wiley. http://site.ebrary.com/id/10317781.

Cichocki, A. (2013). Tensor Decompositions: A New Concept in Brain Data Analysis? *arXiv:1305.0395 [cs, q-bio, stat]*. http://arxiv.org/abs/1305.0395.

Cichocki, A., Mandic, D., Phan, A.-H., Caiafa, C., Zhou, G., Zhao, Q., & De Lathauwer, L. (2014). Tensor Decompositions for Signal Processing Applications From Two-way to Multiway Component Analysis. *arXiv:1403.4462 [cs]*. http://arxiv.org/abs/1403.4462.

Cichocki, A., Mørup, M., Smaragdis, P., Wang, W., & Zdunek, R. (2008). Advances in Nonnegative Matrix and Tensor Factorization. *Comput Intell Neurosci*, 2008, doi:10.1155/2008/852187. http://www.ncbi.nlm.nih.gov/pmc/articles/PMC2443422/.

Cloutman, L. L. & Lambon Ralph, M. A. (2012). Connectivity-based structural and functional parcellation of the human cortex using diffusion imaging and tractography. *Front Neuroanat*, 6, 34, doi:10.3389/fnana.2012.00034.

Collins, D. L., Neelin, P., Peters, T. M., & Evans, A. C. (1994). Automatic 3D intersubject registration of MR volumetric data in standardized Talairach space. *J Comput Assist Tomogr*, 18(2), 192–205.

Connors, B. W., Gutnick, M. J., & Prince, D. A. (1982). Electrophysiological Properties of Neocortical Neurons in Vitro. *J Neurophysiol*, 48(6), 1302–1320. http://jn.physiology.org/content/48/6/1302.

Corbetta, M. & Shulman, G. L. (2002). Control of goal-directed and stimulus-driven attention in the brain. *Nat. Rev. Neurosci.*, 3(3), 201–215, doi:10.1038/nrn755.

Cordes, D., Haughton, V., Carew, J. D., Arfanakis, K., & Maravilla, K. (2002). Hierarchical clustering to measure connectivity in fMRI resting-state data. *Magn Reson Imaging*, 20(4), 305–317, doi:16/S0730-725X(02)00503-9. http://www.sciencedirect.com/science/article/pii/S0730725X02005039.

Cordes, D., et al. (2001). Frequencies Contributing to Functional Connectivity in the Cerebral Cortex in "Resting-State" Data. *AJNR Am J Neuroradiol*, 22(7), 1326–1333. http://www.ajnr.org/content/22/7/1326.

Cordes, D., et al. (2000). Mapping Functionally Related Regions of Brain with Functional Connectivity MR Imaging. *AJNR Am J Neuroradiol*, 21(9), 1636–1644. http://www.ajnr.org/content/21/9/1636.

Costa, M., Goldberger, A. L., & Peng, C.-K. (2002). Multiscale entropy analysis of complex physiologic time series. *Phys Rev Lett*, 89(6), 068102. http://www.ncbi.nlm.nih.gov/pubmed/12190613.

Costa, M., Goldberger, A. L., & Peng, C.-K. (2005). Multiscale entropy analysis of biological signals. *Phys Rev E Stat Nonlin Soft Matter Phys*, 71(2 Pt 1), 021906. http://www.ncbi.nlm.nih.gov/pubmed/15783351.

Craddock, R. C., et al. (2013). Imaging human connectomes at the macroscale. *Nat Meth*, 10(6), 524–539, doi:10.1038/nmeth.2482. http://www.nature.com/nmeth/journal/v10/n6/full/nmeth.2482.html.

Craig, A. D. (2002). How do you feel? Interoception: the sense of the physiological condition of the body. *Nat Rev Neurosci*, 3(8), 655–666, doi:10.1038/nrn894. http://www.nature.com/nrn/journal/v3/n8/full/nrn894.html.

Craig, A. D. (2009). How do you feel — now? The anterior insula and human awareness. *Nat Rev Neurosci*, 10(1), 59–70, doi:10.1038/nrn2555. http://www.nature.com/nrn/journal/v10/n1/full/nrn2555.html.

Crook, S. M., Ermentrout, G. B., & Bower, J. M. (1998). Spike Frequency Adaptation Affects the Synchronization Properties of Networks of Cortical Oscillators. *Neural Computation*, 10(4), 837–854, doi:i:10.1162/089976698300017511</p>. http://dx.doi.org/10.1162/089976698300017511.

Daducci, A., et al. (2012). The Connectome Mapper: An Open-Source Processing Pipeline to Map Connectomes with MRI. *PLoS One*, 7(12), doi:10.1371/journal.pone.0048121. http://www.ncbi.nlm.nih.gov/pmc/articles/PMC3525592/.

Damoiseaux, J. S., Prater, K. E., Miller, B. L., & Greicius, M. D. (2012). Functional connectivity tracks clinical deterioration in Alzheimer's disease. *Neurobiol. Aging*, 33(4), 828.e19–30, doi:10.1016/j.neurobiolaging.2011.06.024. http://www.ncbi.nlm.nih.gov/pubmed/21840627.

Damoiseaux, J. S., Rombouts, S. A. R. B., Barkhof, F., Scheltens, P., Stam, C. J., Smith, S. M., & Beckmann, C. F. (2006). Consistent resting-state networks across healthy subjects. *Proc Natl Acad Sci U S A*, 103(37), 13848 –13853, doi:10.1073/pnas.0601417103. http://www.pnas.org/content/103/37/13848.abstract.

De Luca, M., Beckmann, C. F., De Stefano, N., Matthews, P., & Smith, S. (2006). fMRI resting state networks define distinct modes of long-distance interactions in the human brain. *NeuroImage*, 29(4), 1359–1367,

doi:16/j.neuroimage.2005.08.035. http://www.sciencedirect.com/science/article/pii/S1053811905006257.

De Luca, M., Smith, S., De Stefano, N., Federico, A., & Matthews, P. M. (2005). Blood oxygenation level dependent contrast resting state networks are relevant to functional activity in the neocortical sensorimotor system. *Exp Brain Res*, 167(4), 587–594, doi:10.1007/s00221-005-0059-1.

de Pasquale, F., et al. (2010). Temporal dynamics of spontaneous MEG activity in brain networks. *Proc Natl Acad Sci U S A*, 107(13), 6040 –6045, doi:10.1073/pnas.0913863107. http://www.pnas.org/content/107/13/6040.abstract.

DeCarli, C., et al. (1995). The effect of white matter hyperintensity volume on brain structure, cognitive performance, and cerebral metabolism of glucose in 51 healthy adults. *Neurology*, 45(11), 2077–2084.

Deco, G. & Corbetta, M. (2011). The Dynamical Balance of the Brain at Rest. *Neuroscientist*, 17(1), 107 –123, doi:10.1177/1073858409354384. http://nro.sagepub.com/content/17/1/107.abstract.

Deco, G., Hagmann, P., Hudetz, A. G., & Tononi, G. (2014). Modeling resting-state functional networks when the cortex falls asleep: local and global changes. *Cereb. Cortex*, 24(12), 3180–3194, doi:10.1093/cercor/bht176.

Deco, G. & Jirsa, V. K. (2012). Ongoing Cortical Activity at Rest: Criticality, Multistability, and Ghost Attractors. *J Neurosci*, 32(10), 3366–3375, doi:10.1523/JNEUROSCI.2523-11.2012. http://www.jneurosci.org/content/32/10/3366.

Deco, G., Jirsa, V. K., & McIntosh, A. R. (2013a). Resting brains never rest: computational insights into potential cognitive architectures. *Trends in Neurosciences*, 36(5), 268–274, doi:10.1016/j.tins.2013.03.001. http://www.sciencedirect.com/science/article/pii/S0166223613000398.

Deco, G., Jirsa, V. K., McIntosh, A. R., Sporns, O., & Kötter, R. (2009). Key role of coupling, delay, and noise in resting brain fluctuations. *Proc Natl Acad Sci U S A*, 106(25), 10302.

Deco, G., Jirsa, V. K., Robinson, P. A., Breakspear, M., & Friston, K. J. (2008). The dynamic brain: From spiking neurons to neural masses and cortical fields. *PLoS Comput Biol*, 4(8), e1000092.

Deco, G., Ponce-Alvarez, A., Mantini, D., Romani, G. L., Hagmann, P., & Corbetta, M. (2013b). Resting-state functional connectivity emerges from structurally and dynamically shaped slow linear fluctuations. *J. Neurosci.*, 33(27), 11239–11252, doi:10.1523/JNEUROSCI.1091-13.2013.

Deco, G. & Rolls, E. T. (2006). Decision-making and Weber's law: a neurophysiological model. *Eur J Neurosci*, 24(3), 901–916, doi:10.1111/j.1460-9568.2006.04940.x.

DeFelipe, J. (1993). Neocortical Neuronal Diversity: Chemical Heterogeneity Revealed by Colocalization Studies of Classic Neurotransmitters, Neuropeptides, Calcium-binding Proteins, and Cell Surface Molecules. *Cereb. Cortex*, 3(4), 273–289, doi:10.1093/cercor/3.4.273. http://cercor.oxfordjournals.org/content/3/4/273.

Desgranges, B., Baron, J. C., & Eustache, F. (1998). The functional neuroanatomy of episodic memory: the role of the frontal lobes, the hippocampal formation, and other areas. *Neuroimage*, 8(2), 198–213, doi:10.1006/nimg.1998.0359.

Destexhe, A., Mainen, Z. F., & Sejnowski, T. J. (1998). Kinetic Models of Synaptic Transmission. In *Methods in Neuronal Modeling* (pp. 1–26). Cambridge, MA, USA: MIT Press, 2nd edition edition.

Dogonowski, A.-M., Andersen, K. W., Madsen, K. H., Sørensen, P. S., Paulson, O. B., Blinkenberg, M., & Siebner, H. R. (2013). Multiple sclerosis impairs regional functional connectivity in the cerebellum. *Neuroimage Clin*, 4, 130–138, doi:10.1016/j.nicl.2013.11.005. http://www.ncbi.nlm.nih.gov/pmc/articles/PMC3871286/.

Doucet, G., et al. (2011). Brain activity at rest: a multiscale hierarchical functional organization. *J. Neurophysiol.*, 105(6), 2753–2763, doi:10.1152/jn.00895.2010.

Ermentrout, B., Pascal, M., & Gutkin, B. (2001). The Effects of Spike Frequency Adaptation and Negative Feedback on the Synchronization of Neural Oscillators. *Neural Computation*, 13(6), 1285–1310, doi:i: 10.1162/08997660152002861</p>. http://dx.doi.org/10.1162/08997660152002861.

Ewald, A., Marzetti, L., Zappasodi, F., Meinecke, F. C., & Nolte, G. (2012). Estimating true brain connectivity from EEG/MEG data invariant to linear and static transformations in sensor space. *NeuroImage*, 60(1), 476–488, doi:10.1016/j.neuroimage.2011.11.084. http://www.sciencedirect.com/science/article/pii/S1053811911013668.

Feige, B., Scheffler, K., Esposito, F., Di Salle, F., Hennig, J., & Seifritz, E. (2005). Cortical and Subcortical Correlates of Electroencephalographic Alpha Rhythm Modulation. *Journal of Neurophysiology*, 93(5), 2864–2872, doi:10.1152/jn.00721.2004. http://jn.physiology.org/content/93/5/2864.abstract.

FitzHugh, R. (1961). Impulses and Physiological States in Theoretical Models of Nerve Membrane. *Biophys J*, 1(6), 445–466. http://www.ncbi.nlm.nih.gov/pmc/articles/PMC1366333/.

Fox, M. D. & Greicius, M. (2010). Clinical applications of resting state functional connectivity. *Front. Syst. Neurosci.*, 4, 19, doi:10.3389/fnsys.2010.00019. http://journal.frontiersin.org/Journal/10.3389/fnsys.2010.00019/full.

Fox, M. D. & Raichle, M. E. (2007). Spontaneous fluctuations in brain activity observed with functional magnetic resonance imaging. *Nat Rev Neurosci*, 8(9), 700–711, doi:10.1038/nrn2201. http://dx.doi.org/10.1038/nrn2201.

Fox, M. D., Snyder, A. Z., Vincent, J. L., Corbetta, M., Van Essen, D. C., & Raichle, M. E. (2005). The human brain is intrinsically organized into dynamic, anticorrelated functional networks. *Proc Natl Acad Sci U S A*, 102(27), 9673–9678, doi:10.1073/pnas.0504136102.

Fox, M. D., Zhang, D., Snyder, A. Z., & Raichle, M. E. (2009). The global signal and observed anticorrelated resting state brain networks. *J. Neurophysiol*, 101(6), 3270–3283, doi:10.1152/jn.90777.2008. http://www.ncbi.nlm.nih.gov/pubmed/19339462.

Fransson, P. (2005). Spontaneous low-frequency BOLD signal fluctuations: An fMRI investigation of the resting-state default mode of brain function hypothesis. *Hum Brain Mapp*, 26(1), 15–29, doi:10.1002/hbm.20113. http://onlinelibrary.wiley.com/doi/10.1002/hbm.20113/abstract.

Freyer, F., Aquino, K., Robinson, P. A., Ritter, P., & Breakspear, M. (2009). Bistability and Non-Gaussian Fluctuations in Spontaneous Cortical Activity. *J Neurosci*, 29(26), 8512 –8524, doi:10.1523/JNEUROSCI.0754-09.2009. http://www.jneurosci.org/content/29/26/8512.abstract.

Freyer, F., Roberts, J. A., Becker, R., Robinson, P. A., Ritter, P., & Breakspear, M. (2011). Biophysical Mechanisms of Multistability in Resting-State Cortical Rhythms. *J Neurosci*, 31(17), 6353–6361, doi:10.1523/JNEUROSCI.6693-10.2011. http://www.jneurosci.org/content/31/17/6353.

Freyer, F., Roberts, J. A., Ritter, P., & Breakspear, M. (2012). A Canonical Model of Multistability and Scale-Invariance in Biological Systems. *PLoS Comput Biol*, 8(8), e1002634, doi:10.1371/journal.pcbi.1002634. http://dx.doi.org/10.1371/journal.pcbi.1002634.

Friedlander, M. P. & Hatz, K. (2008). Computing Non-negative Tensor Factorizations. *Optimization Methods Software*, 23(4), 631–647, doi:10.1080/10556780801996244. http://dx.doi.org/10.1080/10556780801996244.

Friston, K. J. (1998). The disconnection hypothesis. *Schizophrenia Research*, 30(2), 115–125, doi:10.1016/S0920-9964(97)00140-0. http://www.sciencedirect.com/science/article/pii/S0920996497001400.

Friston, K. J., Harrison, L. M., & Penny, W. D. (2003). Dynamic causal modelling. *Neuroimage*, 19(4), 1273–1302, doi:16/S1053-8119(03)00202-7. http://www.sciencedirect.com/science/article/pii/S1053811903002027.

Friston, K. J., Mechelli, A., Turner, R., & Price, C. J. (2000). Nonlinear responses in fMRI: the Balloon model, Volterra kernels, and other hemodynamics. *Neuroimage*, 12(4), 466–477, doi:10.1006/nimg.2000.0630.

Fuhrmann, G., Markram, H., & Tsodyks, M. (2002). Spike Frequency Adaptation and Neocortical Rhythms. *J Neurophysiol*, 88(2), 761 –770. http://jn.physiology.org/content/88/2/761.abstract.

Galluzzi, S., Beltramello, A., Filippi, M., & Frisoni, G. B. (2008). Aging. *Neurol Sci*, 29(3), 296–300, doi:10.1007/s10072-008-1002-6. http://link.springer.com/article/10.1007/s10072-008-1002-6.

Garrett, D. D., Kovacevic, N., McIntosh, A. R., & Grady, C. L. (2011a). The importance of being variable. *J Neurosci*, 31(12), 4496–4503, doi:10.1523/JNEUROSCI.5641-10.2011. http://www.ncbi.nlm.nih.gov/pmc/articles/PMC3104038/.

Garrett, D. D., Kovacevic, N., McIntosh, A. R., & Grady, C. L. (2012). The Modulation of BOLD Variability between Cognitive States Varies by Age and Processing Speed. *Cereb Cortex*, doi:10.1093/cercor/bhs055. http://cercor.oxfordjournals.org/content/early/2012/03/14/cercor.bhs055.

Garrett, D. D., McIntosh, A. R., & Grady, C. L. (2011b). Moment-to-moment signal variability in the human brain can inform models of stochastic facilitation now. *Nature Reviews Neuroscience*, 12(10), 612–612, doi:10.1038/nrn3061-c1. http://www.nature.com/nrn/journal/v12/n10/full/nrn3061-c1.html.

Ge, Y., Grossman, R. I., Babb, J. S., Rabin, M. L., Mannon, L. J., & Kolson, D. L. (2002). Age-related total gray matter and white matter changes in normal adult brain. Part I: volumetric MR imaging analysis. *AJNR Am J Neuroradiol*, 23(8), 1327–1333.

Ghosh, A., Rho, Y., McIntosh, A. R., Kötter, R., & Jirsa, V. K. (2008a). Cortical network dynamics with time delays reveals functional connectivity in the resting brain. *Cogn Neurodyn*, 2(2), 115–120, doi:10.1007/s11571-008-9044-2.

Ghosh, A., Rho, Y.-A., McIntosh, A. R., Kötter, R., & Jirsa, V. K. (2008b). Noise during Rest Enables the Exploration of the Brain's Dynamic Repertoire. *PLoS Comput Biol*, 4(10), e1000196, doi:10.1371/journal.pcbi.1000196. http://dx.plos.org/10.1371/journal.pcbi.1000196.

Giorgio, A., Santelli, L., Tomassini, V., Bosnell, R., Smith, S., De Stefano, N., & Johansen-Berg, H. (2010). Age-related changes in grey and white matter structure throughout adulthood. *Neuroimage*, 51(3), 943–951, doi:10.1016/j.neuroimage.2010.03.004. http://www.sciencedirect.com/science/article/pii/S1053811910002740.

Goldberger, A. L., et al. (2000). PhysioBank, PhysioToolkit, and PhysioNet Components of a New Research Resource for Complex Physiologic Signals. *Circulation*, 101(23), e215–e220, doi:10.1161/01.CIR.101.23.e215. http://circ.ahajournals.org/content/101/23/e215.

Goldberger, A. L., Peng, C.-K., & Lipsitz, L. A. (2002). What is physiologic complexity and how does it change with aging and disease? *Neurobiol Aging*, 23(1), 23–26, doi:10.1016/S0197-4580(01)00266-4. http://www.sciencedirect.com/science/article/pii/S0197458001002664.

Goldman, R. I., Stern, J. M., Engel, Jr, J., & Cohen, M. S. (2002). Simultaneous EEG and fMRI of the alpha rhythm. *Neuroreport*, 13(18), 2487–2492, doi:10.1097/01.wnr.0000047685.08940.d0. http://www.ncbi.nlm.nih.gov/pubmed/12499854.

Golland, Y., Golland, P., Bentin, S., & Malach, R. (2008). Data-driven clustering reveals a fundamental subdivision of the human cortex into two global systems. *Neuropsychologia*, 46(2), 540–553, doi:16/j.neuropsychologia.2007.10.003. http://www.sciencedirect.com/science/article/pii/S0028393207003478.

Gonçalves, S., et al. (2006). Correlating the alpha rhythm to BOLD using simultaneous EEG/fMRI: Inter-subject variability. *NeuroImage*, 30(1), 203–213, doi:16/j.neuroimage.2005.09.062. http://www.sciencedirect.com/science/article/pii/S105381190500707X.

Gong, G., He, Y., Concha, L., Lebel, C., Gross, D. W., Evans, A. C., & Beaulieu, C. (2009). Mapping Anatomical Connectivity Patterns of Human Cerebral Cortex Using In Vivo Diffusion Tensor Imaging Tractography. *Cereb Cortex*, 19(3), 524–536, doi:10.1093/cercor/bhn102. http://cercor.oxfordjournals.org/content/19/3/524.

Goodale, M. A. & Milner, A. D. (1992). Separate visual pathways for perception and action. *Trends Neurosci.*, 15(1), 20–25.

Greicius, M. D., Krasnow, B., Reiss, A. L., & Menon, V. (2003). Functional connectivity in the resting brain: a network analysis of the default mode hypothesis. *Proc Natl Acad Sci U S A*, 100(1), 253–258, doi:10.1073/pnas.0135058100. http://www.ncbi.nlm.nih.gov/pubmed/12506194.

Greicius, M. D., Srivastava, G., Reiss, A. L., & Menon, V. (2004). Default-mode network activity distinguishes Alzheimer's disease from healthy aging: evidence from functional MRI. *Proc. Natl. Acad. Sci. U.S.A.*, 101(13), 4637–4642, doi:10.1073/pnas.0308627101.

Greicius, M. D., Supekar, K., Menon, V., & Dougherty, R. F. (2009). Resting-State Functional Connectivity Reflects Structural Connectivity in the Default Mode Network. *Cereb Cortex*, 19(1), 72–78, doi:10.1093/cercor/bhn059. http://cercor.oxfordjournals.org/content/19/1/72.

Grieve, S. M., Williams, L. M., Paul, R. H., Clark, C. R., & Gordon, E. (2007). Cognitive Aging, Executive Function, and Fractional Anisotropy: A Diffusion Tensor MR Imaging Study. *AJNR Am J Neuroradiol*, 28(2), 226–235. http://www.ajnr.org/content/28/2/226.

Griffa, A., Baumann, P. S., Thiran, J.-P., & Hagmann, P. (2013). Structural connectomics in brain diseases. *NeuroImage*, 80, 515–526, doi:10.1016/j.neuroimage.2013.04.056. http:

//www.sciencedirect.com/science/article/pii/S1053811913004035.

Gunning-Dixon, F. M., Brickman, A. M., Cheng, J. C., & Alexopoulos, G. S. (2009). Aging of cerebral white matter: a review of MRI findings. *Int J Geriatr Psychiatry*, 24(2), 109–117, doi:10.1002/gps.2087.

Gunning-Dixon, F. M. & Raz, N. (2000). The cognitive correlates of white matter abnormalities in normal aging: a quantitative review. *Neuropsychology*, 14(2), 224–232.

Gunning-Dixon, F. M. & Raz, N. (2003). Neuroanatomical correlates of selected executive functions in middle-aged and older adults: a prospective MRI study. *Neuropsychologia*, 41(14), 1929–1941.

Gusnard, D. A. & Raichle, M. E. (2001). Searching for a baseline: Functional imaging and the resting human brain. *Nat Rev Neurosci*, 2(10), 685–694, doi:10.1038/35094500. http://www.nature.com/nrn/journal/v2/n10/full/nrn1001-685a.html.

Guttmann, C. R., Jolesz, F. A., Kikinis, R., Killiany, R. J., Moss, M. B., Sandor, T., & Albert, M. S. (1998). White matter changes with normal aging. *Neurology*, 50(4), 972–978.

Haas, L. (2003). Hans Berger (1873-1941), Richard Caton (1842-1926), and electroencephalography. *J Neurol Neurosurg Psychiatry*, 74(1), 9, doi:10.1136/jnnp.74.1.9. http://www.ncbi.nlm.nih.gov/pmc/articles/PMC1738204/.

Hagmann, P., et al. (2010). MR connectomics: Principles and challenges. *J Neurosci Methods*, 194(1), 34–45, doi:10.1016/j.jneumeth.2010.01.014. http://www.sciencedirect.com/science/article/pii/S0165027010000361.

Hagmann, P., Cammoun, L., Gigandet, X., Meuli, R., Honey, C. J., Wedeen, V. J., & Sporns, O. (2008). Mapping the Structural Core of Human Cerebral Cortex. *PLoS Biol*, 6(7), e159, doi:10.1371/journal.pbio.0060159. http://dx.doi.org/10.1371/journal.pbio.0060159.

Hagmann, P., Kurant, M., Gigandet, X., Thiran, P., Wedeen, V. J., Meuli, R., & Thiran, J.-P. (2007). Mapping Human Whole-Brain Structural Networks with Diffusion MRI. *PLoS ONE*, 2(7), e597, doi:10.1371/journal.pone.0000597. http://dx.plos.org/10.1371/journal.pone.0000597.

Haken, H. (1996). *Principles of brain functioning: a synergetic approach to brain activity, behavior, and cognition*. Springer.

Hall, E. L., Woolrich, M. W., Thomaz, C. E., Morris, P. G., & Brookes, M. J. (2013). Using variance information in magnetoencephalography measures of functional connectivity. *NeuroImage*, 67, 203–212, doi:10.1016/j.neuroimage.2012.11.011. http://www.sciencedirect.com/science/article/pii/S105381191201107X.

Harshman, R. A. (1970). Foundations of the PARAFAC procedure: Models and conditions for an" explanatory" multimodal factor analysis. *UCLA Working Papers in Phonetics*, (16, 84). http://www.psychology.uwo.ca/faculty/harshman/wpppfac0.pdf.

Head, D., et al. (2004). Differential vulnerability of anterior white matter in nondemented aging with minimal acceleration in dementia of the Alzheimer type: evidence from diffusion tensor imaging. *Cereb Cortex*, 14(4), 410–423.

Heisz, J. J., Shedden, J. M., & McIntosh, A. R. (2012). Relating brain signal variability to knowledge representation. *Neuroimage*, 63(3), 1384–1392, doi:10.1016/j.neuroimage.2012.08.018. http://www.sciencedirect.com/science/article/pii/S1053811912008117.

Helmchen, F., Imoto, K., & Sakmann, B. (1996). Ca2+ buffering and action potential-evoked Ca2+ signaling in dendrites of pyramidal neurons. *Biophys J*, 70(2), 1069–1081.

Helwig, N. E. & Hong, S. (2013). A critique of Tensor Probabilistic Independent Component Analysis: Implications and recommendations for multi-subject fMRI data analysis. *Journal of Neuroscience Methods*, 213(2), 263–273, doi:10.1016/j.jneumeth.2012.12.009. http://www.sciencedirect.com/science/article/pii/S0165027012004761.

Hill, S. & Tononi, G. (2005). Modeling sleep and wakefulness in the thalamocortical system. *J. Neurophysiol.*, 93(3), 1671–1698, doi:10.1152/jn.00915.2004.

Hillebrand, A. & Barnes, G. R. (2005). Beamformer analysis of MEG data. *Int. Rev. Neurobiol.*, 68, 149–171, doi:10.1016/S0074-7742(05)68006-3.

Hillebrand, A., Barnes, G. R., Bosboom, J. L., Berendse, H. W., & Stam, C. J. (2012). Frequency-dependent functional connectivity within resting-state networks: An atlas-based MEG beamformer solution. *Neuroimage*, 59(4), 3909–3921, doi:10.1016/j.neuroimage.2011.11.005. http://www.ncbi.nlm.nih.gov/pubmed/22122866.

Hindmarsh, J. L. & Rose, R. M. (1984). A model of neuronal bursting using three coupled first order differential equations. *Proc. R. Soc. Lond., B, Biol. Sci.*, 221(1222), 87–102.

Hindriks, R., van Putten, M. J. A. M., & Deco, G. (2014). Intracortical propagation of EEG alpha oscillations. *NeuroImage*, 103, 444–453, doi:10.1016/j.neuroimage.2014.08.027. http://www.sciencedirect.com/science/article/pii/S1053811914007010.

Hipp, J. F., Hawellek, D. J., Corbetta, M., Siegel, M., & Engel, A. K. (2012). Large-scale cortical correlation structure of spontaneous oscillatory activity. *Nat Neurosci*, doi:10.1038/nn.3101. http://www.nature.com/neuro/journal/vaop/ncurrent/full/nn.3101.html.

Hitchcock, F. L. (1927). *The Expression of a Tensor Or a Polyadic as a Sum of Products*. sn.

Holliday, I. E., Barnes, G. R., Hillebrand, A., & Singh, K. D. (2003). Accuracy and applications of group MEG studies using cortical source locations estimated from participants' scalp surfaces. *Hum Brain Mapp*, 20(3), 142–147, doi:10.1002/hbm.10133.

Honey, C. J., Kötter, R., Breakspear, M., & Sporns, O. (2007). Network structure of cerebral cortex shapes functional connectivity on multiple time scales. *Proc Natl Acad Sci U S A*, 104(24), 10240 –10245, doi:10.1073/pnas.0701519104. http://www.pnas.org/content/104/24/10240.abstract.

Honey, C. J. & Sporns, O. (2008). Dynamical consequences of lesions in cortical networks. *Hum Brain Mapp*, 29(7), 802–809, doi:10.1002/hbm.20579.

Honey, C. J., Sporns, O., Cammoun, L., Gigandet, X., Thiran, J.-P., Meuli, R., & Hagmann, P. (2009). Predicting human resting-state functional connectivity from structural connectivity. *Proc Natl Acad Sci U S A*, 106(6), 2035 –2040, doi:10.1073/pnas.0811168106. http://www.pnas.org/content/106/6/2035.abstract.

Honey, C. J., Thivierge, J.-P., & Sporns, O. (2010). Can structure predict function in the human brain? *NeuroImage*, 52(3), 766–776, doi:10.1016/j.neuroimage.2010.01.071. http://www.sciencedirect.com/science/article/pii/S1053811910000935.

Horwitz, B. (2003). The elusive concept of brain connectivity. *Neuroimage*, 19(2 Pt 1), 466–470.

Huang, M. X., Mosher, J. C., & Leahy, R. M. (1999). A sensor-weighted overlapping-sphere head model and exhaustive head model comparison for MEG. *Phys Med Biol*, 44(2), 423–440.

Huisman, T. A. G. M. (2003). Diffusion-weighted imaging: basic concepts and application in cerebral stroke and head trauma. *Eur Radiol*, 13(10), 2283–2297, doi:10.1007/s00330-003-1843-6. http://link.springer.com/article/10.1007/s00330-003-1843-6.

Hyvärinen, A. & Oja, E. (2000). Independent component analysis: algorithms and applications. *Neural Netw*, 13(4-5), 411–430.

Iturria-Medina, Y., Canales-Rodríguez, E. J., Melie-García, L., Valdés-Hernández, P. A., Martínez-Montes, E., Alemán-Gómez, Y., & Sánchez-Bornot, J. M. (2007). Characterizing brain anatomical connections using diffusion weighted MRI and graph theory. *NeuroImage*, 36(3), 645–660, doi:10.1016/j.neuroimage.2007.02.012. http://www.sciencedirect.com/science/article/pii/S105381190700105X.

Izhikevich, E. M. & Edelman, G. M. (2008). Large-Scale Model of Mammalian Thalamocortical Systems. *Proc Natl Acad Sci U S A*, 105(9), 3593–3598, doi:10.1073/pnas.0712231105. http://www.pnas.org/content/105/9/3593.

Jann, K., Kottlow, M., Dierks, T., Boesch, C., & Koenig, T. (2010). Topographic Electrophysiological Signatures of fMRI Resting State Networks. *PLoS ONE*, 5(9), e12945, doi:10.1371/journal.pone.0012945. http://dx.doi.org/10.1371/journal.pone.0012945.

Jbabdi, S., Woolrich, M. W., & Behrens, T. E. J. (2009). Multiple-subjects connectivity-based parcellation using hierarchical Dirichlet process mixture models. *Neuroimage*, 44(2), 373–384, doi:10.1016/j.neuroimage.2008.08.044.

Jenkinson, M., Bannister, P., Brady, M., & Smith, S. (2002). Improved optimization for the robust and accurate linear registration and motion correction of brain images. *NeuroImage*, 17(2), 825–841.

Jenkinson, M., Beckmann, C. F., Behrens, T. E. J., Woolrich, M. W., & Smith, S. M. (2012). FSL. *Neuroimage*, 62(2), 782–790, doi:10.1016/j.neuroimage.2011.09.015.

Jin, S.-H., Jeong, W., Seol, J., Kwon, J., & Chung, C. K. (2013). Functional Cortical Hubs in the Eyes-Closed Resting Human Brain from an Electrophysiological Perspective Using Magnetoencephalography. *PLoS One*, 8(7), doi:10.1371/journal.pone.0068192. http://www.ncbi.nlm.nih.gov/pmc/articles/PMC3706585/.

Jirsa, V. K. (2009). Neural Field Dynamics with Local and Global Connectivity and Time Delay. *Philos Transact A Math Phys Eng Sci*, 367(1891), 1131–1143, doi:10.1098/rsta.2008.0260. http://rsta.royalsocietypublishing.org/content/367/1891/1131.

Jirsa, V. K. & Ding, M. (2004). Will a Large Complex System with Time Delays Be Stable? *Phys Rev Lett*, 93(7), 070602, doi:10.1103/PhysRevLett.93.070602. http://link.aps.org/doi/10.1103/PhysRevLett.93.070602.

Jirsa, V. K. & Stefanescu, R. A. (2011). Neural population modes capture biologically realistic large scale network dynamics. *Bull. Math. Biol.*, 73(2), 325–343, doi:10.1007/s11538-010-9573-9.

Kanwisher, N., McDermott, J., & Chun, M. M. (1997). The Fusiform Face Area: A Module in Human Extrastriate Cortex Specialized for Face Perception. *The Journal of Neuroscience*, 17(11), 4302 –4311. http://www.jneurosci.org/content/17/11/4302.abstract.

Kim, J., He, Y., & Park, H. (2013). Algorithms for nonnegative matrix and tensor factorizations: a unified view based on block coordinate descent framework. *J Glob Optim*, (pp. 1–35)., doi:10.1007/s10898-013-0035-4. http://link.springer.com/article/10.1007/s10898-013-0035-4.

Kim, J. & Park, H. (2011). Fast nonnegative matrix factorization: An active-set-like method and comparisons. *SIAM Journal on Scientific Computing*, 33(6), 3261–3281. http://epubs.siam.org/doi/abs/10.1137/110821172.

Kitzbichler, M. G., Smith, M. L., Christensen, S. R., & Bullmore, E. (2009). Broadband Criticality of Human Brain Network Synchronization. *PLoS Comput Biol*, 5(3), doi:10.1371/journal.pcbi.1000314.

Kiviniemi, V., Kantola, J.-H., Jauhiainen, J., Hyvärinen, A., & Tervonen, O. (2003). Independent component analysis of nondeterministic fMRI signal sources. *Neuroimage*, 19(2 Pt 1), 253–260.

Knock, S., McIntosh, A., Sporns, O., Kötter, R., Hagmann, P., & Jirsa, V. (2009). The effects of physiologically plausible connectivity structure on local and global dynamics in large scale brain models. *J Neurosci Methods*, 183(1), 86–94, doi:10.1016/j.jneumeth.2009.07.007. http://www.sciencedirect.com/science/article/pii/S0165027009003707.

Kolda, T. G. & Bader, B. W. (2009). Tensor Decompositions and Applications. *SIAM Review*, 51(3), 455–500, doi:10.1137/07070111X. http://epubs.siam.org/doi/abs/10.1137/07070111X.

Kötter, R. (2004). Online retrieval, processing, and visualization of primate connectivity data from the CoCoMac Database. *Neuroinform*, 2(2), 127–144, doi:10.1385/NI:2:2:127. http://link.springer.com/article/10.1385/NI%3A2%3A2%3A127.

Kruskal, J. B. (1989). Rank, decomposition, and uniqueness for 3-way and n-way arrays. In R. Coppi & S. Bolasco (Eds.), *Multiway Data Analysis* (pp. 7–18). Amsterdam, The Netherlands, The Netherlands: North-Holland Publishing Co. http://dl.acm.org/citation.cfm?id=120565.120567.

Kuramoto, Y. (1984). *Chemical Oscillations, Waves, and Turbulence*. New York: Springer-Verlag.

Ladenbauer, J., Augustin, M., Shiau, L., & Obermayer, K. (2012). Impact of adaptation currents on synchronization of coupled exponential integrate-and-fire neurons. *PLoS Comput. Biol.*, 8(4), e1002478, doi:10.1371/journal.pcbi.1002478. http://www.ncbi.nlm.nih.gov/pubmed/22511861.

Lancaster, J. L., et al. (2000). Automated Talairach atlas labels for functional brain mapping. *Hum Brain Mapp*, 10(3), 120–131.

Larson-Prior, L. J., et al. (2011). Modulation of the brain's functional network architecture in the transition from wake to sleep. *Prog. Brain Res.*, 193, 277–294, doi:10.1016/B978-0-444-53839-0.00018-1. http://www.ncbi.nlm.nih.gov/pubmed/21854969.

Laufs, H., Krakow, K., Sterzer, P., Eger, E., Beyerle, A., Salek-Haddadi, A., & Kleinschmidt, A. (2003). Electroencephalographic Signatures of Attentional and Cognitive Default Modes in Spontaneous Brain Activity Fluctuations at Rest. *PNAS*, 100(19), 11053–11058, doi:10.1073/pnas.1831638100. http://www.pnas.org/content/100/19/11053.

Le Bihan, D. (2014). Diffusion MRI: what water tells us about the brain. *EMBO Mol Med*, 6(5), 569–573, doi:10.1002/emmm.201404055. http://www.ncbi.nlm.nih.gov/pmc/articles/PMC4023879/.

Le Bihan, D., Breton, E., Lallemand, D., Grenier, P., Cabanis, E., & Laval-Jeantet, M. (1986). MR imaging of intravoxel incoherent motions: application to diffusion and perfusion in neurologic disorders. *Radiology*, 161(2), 401–407, doi:10.1148/radiology.161.2.3763909. http://pubs.rsna.org/doi/abs/10.1148/radiology.161.2.3763909.

Lee, M. H., Hacker, C. D., Snyder, A. Z., Corbetta, M., Zhang, D., Leuthardt, E. C., & Shimony, J. S. (2012). Clustering of Resting State Networks. *PLoS ONE*, 7(7), e40370, doi:10.1371/journal.pone.0040370. http://dx.doi.org/10.1371/journal.pone.0040370.

Lehmann, D., Faber, P. L., Tei, S., Pascual-Marqui, R. D., Milz, P., & Kochi, K. (2012). Reduced functional connectivity between cortical sources in five meditation traditions detected with lagged coherence using EEG tomography. *Neuroimage*, 60(2), 1574–1586, doi:10.1016/j.neuroimage.2012.01.042. http://www.ncbi.nlm.nih.gov/pubmed/22266174.

Liang, M., Zhou, Y., Jiang, T., Liu, Z., Tian, L., Liu, H., & Hao, Y. (2006). Widespread functional disconnectivity in schizophrenia with resting-state functional magnetic resonance imaging. *Neuroreport*, 17(2), 209–213.

Lippé, S., Kovacevic, N., & McIntosh, A. R. (2009). Differential Maturation of Brain Signal Complexity in the Human Auditory and Visual System. *Front Hum Neurosci*, 3, doi:10.3389/neuro.09.048.2009. http://www.ncbi.nlm.nih.gov/pmc/articles/PMC2783025/.

Litvak, V., et al. (2011). EEG and MEG data analysis in SPM8. *Comput Intell Neurosci*, 2011, 852961, doi:10.1155/2011/852961.

Liu, Y., et al. (2008). Disrupted small-world networks in schizophrenia. *Brain*, 131(Pt 4), 945–961, doi:10.1093/brain/awn018.

Liu, Y. H. & Wang, X. J. (2001). Spike-frequency adaptation of a generalized leaky integrate-and-fire model neuron. *J Comput Neurosci*, 10(1), 25–45. http://www.ncbi.nlm.nih.gov/pubmed/11316338.

Liu, Z., Fukunaga, M., de Zwart, J. A., & Duyn, J. H. (2010). Large-Scale Spontaneous Fluctuations and Correlations in Brain Electrical Activity Observed with Magnetoencephalography. *NeuroImage*, 51(1), 102–111, doi:10.1016/j.neuroimage.2010.01.092.

Llinas, R. R. (1988). The Intrinsic Electrophysiological Properties of Mammalian Neurons: Insights into Central Nervous System Function. *Science*, 242(4886), 1654–1664, doi:10.1126/science.3059497. http://www.sciencemag.org/content/242/4886/1654.

Long, Z., Li, R., Wen, X., Jin, Z., Chen, K., & Yao, L. (2013). Separating 4D multi-task fMRI data of multiple subjects by independent component analysis with projection. *Magn Reson Imaging*, 31(1), 60–74, doi:10.1016/j.mri.2012.06.034.

Lopes da Silva, F. (1991). Neural mechanisms underlying brain waves: from neural membranes to networks. *Electroencephalogr Clin Neurophysiol*, 79(2), 81–93. http://www.ncbi.nlm.nih.gov/pubmed/1713832.

Lopes da Silva, F., Vos, J., Mooibroek, J., & van Rotterdam, A. (1980). Relative contributions of intracortical and thalamo-cortical processes in the generation of alpha rhythms, revealed by partial coherence analysis. *Electroencephalography and Clinical Neurophysiology*, 50(5–6), 449–456, doi:10.1016/0013-4694(80)90011-5. http://www.sciencedirect.com/science/article/pii/0013469480900115.

Lopes da Silva, F. H., Hoeks, A., Smits, H., & Zetterberg, L. H. (1974). Model of brain rhythmic activity. The alpha-rhythm of the thalamus. *Kybernetik*, 15(1), 27–37. http://www.ncbi.nlm.nih.gov/pubmed/4853232.

Lowe, M., Mock, B., & Sorenson, J. (1998). Functional Connectivity in Single and Multislice Echoplanar Imaging Using Resting-State Fluctuations. *NeuroImage*, 7(2), 119–132, doi:10.1006/nimg.1997.0315. http://www.sciencedirect.com/science/article/pii/S1053811997903153.

Lowe, M. J., Beall, E. B., Sakaie, K. E., Koenig, K. A., Stone, L., Marrie, R. A., & Phillips, M. D. (2008). Resting state sensorimotor functional connectivity in multiple sclerosis inversely correlates with transcallosal motor pathway transverse diffusivity. *Human Brain Mapping*, 29(7), 818–827, doi:10.1002/hbm.20576. http://onlinelibrary.wiley.com/doi/10.1002/hbm.20576/abstract.

Luckhoo, H., Hale, J. R., Stokes, M. G., Nobre, A. C., Morris, P. G., Brookes, M. J., & Woolrich, M. W. (2012). Inferring task-related networks using independent component analysis in magnetoencephalography. *NeuroImage*, 62(1), 530–541, doi:10.1016/j.neuroimage.2012.04.046.

Lynall, M.-E., Bassett, D. S., Kerwin, R., McKenna, P. J., Kitzbichler, M., Muller, U., & Bullmore, E. (2010). Functional Connectivity and Brain Networks in Schizophrenia. *J Neurosci*, 30(28), 9477–9487, doi:10.1523/JNEUROSCI.0333-10.2010. http://www.jneurosci.org/content/30/28/9477.

Madden, D. J., Bennett, I. J., & Song, A. W. (2009). Cerebral White Matter Integrity and Cognitive Aging: Contributions from Diffusion Tensor Imaging. *Neuropsychol Rev*, 19(4), 415–435, doi:10.1007/s11065-009-9113-2. http://www.ncbi.nlm.nih.gov/pmc/articles/PMC2787975/.

Magee, J. C. (2000). Dendritic integration of excitatory synaptic input. *Nat Rev Neurosci*, 1(3), 181–190, doi:10.1038/35044552. http://www.nature.com/nrn/journal/v1/n3/full/nrn1200_181a.html.

Maguire, E. A. & Mummery, C. J. (1999). Differential modulation of a common memory retrieval network revealed by positron emission tomography. *Hippocampus*, 9(1), 54–61, doi:10.1002/(SICI)1098-1063(1999)9:1<54::AID-HIPO6>3.0.CO;2-O.

Mantini, D., Della Penna, S., Marzetti, L., de Pasquale, F., Pizzella, V., Corbetta, M., & Romani, G. L. (2011). A signal-processing pipeline for magnetoencephalography resting-state networks. *Brain Connect*, 1(1), 49–59, doi:10.1089/brain.2011.0001.

Mantini, D., Franciotti, R., Romani, G. L., & Pizzella, V. (2008). Improving MEG source localizations: an automated method for complete artifact removal based on independent component analysis. *Neuroimage*, 40(1), 160–173, doi:10.1016/j.neuroimage.2007.11.022.

Mantini, D., Perrucci, M. G., Del Gratta, C., Romani, G. L., & Corbetta, M. (2007). Electrophysiological signatures of resting state networks in the human brain. *Proc Natl Acad Sci U S A*, 104(32), 13170 –13175,

doi:10.1073/pnas.0700668104. http://www.pnas.org/content/104/32/13170.abstract.

Martínez-Montes, C. N., Sánchez-Bornot, & Valdés-Sosa (2008a). Penalized PARAFAC analysis of spontaneous EEG recordings. *Statistica Sinica*, 18, 1449–1464. http://www3.stat.sinica.edu.tw/statistica/oldpdf/A18n411.pdf.

Martínez-Montes, E., Vega-Hernández, M., Sánchez-Bornot, J. M., & Valdés-Sosa, P. A. (2008b). Identifying Complex Brain Networks Using Penalized Regression Methods. *J Biol Phys*, 34(3-4), 315–323, doi:10.1007/s10867-008-9077-0. http://link.springer.com/article/10.1007/s10867-008-9077-0.

Marzetti, L., et al. (2013). Frequency specific interactions of MEG resting state activity within and across brain networks as revealed by the multivariate interaction measure. *NeuroImage*, 79, 172–183, doi:10.1016/j.neuroimage.2013.04.062. http://www.sciencedirect.com/science/article/pii/S1053811913004096.

Mazoyer, B., et al. (2001). Cortical networks for working memory and executive functions sustain the conscious resting state in man. *Brain Res Bull*, 54(3), 287–298, doi:16/S0361-9230(00)00437-8. http://www.sciencedirect.com/science/article/pii/S0361923000004378.

Mazzoni, A., Panzeri, S., Logothetis, N. K., & Brunel, N. (2008). Encoding of Naturalistic Stimuli by Local Field Potential Spectra in Networks of Excitatory and Inhibitory Neurons. *PLoS Comput Biol*, 4(12), e1000239, doi:10.1371/journal.pcbi.1000239. http://dx.doi.org/10.1371/journal.pcbi.1000239.

McIntosh, A. R., Kovacevic, N., & Itier, R. J. (2008). Increased Brain Signal Variability Accompanies Lower Behavioral Variability in Development. *PLoS Comput Biol*, 4(7), e1000106, doi:10.1371/journal.pcbi.1000106. http://dx.plos.org/10.1371/journal.pcbi.1000106.

McIntosh, A. R., Kovacevic, N., Lippe, S., Garrett, D., Grady, C., & Jirsa, V. (2010). The Development of a Noisy Brain. *Arch Ital Biol*, 148(3), 323–337, doi:10.4449/aib.v148i3.1225. http://www.architalbiol.org/aib/article/view/148323.

McIntosh, A. R., Vakorin, V., Kovacevic, N., Wang, H., Diaconescu, A., & Protzner, A. B. (2013). Spatiotemporal Dependency of Age-Related Changes in Brain Signal Variability. *Cereb. Cortex*, doi:10.1093/cercor/bht030. http://cercor.oxfordjournals.org/content/early/2013/02/07/cercor.bht030.

Meech, R. W. (1978). Calcium-Dependent Potassium Activation in Nervous Tissues. *Annu. Rev. Biophys. Bioeng.*, 7(1), 1–18, doi:10.1146/annurev.bb.07.060178.000245. http://www.annualreviews.org/doi/abs/10.1146/annurev.bb.07.060178.000245.

Milgram, S. (1967). The Small World Problem. *Psychology Today*, 2, 60–67.

Mishkin, M. & Ungerleider, L. G. (1982). Contribution of striate inputs to the visuospatial functions of parieto-preoccipital cortex in monkeys. *Behav. Brain Res.*, 6(1), 57–77.

Miwakeichi, F., Martínez-Montes, E., Valdés-Sosa, P. A., Nishiyama, N., Mizuhara, H., & Yamaguchi, Y. (2004). Decomposing EEG data into space–time–frequency components using Parallel Factor Analysis. *NeuroImage*, 22(3), 1035–1045, doi:10.1016/j.neuroimage.2004.03.039. http://www.sciencedirect.com/science/article/pii/S1053811904001958.

Mo, J., Liu, Y., Huang, H., & Ding, M. (2013). Coupling between visual alpha oscillations and default mode activity. *Neuroimage*, 68, 112–118, doi:10.1016/j.neuroimage.2012.11.058.

Morcom, A. M. & Fletcher, P. C. (2007). Does the brain have a baseline? Why we should be resisting a rest. *NeuroImage*, 37(4), 1073–1082, doi:16/j.neuroimage.2006.09.013. http://www.sciencedirect.com/science/article/pii/S1053811906009645.

Morris, C. & Lecar, H. (1981). Voltage oscillations in the barnacle giant muscle fiber. *Biophys. J.*, 35(1), 193–213, doi:10.1016/S0006-3495(81)84782-0.

Mørup, M., Hansen, L. K., Herrmann, C. S., Parnas, J., & Arnfred, S. M. (2006). Parallel Factor Analysis as an exploratory tool for wavelet transformed event-related EEG. *NeuroImage*, 29(3), 938–947, doi:10.1016/j.neuroimage.2005.08.005. http://www.sciencedirect.com/science/article/pii/S1053811905005896.

Murphy, K., Birn, R. M., Handwerker, D. A., Jones, T. B., & Bandettini, P. A. (2009). The impact of global signal regression on resting state correlations: are anti-correlated networks introduced? *Neuroimage*, 44(3), 893–905, doi:10.1016/j.neuroimage.2008.09.036.

Murphy, K. R., Stedmon, C. A., Graeber, D., & Bro, R. (2013). Fluorescence spectroscopy and multi-way techniques. PARAFAC. *Anal. Methods*, 5(23), 6557–6566, doi:10.1039/C3AY41160E. http://pubs.rsc.org/en/content/articlelanding/2013/ay/c3ay41160e.

Muthukumaraswamy, S. (2013). High-frequency brain activity and muscle artifacts in MEG/EEG: a review and recommendations. *Front. Hum. Neurosci*, 7, 138, doi:10.3389/fnhum.2013.00138. http://journal.frontiersin.org/Journal/10.3389/fnhum.2013.00138/full.

Nagumo, J., Arimoto, S., & Yoshizawa, S. (1962). An Active Pulse Transmission Line Simulating Nerve Axon. *Proceedings of the IRE*, 50(10), 2061–2070, doi:10.1109/JRPROC.1962.288235.

Nakagawa, T. & Deco, P. D. G. (2014). Multiscale Brain Connectivity. In D. Jaeger & R. Jung (Eds.), *Encyclopedia of Computational Neuroscience* (pp. 1–3). Springer New York. http://link.springer.com/referenceworkentry/10.1007/978-1-4614-7320-6_535-1.

Nakagawa, T. T., Jirsa, V. K., Spiegler, A., McIntosh, A. R., & Deco, G. (2013). Bottom up modeling of the connectome: Linking structure and function in the resting brain and their changes in aging. *Neu-*

roImage, doi:10.1016/j.neuroimage.2013.04.055. http://linkinghub.elsevier.com/retrieve/pii/S1053811913004023.

Nakagawa, T. T., et al. (2014). How delays matter in an oscillatory whole-brain spiking-neuron network model for MEG alpha-rhythms at rest. *NeuroImage*, 87, 383–394, doi:10.1016/j.neuroimage.2013.11.009. http://www.sciencedirect.com/science/article/pii/S1053811913011014.

Neuner, I., Arrubla, J., Werner, C. J., Hitz, K., Boers, F., Kawohl, W., & Shah, N. J. (2014). The default mode network and EEG regional spectral power: a simultaneous fMRI-EEG study. *PLoS ONE*, 9(2), e88214, doi:10.1371/journal.pone.0088214.

Neymotin, S. A., Lee, H., Park, E., Fenton, A. A., & Lytton, W. W. (2011). Emergence of physiological oscillation frequencies in a computer model of neocortex. *Front Comput Neurosci*, 5, 19, doi:10.3389/fncom.2011.00019. http://www.ncbi.nlm.nih.gov/pubmed/21541305.

Nijhuis, E. H. J., van Cappellen van Walsum, A.-M., & Norris, D. G. (2013). Topographic Hub Maps of the Human Structural Neocortical Network. *PLoS ONE*, 8(6), e65511, doi:10.1371/journal.pone.0065511. http://dx.doi.org/10.1371/journal.pone.0065511.

Nikouline, V. V., Linkenkaer-Hansen, K., Huttunen, J., & Ilmoniemi, R. J. (2001). Interhemispheric phase synchrony and amplitude correlation of spontaneous beta oscillations in human subjects: a magnetoencephalographic study. *Neuroreport*, 12(11), 2487–2491. http://www.ncbi.nlm.nih.gov/pubmed/11496135.

Nunez, P. L. (1995). *Neocortical Dynamics and Human EEG Rhythms*. Oxford University Press, USA, 1st edition.

Oostenveld, R., Fries, P., Maris, E., & Schoffelen, J.-M. (2011). FieldTrip: Open source software for advanced analysis of MEG, EEG, and invasive electrophysiological data. *Comput Intell Neurosci*, 2011, 156869, doi:10.1155/2011/156869.

Oosterman, J. M., Sergeant, J. A., Weinstein, H. C., & Scherder, E. J. A. (2004). Timed executive functions and white matter in aging with and without cardiovascular risk factors. *Rev Neurosci*, 15(6), 439–462.

Palva, S. & Palva, J. M. (2012). Discovering oscillatory interaction networks with M/EEG: challenges and breakthroughs. *Trends in Cognitive Sciences*, 16(4), 219–230, doi:10.1016/j.tics.2012.02.004. http://www.sciencedirect.com/science/article/pii/S1364661312000472.

Park, D. C., Lautenschlager, G., Hedden, T., Davidson, N. S., Smith, A. D., & Smith, P. K. (2002). Models of visuospatial and verbal memory across the adult life span. *Psychol Aging*, 17(2), 299–320, doi:10.1037/0882-7974.17.2.299.

Pfefferbaum, A. & Sullivan, E. V. (2003). Increased brain white matter diffusivity in normal adult aging: relationship to anisotropy and partial voluming. *Magn Reson Med*, 49(5), 953–961, doi:10.1002/mrm.10452.

Pfefferbaum A, M. D. (1994). A quantitative magnetic resonance imaging study of changes in brain morphology from infancy to late adulthood. *Arch Neurol*, 51(9), 874–887, doi:10.1001/archneur.1994.00540210046012. http://dx.doi.org/10.1001/archneur.1994.00540210046012.

Phan, A. H., Tichavsky, P., & Cichocki, A. (2012). CANDECOMP/PARAFAC decomposition of high-order tensors through tensor reshaping. *arXiv preprint arXiv:1211.3796*. http://arxiv.org/abs/1211.3796.

Pincus, S. M. & Goldberger, A. L. (1994). Physiological time-series analysis: what does regularity quantify? *Am J Physiol*, 266(4 Pt 2), H1643–1656.

Poil, S.-S., Hardstone, R., Mansvelder, H. D., & Linkenkaer-Hansen, K. (2012). Critical-state dynamics of avalanches and oscillations jointly emerge from balanced excitation/inhibition in neuronal networks. *J Neurosci*, 32(29), 9817–9823, doi:10.1523/JNEUROSCI.5990-11.2012.

Poil, S.-S., van Ooyen, A., & Linkenkaer-Hansen, K. (2008). Avalanche dynamics of human brain oscillations: Relation to critical branching

processes and temporal correlations. *Hum Brain Mapp*, 29(7), 770–777, doi:10.1002/hbm.20590. http://onlinelibrary.wiley.com/doi/10.1002/hbm.20590/abstract.

Popovych, O. V., Maistrenko, Y. L., & Tass, P. A. (2005). Phase chaos in coupled oscillators. *Phys Rev E Stat Nonlin Soft Matter Phys*, 71(6 Pt 2), 065201.

Prins, N. D., et al. (2005). Cerebral small-vessel disease and decline in information processing speed, executive function and memory. *Brain*, 128(Pt 9), 2034–2041, doi:10.1093/brain/awh553.

Rabinovich, M., Volkovskii, A., Lecanda, P., Huerta, R., Abarbanel, H. D., & Laurent, G. (2001). Dynamical encoding by networks of competing neuron groups: winnerless competition. *Phys Rev Lett*, 87(6), 068102.

Rabinovich, M. I., Huerta, R., Varona, P., & Afraimovich, V. S. (2008). Transient cognitive dynamics, metastability, and decision making. *PLoS Comput Biol*, 4(5), e1000072, doi:10.1371/journal.pcbi.1000072.

Raichle, M. E., MacLeod, A. M., Snyder, A. Z., Powers, W. J., Gusnard, D. A., & Shulman, G. L. (2001). A default mode of brain function. *Proc. Natl. Acad. Sci. U.S.A*, 98(2), 676–682, doi:10.1073/pnas.98.2.676. http://www.ncbi.nlm.nih.gov/pubmed/11209064.

Rechtschaffen, A. & Kales, A. (1968). *A manual of standardized terminology, techniques and scoring system for sleep stages of human subjects*. Bethesda, Md.: U.S. National Institute of Neurological Diseases and Blindness, Neurological Information Network.

Reijneveld, J. C., Ponten, S. C., Berendse, H. W., & Stam, C. J. (2007). The application of graph theoretical analysis to complex networks in the brain. *Clinical Neurophysiology*, 118(11), 2317–2331, doi:16/j.clinph.2007.08.010. http://www.sciencedirect.com/science/article/pii/S1388245707004257.

Resnick, S. M., Pham, D. L., Kraut, M. A., Zonderman, A. B., & Davatzikos, C. (2003). Longitudinal Magnetic Resonance Imaging Studies of Older Adults: A Shrinking Brain. *J Neurosci*, 23(8), 3295–3301. http://www.jneurosci.org/content/23/8/3295.

Richman, J. S. & Moorman, J. R. (2000). Physiological time-series analysis using approximate entropy and sample entropy. *Am J Physiol Heart Circ Physiol*, 278(6), H2039–H2049. http://ajpheart.physiology.org/content/278/6/H2039.

Ritter, P., Moosmann, M., & Villringer, A. (2009). Rolandic alpha and beta EEG rhythms' strengths are inversely related to fMRI-BOLD signal in primary somatosensory and motor cortex. *Hum. Brain Mapp.*, 30(4), 1168–1187, doi:10.1002/hbm.20585. http://onlinelibrary.wiley.com/doi/10.1002/hbm.20585/abstract.

Ritter, P., Schirner, M., McIntosh, A. R., & Jirsa, V. K. (2013). The Virtual Brain Integrates Computational Modeling and Multimodal Neuroimaging. *Brain Connectivity*, 3(2), 121–145, doi:10.1089/brain.2012.0120. http://online.liebertpub.com/doi/abs/10.1089/brain.2012.0120.

Robinson, P., Rennie, C., Wright, J., Bahramali, H., Gordon, E., & Rowe, D. (2001). Prediction of electroencephalographic spectra from neurophysiology. *Physical Review E*, 63(2), doi:10.1103/PhysRevE.63.021903. http://adsabs.harvard.edu/abs/2001PhRvE..63b1903R.

Rodrigue, K. M. & Raz, N. (2004). Shrinkage of the entorhinal cortex over five years predicts memory performance in healthy adults. *J Neurosci*, 24(4), 956–963, doi:10.1523/JNEUROSCI.4166-03.2004.

Rogers, B. P., Morgan, V. L., Newton, A. T., & Gore, J. C. (2007). Assessing functional connectivity in the human brain by fMRI. *Magnetic Resonance Imaging*, 25(10), 1347–1357, doi:16/j.mri.2007.03.007. http://www.sciencedirect.com/science/article/pii/S0730725X07002238.

Roosendaal, S. D., Schoonheim, M. M., Hulst, H. E., Sanz-Arigita, E. J., Smith, S. M., Geurts, J. J. G., & Barkhof, F. (2010). Resting state networks change in clinically isolated syndrome. *Brain*, 133, 1612–1621, doi:10.1093/brain/awq058.

Rosen, A. C., et al. (2003). Differential associations between entorhinal and hippocampal volumes and memory performance in older adults. *Behav Neurosci*, 117(6), 1150–1160, doi:10.1037/0735-7044.117.6.1150.

Roy, D., Sigala, R., Breakspear, M., McIntosh, A. R., Jirsa, V. K., Deco, G., & Ritter, P. (2014). Using the Virtual Brain to Reveal the Role of Oscillations and Plasticity in Shaping Brain's Dynamical Landscape. *Brain Connectivity*, doi:10.1089/brain.2014.0252. http://online.liebertpub.com/doi/abs/10.1089/brain.2014.0252.

Rubinov, M. & Sporns, O. (2010). Complex network measures of brain connectivity: Uses and interpretations. *NeuroImage*, 52(3), 1059–1069, doi:10.1016/j.neuroimage.2009.10.003. http://www.sciencedirect.com/science/article/pii/S105381190901074X.

Salat, D., et al. (2005). Age-related alterations in white matter microstructure measured by diffusion tensor imaging. *Neurobiol Aging*, 26(8), 1215–1227, doi:10.1016/j.neurobiolaging.2004.09.017. http://www.sciencedirect.com/science/article/pii/S0197458004003173.

Salat, D. H., Kaye, J. A., & Janowsky, J. S. (2002). Greater orbital prefrontal volume selectively predicts worse working memory performance in older adults. *Cereb Cortex*, 12(5), 494–505.

Salomon, R., et al. (2011). Global Functional Connectivity Deficits in Schizophrenia Depend on Behavioral State. *J. Neurosci.*, 31(36), 12972–12981, doi:10.1523/JNEUROSCI.2987-11.2011. http://www.jneurosci.org/content/31/36/12972.

Salthouse, T. A. (1996). The processing-speed theory of adult age differences in cognition. *Psychol Rev*, 103(3), 403–428, doi:10.1037/0033-295X.103.3.403.

Salvador, R., Suckling, J., Schwarzbauer, C., & Bullmore, E. (2005). Undirected graphs of frequency-dependent functional connectivity in whole brain networks. *Philos Trans R Soc Lond B Biol Sci*, 360(1457), 937–946, doi:10.1098/rstb.2005.1645. http://www.ncbi.nlm.nih.gov/pmc/articles/PMC1854928/.

Samu, D., Seth, A. K., & Nowotny, T. (2014). Influence of Wiring Cost on the Large-Scale Architecture of Human Cortical Connectivity. *PLoS Comput Biol*, 10(4), e1003557, doi:10.1371/journal.pcbi.1003557. http://dx.doi.org/10.1371/journal.pcbi.1003557.

Sanz Leon, P., Knock, S. A., Woodman, M. M., Domide, L., Mersmann, J., McIntosh, A. R., & Jirsa, V. (2013). The Virtual Brain: a simulator of primate brain network dynamics. *Front Neuroinform*, 7, doi:10.3389/fninf.2013.00010. http://www.ncbi.nlm.nih.gov/pmc/articles/PMC3678125/.

Sarter, M. & Bruno, J. (1999). Cortical cholinergic inputs mediating arousal, attentional processing and dreaming: differential afferent regulation of the basal forebrain by telencephalic and brainstem afferents. *Neuroscience*, 95(4), 933–952, doi:10.1016/S0306-4522(99)00487-X. http://www.sciencedirect.com/science/article/pii/S030645229900487X.

Sato, J. R., Rondinoni, C., Sturzbecher, M., de Araujo, D. B., & Amaro Jr, E. (2010). From EEG to BOLD: Brain mapping and estimating transfer functions in simultaneous EEG-fMRI acquisitions. *NeuroImage*, 50(4), 1416–1426, doi:10.1016/j.neuroimage.2010.01.075. http://www.sciencedirect.com/science/article/pii/S1053811910000972.

Scheeringa, R., Petersson, K. M., Kleinschmidt, A., Jensen, O., & Bastiaansen, M. C. (2012). EEG alpha power modulation of fMRI resting state connectivity. *Brain Connectivity*, (pp. 120903045147002)., doi:10.1089/brain.2012.0088. http://online.liebertpub.com/doi/abs/10.1089/brain.2012.0088?url_ver=Z39.88-2003&rfr_id=ori:rid:crossref.org&rfr_dat=cr_pub%3dpubmed.

Schilbach, L., Müller, V. I., Hoffstaedter, F., Clos, M., Goya-Maldonado, R., Gruber, O., & Eickhoff, S. B. (2014). Meta-Analytically Informed Network Analysis of Resting State fMRI Reveals Hyperconnectivity in an Introspective Socio-Affective Network in Depression. *PLoS ONE*, 9(4), e94973,

doi:10.1371/journal.pone.0094973. http://dx.doi.org/10.1371/journal.pone.0094973.

Schmahmann, J. D., Pandya, D. N., Wang, R., Dai, G., D'Arceuil, H. E., Crespigny, A. J. d., & Wedeen, V. J. (2007). Association fibre pathways of the brain: parallel observations from diffusion spectrum imaging and autoradiography. *Brain*, 130(3), 630–653, doi:10.1093/brain/awl359. http://brain.oxfordjournals.org/content/130/3/630.

Schölvinck, M. L., Maier, A., Ye, F. Q., Duyn, J. H., & Leopold, D. A. (2010). Neural basis of global resting-state fMRI activity. *Proceedings of the National Academy of Sciences*, 107(22), 10238 –10243, doi:10.1073/pnas.0913110107. http://www.pnas.org/content/107/22/10238.abstract.

Sekihara, K., Nagarajan, S. S., Poeppel, D., Marantz, A., & Miyashita, Y. (2001). Reconstructing spatio-temporal activities of neural sources using an MEG vector beamformer technique. *IEEE Trans Biomed Eng*, 48(7), 760–771, doi:10.1109/10.930901.

Senden, M., Goebel, R., & Deco, G. (2012). Structural connectivity allows for multi-threading during rest: The structure of the cortex leads to efficient alternation between resting state exploratory behavior and default mode processing. *NeuroImage*, 60(4), 2274–2284, doi:10.1016/j.neuroimage.2012.02.061. http://www.sciencedirect.com/science/article/pii/S105381191200239X.

Sharma, N. & Baron, J.-C. (2013). Does motor imagery share neural networks with executed movement: a multivariate fMRI analysis. *Front Hum Neurosci*, 7, 564, doi:10.3389/fnhum.2013.00564.

Shaw, J. C. (2003). *The Brain's alpha rhythms and the mind: a review of classical and modern studies of the alpha rhythm component of the electroencephalogram with commentaries on associated neuroscience and neuropsychology*. Elsevier Health Sciences.

Shulman, G. L., Fiez, J. A., Corbetta, M., Buckner, R. L., Miezin, F. M., Raichle, M. E., & Petersen, S. E. (1997). Common Blood Flow Changes across Visual Tasks: II. Decreases in Cerebral Cortex. *Journal of Cognitive Neuroscience*,

9(5), 648–663, doi:i: 10.1162/jocn.1997.9.5.648</p>. http://dx.doi.org/10.1162/jocn.1997.9.5.648.

Skudlarski, P., Jagannathan, K., Calhoun, V. D., Hampson, M., Skudlarska, B. A., & Pearlson, G. (2008). Measuring brain connectivity: diffusion tensor imaging validates resting state temporal correlations. *Neuroimage*, 43(3), 554–561, doi:10.1016/j.neuroimage.2008.07.063. http://www.ncbi.nlm.nih.gov/pubmed/18771736.

Smith, S. M., et al. (2009). Correspondence of the brain's functional architecture during activation and rest. 106(31), 13040–13045, doi:10.1073/pnas.0905267106.

Smith, S. M., et al. (2012). Temporally-independent functional modes of spontaneous brain activity. *PNAS*, 109(8), 3131–3136, doi:10.1073/pnas.1121329109. http://www.pnas.org/content/109/8/3131.

Sokoloff, L., Mangold, R., Wechsler, R. L., Kennedy, C., & Kety, S. S. (1955). THE EFFECT OF MENTAL ARITHMETIC ON CEREBRAL CIRCULATION AND METABOLISM 1. *Journal of Clinical Investigation*, 34(7 Pt 1), 1101–1108, doi:10.1172/JCI103159. http://www.jci.org/articles/view/103159.

Spiegler, A. & Jirsa, V. (2013). Systematic approximations of neural fields through networks of neural masses in the virtual brain. *Neuroimage*, 83C, 704–725, doi:10.1016/j.neuroimage.2013.06.018.

Sporns, O. (2011). The human connectome: a complex network. *Annals of the New York Academy of Sciences*, 1224(1), 109–125, doi:10.1111/j.1749-6632.2010.05888.x. http://onlinelibrary.wiley.com/doi/10.1111/j.1749-6632.2010.05888.x/abstract.

Sporns, O. (2012). From simple graphs to the connectome: Networks in neuroimaging. *NeuroImage*, 62(2), 881–886, doi:10.1016/j.neuroimage.2011.08.085. http://www.sciencedirect.com/science/article/pii/S1053811911010172.

Sporns, O. (2013). Structure and function of complex brain networks. *Dialogues Clin Neurosci*, 15(3), 247–262. http://www.ncbi.nlm.nih.gov/pmc/articles/PMC3811098/.

Sporns, O. (2014). Contributions and challenges for network models in cognitive neuroscience. *Nat Neurosci*, 17(5), 652–660, doi:10.1038/nn.3690. http://www.nature.com/neuro/journal/v17/n5/full/nn.3690.html.

Sporns, O., Honey, C. J., & Kötter, R. (2007). Identification and Classification of Hubs in Brain Networks. *PLoS ONE*, 2(10), e1049, doi:10.1371/journal.pone.0001049. http://dx.plos.org/10.1371/journal.pone.0001049.

Sporns, O., Tononi, G., & Kötter, R. (2005). The Human Connectome: A Structural Description of the Human Brain. *PLoS Comput Biol*, 1(4), e42, doi:10.1371/journal.pcbi.0010042. http://dx.plos.org/10.1371/journal.pcbi.0010042.

Stam, C. & van Straaten, E. (2012). The organization of physiological brain networks. *Clinical Neurophysiology*, 123(6), 1067–1087, doi:10.1016/j.clinph.2012.01.011. http://www.sciencedirect.com/science/article/pii/S1388245712000570.

Stefanescu, R. A. & Jirsa, V. K. (2008). A Low Dimensional Description of Globally Coupled Heterogeneous Neural Networks of Excitatory and Inhibitory Neurons. *PLoS Comput Biol*, 4(11), e1000219, doi:10.1371/journal.pcbi.1000219. http://dx.doi.org/10.1371/journal.pcbi.1000219.

Stefanescu, R. A. & Jirsa, V. K. (2011). Reduced representations of heterogeneous mixed neural networks with synaptic coupling. *Phys Rev E Stat Nonlin Soft Matter Phys*, 83(2 Pt 2), 026204.

Stegeman, A. (2007). *Comparing Independent Component Analysis and the Parafac model for artificial multi-subject fMRI data*. Technical report, University of Groningen, Groningen. http://www.gmw.rug.nl/~stegeman/Stegeman%20-%20parafac%20&%20ica.pdf.

Stegeman, A. (2014). Finding the limit of diverging components in three-way Candecomp/Parafac—A demonstration of its practical merits. *Computational Statistics & Data Analysis*, 75, 203–216, doi:10.1016/j.csda.2014.02.010. http://www.sciencedirect.com/science/article/pii/S0167947314000504.

Stephan, K. E., Kamper, L., Bozkurt, A., Burns, G. A. P. C., Young, M. P., & Kötter, R. (2001). Advanced database methodology for the Collation of Connectivity data on the Macaque brain (CoCoMac). *Phil. Trans. R. Soc. Lond. B*, 356(1412), 1159–1186, doi:10.1098/rstb.2001.0908. http://rstb.royalsocietypublishing.org/content/356/1412/1159.

Stephan, K. E., Zilles, K., & Kötter, R. (2000). Coordinate-independent mapping of structural and functional data by objective relational transformation (ORT). *Philos Trans R Soc Lond B Biol Sci*, 355(1393), 37–54. http://www.ncbi.nlm.nih.gov/pmc/articles/PMC1692724/.

Steriade, M. (1997). Synchronized activities of coupled oscillators in the cerebral cortex and thalamus at different levels of vigilance. *Cereb. Cortex*, 7(6), 583–604.

Stiefel, K. M., Gutkin, B. S., & Sejnowski, T. J. (2009). The effects of cholinergic neuromodulation on neuronal phase-response curves of modeled cortical neurons. *J Comput Neurosci*, 26(2), 289–301, doi:10.1007/s10827-008-0111-9. http://www.ncbi.nlm.nih.gov/pmc/articles/PMC2857973/.

Strogatz, S. H. (2000). From Kuramoto to Crawford: exploring the onset of synchronization in populations of coupled oscillators. *Phys. D*, 143(1-4), 1–20, doi:10.1016/S0167-2789(00)00094-4. http://dx.doi.org/10.1016/S0167-2789(00)00094-4.

Sullivan, E. V. & Pfefferbaum, A. (2007). Neuroradiological characterization of normal adult ageing. *Brit J Radiol*, 80(Special Issue 2), S99–S108, doi:10.1259/bjr/22893432.

Supekar, K., Menon, V., Rubin, D., Musen, M., & Greicius, M. D. (2008). Network Analysis of Intrinsic Functional Brain Connectivity in Alzheimer's Dis-

ease. *PLoS Comput Biol*, 4(6), doi:10.1371/journal.pcbi.1000100. http://www.ncbi.nlm.nih.gov/pmc/articles/PMC2435273/.

Svoboda, K., Denk, W., Kleinfeld, D., & Tank, D. W. (1997). In vivo dendritic calcium dynamics in neocortical pyramidal neurons. *Nature*, 385(6612), 161–165, doi:10.1038/385161a0. http://dx.doi.org/10.1038/385161a0.

Tagliazucchi, E., Balenzuela, P., Fraiman, D., & Chialvo, D. R. (2012a). Criticality in large-scale brain FMRI dynamics unveiled by a novel point process analysis. *Front Physiol*, 3, 15, doi:10.3389/fphys.2012.00015.

Tagliazucchi, E., von Wegner, F., Morzelewski, A., Brodbeck, V., & Laufs, H. (2012b). Dynamic BOLD functional connectivity in humans and its electrophysiological correlates. *Frontiers in Human Neuroscience*, (DEC), doi:10.3389/fnhum.2012.00339.

Takahashi, T., et al. (2009). Age-related variation in EEG complexity to photic stimulation: a multiscale entropy analysis. *Clin Neurophysiol*, 120(3), 476–483, doi:10.1016/j.clinph.2008.12.043.

Taulu, S., Simola, J., & Kajola, M. (2005). Applications of the Signal Space Separation Method. *IEEE Trans Signal Process*, 53(9), 3359 – 3372, doi:10.1109/TSP.2005.853302.

Tisserand, D. J., Visser, P. J., van Boxtel, M. P., & Jolles, J. (2000). The relation between global and limbic brain volumes on MRI and cognitive performance in healthy individuals across the age range. *Neurobiol Aging*, 21(4), 569–576.

Tononi, G., Sporns, O., & Edelman, G. M. (1994). A measure for brain complexity: relating functional segregation and integration in the nervous system. *Proc Natl Acad Sci U S A*, 91(11), 5033–5037. http://www.pnas.org/content/91/11/5033.

Travers, J. & Milgram, S. (1969). An Experimental Study of the Small World Problem. *Sociometry*, 32(4), 425–443, doi:10.2307/2786545. http://www.jstor.org/stable/2786545.

Tzourio-Mazoyer, N., et al. (2002). Automated Anatomical Labeling of Activations in SPM Using a Macroscopic Anatomical Parcellation of the MNI MRI Single-Subject Brain. *NeuroImage*, 15(1), 273–289, doi:10.1006/nimg.2001.0978. http://www.sciencedirect.com/science/article/pii/S1053811901909784.

Uddin, L. Q., Kelly, A. M., Biswal, B. B., Xavier Castellanos, F., & Milham, M. P. (2009). Functional connectivity of default mode network components: correlation, anticorrelation, and causality. *Hum Brain Mapp*, 30(2), 625–637, doi:10.1002/hbm.20531. http://www.ncbi.nlm.nih.gov/pubmed/18219617.

Vakorin, V. A., Lippé, S., & McIntosh, A. R. (2011). Variability of Brain Signals Processed Locally Transforms into Higher Connectivity with Brain Development. *J Neurosci*, 31(17), 6405–6413, doi:10.1523/JNEUROSCI.3153-10.2011. http://www.jneurosci.org/content/31/17/6405.

van den Heuvel, M. P. & Hulshoff Pol, H. E. (2010). Exploring the brain network: A review on resting-state fMRI functional connectivity. *European Neuropsychopharmacology*, 20(8), 519–534, doi:16/j.euroneuro.2010.03.008. http://www.sciencedirect.com/science/article/pii/S0924977X10000684.

van den Heuvel, M. P., Mandl, R., & Hulshoff Pol, H. (2008). Normalized Cut Group Clustering of Resting-State fMRI Data. *PLoS One*, 3(4), e2001, doi:10.1371/journal.pone.0002001. http://dx.plos.org/10.1371/journal.pone.0002001.

van den Heuvel, M. P. & Sporns, O. (2013). Network hubs in the human brain. *Trends in Cognitive Sciences*, 17(12), 683–696, doi:10.1016/j.tics.2013.09.012. http://www.sciencedirect.com/science/article/pii/S1364661313002167.

van der Want, J. J. L., Klooster, J., Nunes Cardozo, B., de Weerd, H., & Liem, R. S. B. (1997). Tract-tracing in the nervous system of vertebrates using horseradish peroxidase and its conjugates: tracers, chromogens and stabilization for light and electron microscopy. *Brain*

Research Protocols, 1(3), 269–279, doi:10.1016/S1385-299X(96)00042-6. http://www.sciencedirect.com/science/article/pii/S1385299X96000426.

Van Essen, D. & Ugurbil, K. (2012). The future of the human connectome. *Neuroimage*, 62(2), 1299–1310, doi:10.1016/j.neuroimage.2012.01.032. http://www.sciencedirect.com/science/article/pii/S1053811912000493.

Van Essen, D., et al. (2012). The Human Connectome Project: A data acquisition perspective. *Neuroimage*, 62(4), 2222–2231, doi:10.1016/j.neuroimage.2012.02.018. http://www.sciencedirect.com/science/article/pii/S1053811912001954.

Van Steen, M. (2010). Graph Theory and Complex Networks. *An Introduction*. http://www.di.unipi.it/~ricci/book-watermarked.pdf.

Van Veen, B. D., van Drongelen, W., Yuchtman, M., & Suzuki, A. (1997). Localization of brain electrical activity via linearly constrained minimum variance spatial filtering. *IEEE Trans Biomed Eng*, 44(9), 867–880, doi:10.1109/10.623056.

Vazquez, J. & Baghdoyan, H. A. (2001). Basal forebrain acetylcholine release during REM sleep is significantly greater than during waking. *Am J Physiol Regul Integr Comp Physiol*, 280(2), R598–R601. http://ajpregu.physiology.org/content/280/2/R598.

Vigário, R., Särelä, J., Jousmäki, V., Hämäläinen, M., & Oja, E. (2000). Independent component approach to the analysis of EEG and MEG recordings. *IEEE Trans Biomed Eng*, 47(5), 589–593, doi:10.1109/10.841330.

Vincent, J. L., Kahn, I., Snyder, A. Z., Raichle, M. E., & Buckner, R. L. (2008). Evidence for a Frontoparietal Control System Revealed by Intrinsic Functional Connectivity. *J Neurophysiol*, 100(6), 3328–3342, doi:10.1152/jn.90355.2008. http://www.ncbi.nlm.nih.gov/pmc/articles/PMC2604839/.

Wang, J., et al. (2009). Parcellation-dependent small-world brain functional networks: A resting-state fMRI study. *Hum Brain Mapp*, 30(5), 1511–1523, doi:10.1002/hbm.20623. http://onlinelibrary.wiley.com/doi/10.1002/hbm.20623/abstract.

Wang, Z., Maier, A., Logothetis, N. K., & Liang, H. (2008). Single-Trial Decoding of Bistable Perception Based on Sparse Nonnegative Tensor Decomposition. *Comput Intell Neurosci*, 2008, doi:10.1155/2008/642387. http://www.ncbi.nlm.nih.gov/pmc/articles/PMC2396775/.

Watts, D. J. & Strogatz, S. H. (1998). Collective dynamics of 'small-world' networks. *Nature*, 393(6684), 440–442, doi:10.1038/30918. http://www.nature.com/nature/journal/v393/n6684/full/393440a0.html.

Wedeen, V. J., Hagmann, P., Tseng, W.-Y. I., Reese, T. G., & Weisskoff, R. M. (2005). Mapping complex tissue architecture with diffusion spectrum magnetic resonance imaging. *Magn. Reson. Med.*, 54(6), 1377–1386, doi:10.1002/mrm.20642. http://onlinelibrary.wiley.com/doi/10.1002/mrm.20642/abstract.

Whitfield-Gabrieli, S. & Ford, J. M. (2012). Default Mode Network Activity and Connectivity in Psychopathology. *Annu Rev Clin Psychol*, 8(1), 49–76, doi:10.1146/annurev-clinpsy-032511-143049. http://www.annualreviews.org/doi/abs/10.1146/annurev-clinpsy-032511-143049.

Wilson, H. R. & Cowan, J. D. (1972). Excitatory and Inhibitory Interactions in Localized Populations of Model Neurons. *Biophys J*, 12(1), 1–24.

Wilson, H. R. & Cowan, J. D. (1973). A mathematical theory of the functional dynamics of cortical and thalamic nervous tissue. *Kybernetik*, 13(2), 55–80.

Wise, R. G., Ide, K., Poulin, M. J., & Tracey, I. (2004). Resting fluctuations in arterial carbon dioxide induce significant low frequency variations in BOLD signal. *NeuroImage*, 21(4), 1652–1664, doi:16/j.neuroimage.2003.11.025. http://www.sciencedirect.com/science/article/pii/S1053811903007663.

Wong, K.-F. & Wang, X.-J. (2006). A Recurrent Network Mechanism of Time Integration in Perceptual Decisions. *J Neurosci*, 26(4), 1314–1328, doi:10.1523/JNEUROSCI.3733-05.2006. http://www.jneurosci.org/cgi/content/abstract/26/4/1314.

Woodman, M. M. & Jirsa, V. K. (2013). Emergent Dynamics from Spiking Neuron Networks through Symmetry Breaking of Connectivity. *PLoS ONE*, 8(5), e64339, doi:10.1371/journal.pone.0064339. http://dx.doi.org/10.1371/journal.pone.0064339.

Woolrich, M., Hunt, L., Groves, A., & Barnes, G. (2011). MEG beamforming using Bayesian PCA for adaptive data covariance matrix regularization. *Neuroimage*, 57(4), 1466–1479, doi:10.1016/j.neuroimage.2011.04.041.

Xiong, J., Parsons, L. M., Gao, J.-H., & Fox, P. T. (1999). Interregional connectivity to primary motor cortex revealed using MRI resting state images. *Human Brain Mapping*, 8(2-3), 151–156, doi:10.1002/(SICI)1097-0193(1999)8:2/3<151::AID-HBM13>3.0.CO;2-5. http://onlinelibrary.wiley.com/doi/10.1002/(SICI)1097-0193(1999)8:2/3<151::AID-HBM13>3.0.CO;2-5/abstract.

Yang, A. C., et al. (2012). Complexity of spontaneous BOLD activity in default mode network is correlated with cognitive function in normal male elderly: a multiscale entropy analysis. *Neurobiology of aging*, doi:10.1016/j.neurobiolaging.2012.05.004.

Yang, L., Liu, Z., & He, B. (2010). EEG-fMRI reciprocal functional neuroimaging. *Clinical Neurophysiology*, 121(8), 1240–1250, doi:16/j.clinph.2010.02.153. http://www.sciencedirect.com/science/article/pii/S1388245710002567.

Yeung, M. K. S. & Strogatz, S. H. (1999). Time Delay in the Kuramoto Model of Coupled Oscillators. *Phys. Rev. Lett.*, 82(3), 648–651, doi:10.1103/PhysRevLett.82.648. http://link.aps.org/doi/10.1103/PhysRevLett.82.648.

Yuan, H., Zotev, V., Phillips, R., Drevets, W. C., & Bodurka, J. (2012). Spatiotemporal dynamics of the brain at rest–exploring EEG microstates as electrophysiological signatures of BOLD resting state networks. *Neuroimage*, 60(4), 2062–2072, doi:10.1016/j.neuroimage.2012.02.031.

Zalesky, A., Fornito, A., Harding, I. H., Cocchi, L., Yücel, M., Pantelis, C., & Bullmore, E. T. (2010). Whole-brain anatomical networks: Does the choice of nodes matter? *NeuroImage*, 50(3), 970–983, doi:10.1016/j.neuroimage.2009.12.027. http://www.sciencedirect.com/science/article/pii/S1053811909013159.

Zeng, L.-L., et al. (2012). Identifying major depression using whole-brain functional connectivity: a multivariate pattern analysis. *Brain*, 135(Pt 5), 1498–1507, doi:10.1093/brain/aws059. http://www.ncbi.nlm.nih.gov/pubmed/22418737.

Zhou, C., Zemanová, L., Zamora, G., Hilgetag, C. C., & Kurths, J. (2006). Hierarchical organization unveiled by functional connectivity in complex brain networks. *Phys. Rev. Lett.*, 97(23), 238103.

Zhou, G. & Cichocki, A. (2013). A Brief Guide for TDALAB Ver 1.1. http://bsp.brain.riken.jp/~zhougx/tdalab/tdalab_guide.pdf.

Zhou, J., et al. (2010). Divergent network connectivity changes in behavioural variant frontotemporal dementia and Alzheimer's disease. *Brain*, 133(Pt 5), 1352–1367, doi:10.1093/brain/awq075.

Zhu, Z., et al. (2009). The relationship between magnetic and electrophysiological responses to complex tactile stimuli. *BMC Neurosci*, 10, 4, doi:10.1186/1471-2202-10-4.

Zimmerman, D. W., Zumbo, B. D., & Williams, R. H. (2003). Bias in Estimation and Hypothesis Testing of Correlation. *Psicológica*, (001). http://redalyc.uaemex.mx/src/inicio/ArtPdfRed.jsp?iCve=16924109.

Abbreviations and Glossary

Abbreviations

- **AAL**: **Automated Anatomical Labeling**
- **AMPA**: **α-amino-3-hydroxy-5-methyl-4-isoxazolepropionic acid**
- **ACC**: **Anterior Cingulate Cortex**
- **ACh**: **Acetylcholine**
- **AHP**: **After-hyper-polarization**
- **CC**: **Corcondia**
- **CP** or CANDECOMP: **Canonical polyadic (Decomposition)**, see PARAFAC
- **BA**: **Brodman Area**
- **BLP**: **Bandlimited Power**
- **BOLD**: **Blood Oxygen Level Dependent**
- **DAN**: **Dorsal Attention Network**
- **DPFC**: **Dorsolateral Prefrontal Cortex**
- **DMN**: **Default Mode Network**
- **DSI**: **Diffusion Spectrum Imaging**
- **DTI**: **Diffustion Tensor Imaging**
- **DWI**: **Diffusion Weighted Imaging**
- **EEG** : **Electroencephalography**
- **FC**: **Functional Connectivity**
- **fcMRI**: **Functional connectivity MRI**

- **fMRI**: **Functional Mangnetic Resonance Imaging**
- **FPN**: **Frontoparietal Network**
- **GABA**: γ**-Aminobutyric acid**
- **IC**: **Independent Component**
- **ICA**: **Independent Component Analysis**
- **IPS**: **Intraparietal Sulcus**
- **LCMV**: **Linearly Constrained Minimum Variance**
- **LIF**: **Leaky-integrate-and-fire**
- **LPC**: **Lateral Parietal Cortex**
- **MEEG**: **MEG/EEG**
- **MEG**: **Magnetoencephalography**
- **MI**: **Mutual Information**
- **MNI**: **Montreal Neurological Institute**
- **MPFC**: **Medial Prefrontal Cortex**
- **MSE**: **Multiscale Entropy**
- **MT+**: **Medial Temporal Area - visual motion area**
- **NMDA**: **N-Methyl-D-aspartic acid**
- **NREM**: **Non-REM**
- **PARAFAC**: **Parallel Factor Analysis**
- **PCA**: **Principal Component Analysis**
- **PCC**: **Posterior Cingulate Cortex**
- **PET**: **Positron Emmition Tomography**

- **PFC**: **Prefrontal Cortex**
- **PICA**: **Probabilistic ICA**
- **ROI/ROIs**: **Region of Interest**
- **REM**: **Rapid Eye Movement**
- **RS**: **Resting State**
- **rsfMRI**: **Resting State fMRI**
- **RSN/RSNs**: **Resting State Network**
- **SC**: **Structural Connectivity**
- **SFA**: **Spike-Frequency Adaptation**
- **SMN**: **Somatosensory Network**
- **SWS**: **Slow Wave Sleep**
- **TVB**: **The Virtual Brain**
- **VAN**: **Ventral Attention Network**
- **VN**: **Visual Network**

Glossary

- **After-hyper-polarization** (**AHP**): The hyperpolarized state of a neuron after the occurence of an action potential where the membrane potential falls below the resting potential, inhibiting further firing of the cell for its duration. AHP is partly caused by Ca^{2+}-dependent Kˆ+-channel opening during the action potential, but other aspects are not well understood yet. There are AHP on several time scales.

- **Corcondia**: A model appropriateness measure for PARAFAC, expressing the similarity between a decomposition allowing or not allowing for interaction between the components.

- **Criticality**: (or self-organized criticality - SOC) refers to systems with a critical point attractor at the edge of bifurcation, or phase transitioning of the system. In critical systems, scale-free, power-law or at least heavy-tailed complex dynamics arise.

- **Default Mode Network** (**DMN**): A network of brain regions whose activity is more correlated to each other than to other regions during resting-state brain activity, and which is deactivated during a range of tasks. Main hubs are medial prefrontal cortex, posterior cingulate cortex, and precuneus.

- **Dorsal Attention Network** (**DAN**): Also reffered to as the TPN / Task positive network, due to its implication in many visual and attention tasks. It includes areas in inferior parietal cortex, (pre-)sensorimotor cortex, and frontal eye fields.

- **Electroencephalography** (**EEG**): A technology to measure electric currents originating in the brain through electrodes attached to the human scalp. EEG is closely related to MEG and Ecog (Scholarpedia: Electroencephalography).

- **Human Brain Project** (**HBP**): A 10-year European Union flagship research project established in 2013 which aims to build a detailed computer model of the human brain and its dynamics (Project Homepage).

- **Inverse problem**: In neurophysiology, this describes the problem that while we are interested in brain signals, in M/EEG we only have a limited amount of remote sensor data available, which can be potentially caused by many different patterns of internal brain source patterns so that no single unique solution exists (Scholarpedia: Source localization).
- **Magnetoencephalography** (**MEG**): A technology to measure magnetic field emitted by the electric firing of neurons. MEG is mainly sensitive to the postsynaptic intracellular currents flowing across pyramidal neurons in cortical sulci, due to the fact that MEG is only affected by the tangential component and signal strength drops stronger with distance than for EEG, but it is less affected by skull and tissue conductivities, complementing its strengths and weaknesses with EEG. (Scholarpedia: Magnetoencephalography)
- **Mean field**: The representation of a large number of units in a population, here populations of neurons, by a single mean field equation, taking into account the mean or mean and variance.
- **M/EEG**: MEG and/or EEG.
- **Multiscale Connectivity**: Multiscale brain connectivity refers to physical and functional connection patterns between a set of brain units on multiple levels of spatial extent (Springer Encyclopedia: Nakagawa & Deco, 2014).
- **Multiscale Entropy**: A measure of complexity of physiological data, e.g. of the heartbeat.
- **Multistability**: Description for systems that have multiple stable configurations, and may settle into (or, in the presence of noise, switch between) different stable states depending on initial conditions or inputs.
- **Multivariate Interaction Measure** (**MIM**): phase-shifted interaction measure introduced by (Ewald et al., 2012).
- **Mutual Information**: A mutual dependency measure between variables, measured in bits (Scholarpedia: MI)

- **Maximal Correlation Window** (**MCW**): An algorithm "which iteratively locates epochs in which the correlation between a seed region (e.g., LpIPS) and a subset of network nodes is high while, concurrently, the correlation with a region outside of the network is minimal" (de Pasquale et al., 2010).

- **Parallel Factor Analysis** (PARAFAC): A datadriven tensor decomposition method based on a generalization of matrix singular value decomposition.

- **Resting State Network / Resting State Networks** (RSN, RSNs): Distinguishable networks of brain regions that are functionally linked during spontaneous brain activity, such as the DMN or the DAN

- **Source leakage** : A term for the phenomenon that an electric or magnetic signal originating in the brain travels, is picked up by various sensors at the same time, and may be confoundedly attributed to several sources. Related intimately to the inverse problem.

- **Spike Frequency Adaptation** (SFA): The phenomenon that some neurons show a decrease of response to continuous stimulation after the initial response, e.g. through AHP. (Scholarpedia: SFA)